

Alma Mater Studiorum – Università di Bologna

DOTTORATO DI RICERCA IN
Scienze Biomediche e Neuromotorie

Ciclo XXXII

Settore Concorsuale: 05/H1

Settore Scientifico Disciplinare: BIO/16

**ROLE OF NUCLEAR REDOX CONTROL, INTRA-POPULATION
HETEROGENEITY AND OXYGEN TENSION IN HUMAN AMNIOTIC FLUID
STEM CELLS AGING**

Presentata da:
Francesca Casciaro

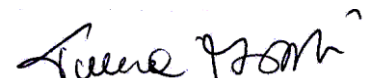
Coordinatore Dottorato
Prof. Pietro Cortelli



Supervisore
Prof.ssa Matilde Yung Follo



Co-Supervisore
Dott.ssa Tullia Maraldi



Esame finale anno 2019

ABSTRACT FRANCESCA CASCIARO

Thanks to their unique properties, mesenchymal stem cells (MSCs) have emerged as a potential therapeutic approach for various disorders. The effects of MSCs treatments could be due to the combination of different factors, such as the ability to support other cell types during tissue regeneration, the secretion of growth factors and cytokines and immunomodulation properties.

MSCs are present both in foetal and adult tissues and in the last years more interest has been focused toward amniotic fluid stem cells (hAFSC). hAFSC have gained the interest of scientific research since they express multiple pluripotent markers and are able to differentiate into mesodermal and nonmesodermal lineages under appropriate differentiation conditions, but unlike embryonic stem cells or iPS, they do not form tumors *in vivo*.

The low number of available MSCs requires their *ex vivo* expansion prior to clinical use. However, during their *in vitro* culture, MSCs quickly reach replicative senescence.

For sure, different mechanisms are involved into stem cell aging and include the accumulation of toxic metabolites as reactive oxygen species (ROS). Among the ROS producing enzymes, NADPH oxidase 4 (Nox4) has been shown to have a peculiar role in regulating amniotic fluid stem cells biology, playing an essential role in the maintenance of pluripotency, through modulation of both nuclear signalling and DNA damage, consequently influencing the proliferation rate and their differentiation ability.

Moreover, recent data have shown a relationship among lamins mutations (nucleoskeleton proteins), altered ROS metabolism and physiological aging. In fact, it has been suggested that lamin A can be oxidized acting as a ROS-sink inside the nucleus.

The principal aim of this study was to investigate the aging process occurring during *in vitro* expansion of human amniotic fluid stem cells, focusing in particular on the redox control involving Nox4 and prelamin A, an immature form of lamin A, that has been reported to accumulate both in premature aging syndromes and in physiological aging.

My results show that a strong heterogeneity is present among samples that reflects their different behaviour in culture and should be considered in their application in regenerative medicine.

I identified three proteins, namely Nox4, prelamin A and PML, which expression increases during hAFSC aging process and could be used as new biomarkers to screen stem cells samples before their use. In particular, I found out that Nox4 degradation is regulated by sumoylation process *via* proteasome pathway and involved interactions with PML bodies and prelamin A. So, all these interactions should be studied in deep to identify new targets for pharmaceutical interventions that could slow down and ameliorate the aging process not only in stem cells but also in normal ones.

Furthermore, since various studies revealed that donor-dependent differences are in part due and explained by cell-to-cell variation within each patient population, I studied in deep this phenomenon.

My results showed that the heterogeneity among samples is also accompanied by a strong intra-population heterogeneity, with cells having different dimensions and morphology. In this sense, separation of different c-kit⁺ hAFSC subpopulations from the same donor, using Celector® technology, which eluates cells with different characteristics at different times, showed that an enrichment in the last eluted fraction could improve hAFSC application in regenerative medicine.

In fact, the analysis of the stemness markers revealed that Oct4 expression was significantly higher in the last part of the eluates and it was accompanied by a less expression of mesenchymal markers compared to the first part of collected cells, indicating that the last eluted cells maintain a higher plasticity.

One of the other problems that could influence stem cell aging is that, at present, most of the expansion procedures of MSCs are performed under atmospheric O₂ concentration (20% O₂), which is approximately 4–10 times higher than the O₂ tension in their natural niches. This higher O₂ concentration might cause environmental stress to the *in vitro* cultured MSCs, due to the increased ROS level and accelerates their aging process.

For this reason, the influence of oxygen tension in morphology, phenotype, proliferative capacity, and functionality of stem cells has been increasingly studied with controversial results.

Here, I showed that, after a month *in vitro*, prolonged low oxygen tension exposure preserves hAFSC stemness properties, increasing proliferation ability, glycolytic metabolism and enhancing osteogenic differentiation ability, while reducing senescence-associated markers, apoptosis process and adipogenic capability.

In conclusion, my study pointed different approaches to improve *in vitro* hAFSC expansion and manipulation with the purpose to land at stem cell therapy.

Index

| | |
|---|----|
| 1. INTRODUCTION | 4 |
| 1.1. Mesenchymal stem cells | 4 |
| 1.2. Amniotic fluid stem cells..... | 6 |
| 1.3. Therapeutic applications of mesenchymal stem cells | 9 |
| 1.4. General features of cellular senescence in mesenchymal stem cells | 12 |
| 1.5. Reactive oxygen species and stem cells aging | 14 |
| 1.6. NADPH oxidase 4 (NOX4) and its role in stem cell biology | 17 |
| 1.7. Lamins as mediators of oxidative stress and their role in aging | 19 |
| 1.8. Role of PML bodies and sumoylation in stress response and senescence | 26 |
| 1.9. Implications of stem cells heterogeneity in <i>in vitro</i> amplification and senescence | 31 |
| 1.10. Effect of hypoxia on stem cells properties | 33 |
| 2. AIM OF THE PROJECT..... | 36 |
| 3. MATERIALS AND METHODS | 39 |
| 3.1. Amniotic fluid collection..... | 39 |
| 3.2. Amniotic fluid stem cells selection..... | 39 |
| 3.3. Cellular culture | 40 |
| 3.4. Evaluation of ROS levels | 40 |
| 3.5. Cellular viability..... | 41 |
| 3.6. Cellular proliferation..... | 41 |
| 3.7. EdU Proliferation assay | 42 |
| 3.8. Differentiation assays | 42 |
| 3.9. Senescence assay..... | 43 |
| 3.10. Cellular morphology | 43 |
| 3.11. Flow cytometer immune-assay | 44 |

| | |
|---|----|
| 3.12. Cells treatments | 44 |
| 3.13. Cellular extracts preparation | 45 |
| 3.14. Protein quantification..... | 45 |
| 3.15. Nuclei purification | 45 |
| 3.16. Immunoprecipitation..... | 46 |
| 3.17. SDS page and western blot..... | 46 |
| 3.18. Mass Spectrometry..... | 48 |
| 3.19. Immunofluorescence and confocal microscopy..... | 48 |
| 3.20. AFSC subpopulations sorting..... | 49 |
| 3.21. RNA isolation and quantification | 51 |
| 3.22. cDNA retrotranscription and qRT-PCR | 51 |
| 3.23. RNA and DNA quality check..... | 53 |
| 3.24. Library preparation and RNAseq | 54 |
| 3.25. Statistical Analysis..... | 56 |
| 4. RESULTS..... | 57 |
| 4.1. Nuclear redox control of stem cell aging..... | 57 |
| 4.1.1. Characterization of Human Amniotic Fluid Stem Cells samples..... | 57 |
| 4.1.2. Senescence-associated molecular changes in AFSCs culture | 60 |
| 4.1.3. Differences in nuclear redox state of AFSC groups during their culture | 64 |
| 4.1.4. Nox4 and prelamin A interaction in human amniotic stem cells | 68 |
| 4.1.5. Exploring the meaning of Nox4 and prelamin A interaction | 73 |
| 4.2. Investigation of c-kit ⁺ hAFSC intrapopulation heterogeneity..... | 78 |
| 4.2.1. hAFSC sorting | 78 |
| 4.2.2. Characterization of hAFSC sorted cells..... | 79 |
| 4.2.3. Evaluation of fractions proliferation ability | 84 |

| | | |
|--------|--|-----|
| 4.2.4. | Analysis of senescence-associated molecular markers | 88 |
| 4.2.5. | Evaluation of overall transcriptome differences among sorted fractions | 89 |
| 4.3. | Effect of prolonged low oxygen tension on hAFSC | 99 |
| 4.3.1. | Evaluation of stemness properties of hAFSC cultured at different oxygen tensions..... | 99 |
| 4.3.2. | Proliferation ability of AFSC at different oxygen tensions | 100 |
| 4.3.3. | Senescence-associated markers in AFSC cultivated at different oxygen concentrations | 104 |
| 4.3.4. | Metabolism variations at different oxygen tensions | 111 |
| 4.3.5. | Hypoxia and resistance to stress..... | 113 |
| 4.3.6. | Differentiation ability in hypoxia | 115 |
| 5. | DISCUSSION AND CONCLUSIONS | 117 |
| 6. | REFERENCES..... | 125 |

1. INTRODUCTION

1.1. Mesenchymal stem cells

Stem cells are implicated in preserving tissue homeostasis throughout life by replacing damaged or lost cells thanks to two defined properties: pluri/multipotency and self-renewal capacity. In fact, they can give rise to all cells within the body (pluripotency) or a given tissue (multipotency) if they are stimulated to differentiate. Furthermore, during each cell division, stem cells have the capacity to generate another cell that shows the same staminal markers in order to maintain a defined stem cell pool (self-renewal capacity)¹.

Because of clinical applications and biological importance, nowadays stem cells have become an important research subject.

Based on their origin, stem cells are divided into different categories.

In particular, embryonic stem cells (ESCs) derive predominantly from blastocyst-stage embryos. They possess distinctive self-renewal capacity, pluripotency, a high telomerase activity and can give rise to all the cellular lineages².

Since their very first isolation, human ESCs aroused the interest of scientists for drug screening, immunotherapy and regenerative medicine, but their use has been restricted for different reasons, such as ethical concerns and their potential tumorigenicity³.

Induced pluripotent stem cells (iPSCs) are generated from adult cells by the overexpression of four pluripotency related transcription factors (Oct4, Sox2, Klf4 and c-Myc)⁴. They are similar to ESCs at cellular level, as they have the capacity of self-renewal, differentiation potential and the ability to produce germ line competent-chimeras⁵. Though iPSCs possess great potential for cell therapy, their genomic stability is still questionable⁵.

Stem cells can also be found in adult tissues but they have a more restrictive differentiation potential than the other types, since their primary roles in a living organism are to maintain and repair the tissue in which they are resident⁶.

For example, stem cells isolated from bone marrow exhibit, upon culture, the ability to differentiate into specialized cells developing from mesoderm and for this reason they are named as mesenchymal stem cells (MSCs)⁷.

MSCs are self-renewable, multipotent, easily accessible and culturally expandable *in vitro* with genomic stability and few ethical issues, characteristics that recognize their importance in cell therapy, regenerative medicine and tissue repair.

MSCs are present both in foetal and adult tissues. Efficient populations of MSCs have been obtained from bone marrow⁸, adipose tissue⁹, amniotic fluid^{10,11}, amniotic membrane¹², dental tissues¹³, endometrium¹⁴, limb bud¹⁵, menstrual blood¹⁶, peripheral blood¹⁷, placenta and foetal membrane¹⁸, salivary gland¹⁹, skin and foreskin²⁰, sub-amniotic umbilical cord lining membrane²¹, synovial fluid²² and Wharton's jelly²³.

According to the International Society for Cellular Therapy, the expression of a specific set of cell surface markers is one of the essential characteristics of hMSCs. In particular, these cells are positive for CD73, CD90, CD105, whereas they do not express CD14, CD34, CD45 and HLA-DR²⁴.

hMSCs have the capacity to differentiate into cellular lines belonging to all the three lineages, ectoderm, mesoderm and endoderm, by employing media and growth supplements which induce lineage differentiation⁵.

In vitro and *in vivo* studies have provided evidences for the immunomodulatory role of MSCs, due to their low expression of MHC I and lack expression of MHC class II along with co-stimulatory molecules, like CD80, CD40 and CD86²⁵.

The identification of MSC paracrine effects on immune cells has led to several stem cell-based clinical applications targeting immune-mediated and autoimmune pathologies.

For example, exposure to inflammatory cytokines, such as TNF α , IFN-g, and IL-1 β , stimulates MSC immunosuppressive activities²⁶, suggesting a cellular negative feedback loop mediated by MSC responses that serves to dampen inflammatory reactions. Activated MSCs, indeed, recruit T lymphocytes by chemokine secretion and reduce T lymphocyte proliferation, activation-antigen expression, and inflammatory cytokine secretion²⁷.

Several studies show that MSCs secreted factors promote angiogenesis, protect compromised host cells from apoptosis, recruit and stimulate resident stem cells, while concurrently inhibiting inflammation and subsequent fibrosis²⁸.

1.2. Amniotic fluid stem cells

In the last years, great interest has been devoted to the use of Induced Pluripotent Stem cells for modelling of human genetic diseases, due to the possibility of reprogramming somatic cells of affected patients into pluripotent cells, enabling differentiation towards several cell types and allowing investigations on the molecular mechanisms of the disease. However, the protocol of iPS generation still suffers from technical limitations, showing low efficiency, being expensive and time consuming²⁹.

In fact, the artificial methods involved in generating them lead to concern about how much they can resemble the identity and the function of both normal and disease-specific differentiated adult cells, for example, and even more if the epigenetic memory of the deriving adult cells is perfectly erased³⁰.

For these reasons, the finding of alternative models able to overcome these criticisms, could be useful for the study of human genetic diseases. In this sense, human amniotic fluid stem cells (hAFSC) have been proposed as a potential alternative for both disease modelling and therapeutic use¹¹.

Human amniotic fluid can be obtained during amniocentesis at the second trimester³¹, or during a procedure called “amnio reduction”³² performed at the third trimester or during the caesarean section³³. In all cases, this material is discarded after the diagnostic procedures, meaning that there are minimal ethical and legal issues associated with their collection and use.

Amniotic fluid contains a mixture of different cell types, derived for example from the foetal amnion membrane and skin, as well as from the alimentary, respiratory, and urogenital tracts of the foetus³⁴.

Nevertheless, the cell population changes with time and reflects the changes in the developing foetus³⁵.

Based on morphological and growth characteristics, hAFSC can be classified into epithelioid (E-type) cells, amniotic fluid specific (AF-type) cells and fibroblastic (F-type) cells³⁶.

A highly multipotent subpopulation can be isolated through positive selection for the membrane receptor c-kit (CD117), a protein tyrosine - kinase receptor that specifically binds to the ligand stem cell factor (SCF). Approximately, only 1% of total amniotic fluid cells has been shown to be c-kit positive^{11,37}.

It has been demonstrated that the fibroblast-shaped cell subpopulation is positive for the mesenchymal markers CD90, CD105, CD73 and CD166, but negative for the hematopoietic markers CD45, CD34 and CD1³⁸.

Furthermore, cultured human AFS cells express a wide range of pluripotency markers, such as Oct4, Sox2, Ssea4, Ssea3, c-Myc, Klf4³⁹.

Consistently with these assumptions, AF-MSCs were found to be able to differentiate into mesodermal and non-mesodermal lineages under appropriate differentiation conditions, although functional *in vivo* differentiation toward endoderm and ectoderm has not yet been fully proved^{11,40}.

It is debated how to classify AFS cells, since they seem to have intermediate properties between embryonic and adult stem cell types in terms of their versatility. In fact, even if they have a large differentiation potential, they cannot be considered pluripotent because they do not form tumors *in vivo* and there is no evidence on their ability to form chimeras when injected into blastocysts⁴¹. Since the unique abilities of pluripotent cells consist of self-renewal, differentiation into derivatives of all three germ layers but also the formation of clonal lines *in vitro* and teratomas *in vivo*, we can conclude that AFS cells are not pluripotent stem cells.

However, AFS cells certainly display molecular and biological characteristics closer to pluripotent than to multipotent stem cells. In 2010, for the first time, it was reported that AFS cells have even the ability to form embryoid bodies (EB) just as embryonic stem cells⁴². So, for all these reasons AFS cells can be defined as largely multipotent¹¹.

Interestingly, these cells are positive for antigens HLA-ABC (MHC class I), but only a small fraction for HLA-DR (MHC class II), otherwise showing the expression of immunosuppressive factors such as CD59 (protectin) and HLA-G, making them promising candidates for allogeneic transplantation and clinical applications in regenerative medicine^{11,43}.

Recently, a number of studies have shown that their secretome is an important source of cytokines, chemokines and pro-angiogenic soluble factors, such as monocyte chemoattractant protein-1 (MCP-1), stromal cell-derived factor-1 (SDF-1) HGF, and VEGF⁴⁴⁻⁴⁷. In particular, the conditioned medium of AFS cells is able to exert a remarkable pro-survival and anti-apoptotic effect in regeneration of injured tissues where, usually, a chronic inflammation status is present^{48,49}. Basing on these

assumptions, in the last decade more attention has been paid to the secretome of stem cells and, therefore, on the paracrine effect. Conditioned medium includes soluble factors and extracellular vesicles. In addition to their role as biomarkers, released extracellular vesicles (EV) have been included among the players contributing to MSC regenerative potential. In a very recent study, my group showed that the secretome components differently affect the immune response. In particular, it seems that the principal effect of AFSC conditioned media (without exosomes) is the induction of apoptosis in lymphocytes, whereas exposure to AFSC-derived exosomes decreases lymphocyte's proliferation, affecting particularly the CD4⁺ subpopulation⁵⁰.

All these considerations have increased during the years the interest towards amniotic fluid stem cells, motivated by their high accessibility, the capability to differentiate in lineages representative of the three germ layers, the ability to form embryoid bodies and the therapeutic safety [Figure 1.2.1]²⁹.

| Properties | ES | iPS | AFS |
|--------------------------------------|-----|-----|-----|
| Naturally existing stem cells | Yes | No | Yes |
| Self renewal capacity | Yes | Yes | Yes |
| High proliferation efficiency | Yes | Yes | Yes |
| Pluripotent marker expression | Yes | Yes | Yes |
| Differentiation in three germ layers | Yes | Yes | Yes |
| Risk for teratoma formation | Yes | Yes | No |
| Ectopic oncogene expression | No | Yes | No |

| Properties | ES | iPS | AFS |
|--|--------|--------|--------|
| Immunological compatibility with recipient | Yes/No | Yes/No | Yes/No |
| Possessing prenatally lethal mutations | Yes | No | Yes/No |
| Disease-specific stem cells | Yes | Yes | Yes |
| Disease specific stem cells with known patient's phenotype | No | Yes | Yes |
| Risk for chromosomal aberrations from the donor cells | No | Yes/No | No |
| Risk for aberrations acquired during reprogramming | No | Yes | No |
| Epigenetic deregulation | No | Yes | No |
| Studies on drug testing | Yes | Yes | Yes |
| Legal restrictions | Yes | No | No |
| Ethical concerns | Yes | No | No |

Figure 1.2.1 Comparison among embryonic stem cells, induced pluripotent stem cells and amniotic fluid stem cells

Antonucci I, Provenzano M, Rodrigues M, et al. *Int J Mol Sci.* 2016;17(4):607

1.3. Therapeutic applications of mesenchymal stem cells

Thanks to their unique properties, mesenchymal stem cells have emerged as a potential therapeutic approach for various disorders. The effects of MSCs treatments could be due to the combination of different factors, such as the ability to support other cell types during tissue regeneration⁵¹, the secretion of growth factors and cytokines⁵² and immunomodulation properties⁵³.

The ability of MSCs to differentiate into osteoblasts, tenocytes, and chondrocytes has attracted interest in the orthopaedic field, mostly in the treatment of bone disorders, such as osteogenesis imperfecta⁵⁴. There are multiple ways to implant cells during tissue regeneration, together with vehicles or scaffolds which are also known as systemic application or local application.

Although the results from most of the studies proved that only 5% of transplanted cells survived after 2 weeks of their administration⁵⁵, a follow-up study demonstrated continued improvements in patients with osteogenesis imperfecta for 18 to 36 months post-transplantation⁵⁶.

Recently, new strategies have been proposed to increase the success of bone graft. For example, researchers suggest the use of scaffolds treated with promoting factors together with stem cells^{57,58}.

Similarly, there is a limited number of reports demonstrating the efficacy of MSCs also in promoting cartilage repair even if the mechanisms remain unclear^{59,60}.

Despite improvements in medical and surgical therapies, heart disease and heart failure continue to be one of the major causes of mortality. Thanks to its regenerative and immunomodulatory properties, MSC therapy is an attractive candidate for cardiovascular repair. In particular, cardio-protection seems to be achieved through different secreted MSCs factors, such as vascular endothelial growth factor (VEGF), hepatocyte growth factor (HGF), granulocyte colony stimulating factor (G-CSF), fibroblast growth factor (FGF-2) and transforming growth factor beta 1 (TGF-1)⁶¹. In addition, some studies reported that engrafted MSCs could differentiate into cardiomyocytes after local injection⁶².

The paracrine function of the MSCs may play an important role also in kidney injury repair. In fact, it has been proved that MSCs-derived GM-CSF, EGF, CXCL1, IL-6, IL-

8, MCP-1, PDGF-AA, and CCL5 may promote repair of kidney injury by promoting macrophage polarization⁶³.

Thanks to their immunomodulatory properties, MSCs represent an attractive therapeutic approach also to minimize the toxicity of the conditioning regimens and decreasing the incidence and the severity of the graft versus host disease (GVHD). Different studies show promising results in the treatment of acute GVHD, while more analysis should be carried out to prove the effect on the chronic GVHD. Anyway, in studies where MSC therapy was tested both on aGVHD and cGVHD, the response rates were always higher in the treatment of the acute one⁶⁴.

Moreover, also based on all these results, it has been proposed to take advantage of these immunomodulatory functions to treat autoimmune diseases. In fact, patients suffering from severe autoimmune diseases, do not often respond to standard therapy and require autologous or allogeneic haemopoietic stem cells transplantation⁶⁵, which can however induce toxicity or GVHD. In this case, the administration of MSCs may be a safer and more feasible method of treatment.

First, the therapeutic role of MSCs has been investigated in patients with Crohn disease, a chronic inflammatory disorder in which the immune system attacks the gastrointestinal tract. Five patients were treated with autologous adipose tissue derived MSCs. Promising results were showed in two patients after 8 weeks: the 75% of treated fistulas had closed and showed signs of significant repair⁶⁶, leading the researchers to start a phase II - clinical trial⁶⁷.

Other studies have been carried out in multiple sclerosis, a chronic autoimmune demyelinating disease of the central nervous system, but until now the results seem to claim that MSCs therapy is less efficient in this pathology⁶⁸.

Mesenchymal stem cells efficacy has also been tested in systemic lupus erythematosus (SLE), an autoimmune inflammatory disease with multiorgan involvement including the kidney, brain, lung, and hematopoietic systems. Even if MSCs seem to be an attractive therapeutic approach, a recent study showed that MSCs derived from SLE patients have an abnormal functionality⁶⁹, suggesting in this way that heterologous MSC transplantation may be more effective compared to the autologous treatment.

Finally, MSC anti-inflammatory properties and regenerative potential indicate that they could represent a novel therapeutic approach to treat rheumatoid arthritis (RA), a T cell-

mediated autoimmune disease characterized by cartilage and bone destruction. However, since preclinical studies have showed controversial results^{70,71}, their application in clinical trials may be delayed [Figure 1.3.1]⁷².

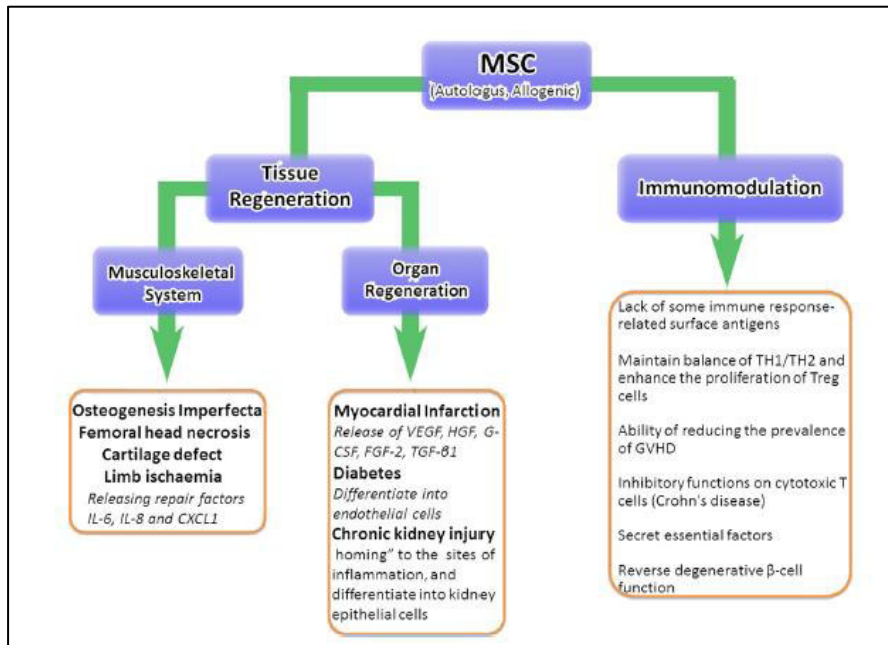


Figure 1.3.1 MSCs application in regenerative medicine and their potential mechanisms of action
Morito T, Muneta T, Hara K, et al. *Rheumatology*. 2008;47(8):1137-1143

Besides to be a tool in regenerative medicine, MSCs are emerging as a novel approach in cancer therapy. Even if it is not clear if MSCs themselves promote^{73,74} or inhibit^{75,76} tumor growth, they have been genetically modified to overexpress different anticancer genes, such as ILs⁷⁷, IFNs⁷⁸, prodrugs⁷⁹, oncolytic viruses⁸⁰, antiangiogenic agents⁸¹, proapoptotic proteins⁸² and growth factor antagonists⁸³, in order to target the tumor mass.

Since the safety of MSCs carrying potential adverse molecules remains uncertain, recently a system that controls their growth and survival has been developed. It consists in a suicide system based on an inducible caspase-9 protein that is activated using a specific chemical inducer of dimerization (CID), which induces death within 24 hours after exposure. So, once administrated, CID provokes rapidly the death of MSCs⁸⁴. This safety mechanisms may allow extensive use of genetically engineered MSCs [Figure 1.3.2]⁸⁵.

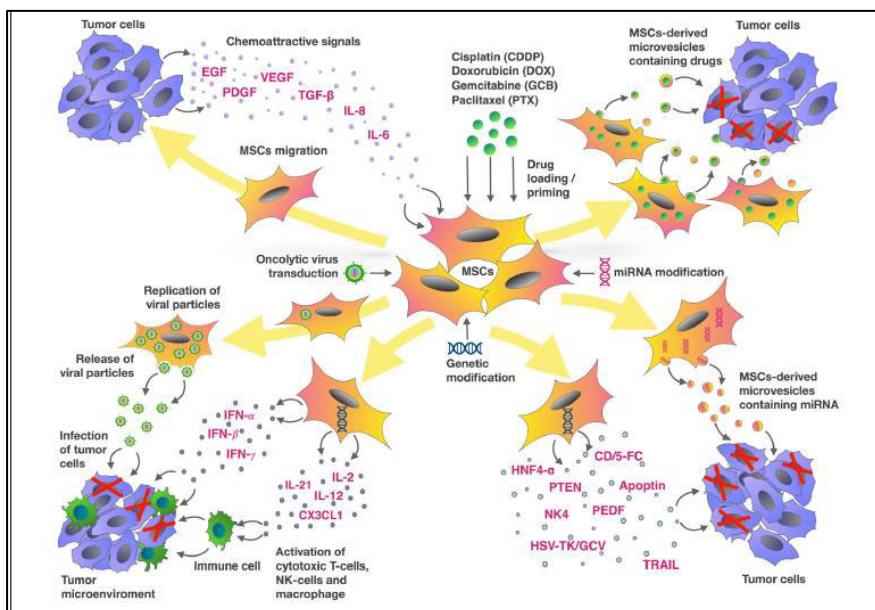


Figure 1.3.2 Mesenchymal stem cells in cancer therapy

Chulpanova DS, Kitaeva K V., Tazetdinova LG, James V, Rizvanov AA, Solovyeva V V. *Front Pharmacol.* 2018;9:259

1.4. General features of cellular senescence in mesenchymal stem cells

The low number of available MSCs requires their *ex vivo* expansion prior to clinical use⁸⁶. However, during their *in vitro* culture, MSCs quickly reach replicative senescence⁸⁷. Cellular senescence is a permanent state of cell cycle arrest that can also contribute to the decline of the regenerative potential^{88,89}.

Originally, cellular senescence was defined as a loss of replicative capacity⁹⁰ caused by a progressive shortening of the tandem repeats protecting chromosome ends, eventually leading to chromosomal damage and replicative arrest⁹¹. More recently was discovered that it can also be induced by stress⁹² and oncogenes⁹³, demonstrating that cellular senescence is not only caused by exhaustion of replicative capacity as first thought.

The senescence phenotype is often characterized by the activation of a chronic DNA damage response (DDR) and the engagement of various cyclin-dependent kinase inhibitors (CDKi) like p16 and p21 that lead to cell cycle arrest. In particular, p16 directly interacts and inhibits CDK4/6, while p21 is able to inhibit a range of CDKs but, paradoxically, is also necessary for cell cycle progression. Although p21 can be upregulated in response to different senescence-inducing stimuli, its expression is part

of a more generic DDR mainly controlled by direct transactivation *via* p53, even if it can also be activated in a p53-independent manner⁹⁴.

Furthermore, senescent cells can show enhanced secretion of proinflammatory and tissue-remodelling factors, induction of antiapoptotic genes, altered metabolic rates and endoplasmic reticulum (ER) stress. Because of these signalling pathways, senescent cells show also structural aberrations⁹⁴. In fact, senescent MSCs usually become flat and hypertrophic with altered nuclei and granular cytoplasm resulting from accumulation of cell debris, enrichment in lysosomes (higher expression of lysosomal β -galactosidase enzyme) and mitochondria

Understanding the molecular processes controlling stem cell survival, self-renewal, quiescence, proliferative expansion and commitment to specific differentiated cell lineages is essential to determine the drivers and effectors of age-associated stem cell dysfunction.

Furthermore, such knowledge will help the development of therapeutic interventions that can slow age-related degenerative changes, in turn enhancing repair processes and maintaining healthy function in aging tissues but also will improve their manipulation methods used in regenerative medicine.

For sure, different mechanisms are involved into stem cell aging and include the accumulation of toxic metabolites like reactive oxygen species (ROS) that can be responsible of DNA and proteins damage, mitochondrial dysfunction, proliferative exhaustion, extracellular signalling and epigenetic remodelling [Figure 1.4.1]⁹⁵.

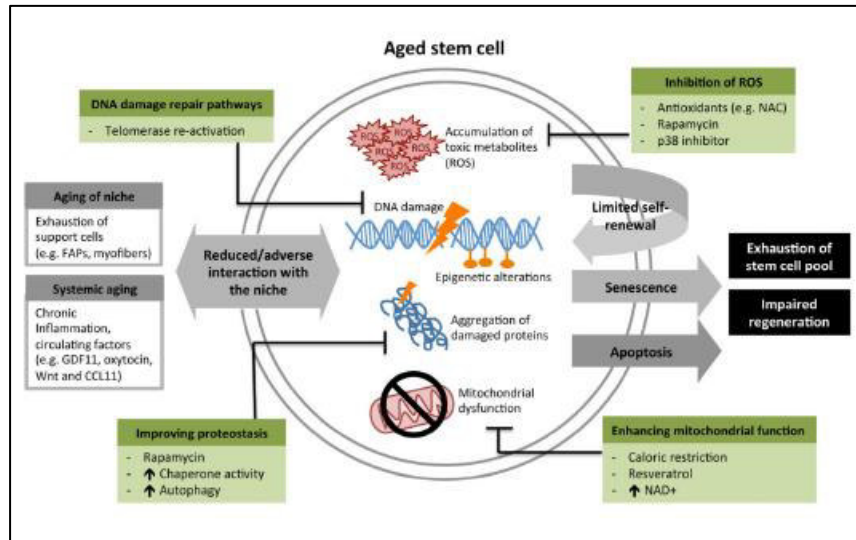


Figure 1.4.1 Mechanisms involved into stem cells aging and possible interventions
Oh J, Lee YD, Wagers AJ.. *Nat Med.* 2014;20(8):870-880

1.5. Reactive oxygen species and stem cells aging

The free radical theory of aging, first proposed in 1956, postulates that the production of intracellular ROS is the major determinant of lifespan⁹⁶. Free radicals are unstable molecules that have an unpaired electron, including nitric oxide (NO), several of the reactive oxygen species (ROS), and their reactive products. ROS include superoxide anions (O_2^-), hydrogen peroxide (H_2O_2) and hydroxyl radicals (OH^\bullet). Most of these molecules are generated by the mitochondrial respiratory chain⁹⁷, but other very important sources are NADPH Nox family of oxidases⁹⁸. Moreover, also extrinsic factors (radiation, ultraviolet light and growth factors) cause ROS production.

An appropriate balance between self-renewal and differentiation is crucial for stem cell function during both early development and adult life: recent studies suggest that this balance is partly regulated by ROS⁹⁹ [Figure 1.5.1]¹⁰⁰.

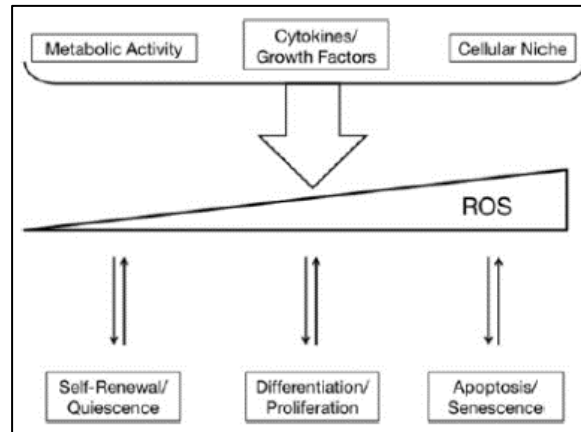


Figure 1.5.1 ROS levels regulate stem cells biology

Liang R, Ghaffari S. *Antioxid Redox Signal.* 2014;20(12):1902.

ROS are thought to be involved in many biological processes including gene transcription, protein translation, protein-protein interaction and, furthermore, they can function as cellular signalling molecules involved in the maintenance of stem cells homeostasis¹⁰¹. In particular, oxidative stress is known to play an important role in modulating different stem cells properties, such as self-renewal, proliferation, differentiation and senescence¹⁰². For example, the metabolic shift observed during stem cell commitment leads to increased ROS levels, which are intrinsically linked to the differentiation stage of stem cells, whereas low levels of ROS are reported to enhance MSCs proliferation and migration⁸⁷.

As well as a role in redox regulation, ROS might also function to modify the epigenetic landscape, which plays a particularly pertinent role in regulating stem cell fate¹⁰³.

Under physiological conditions ROS levels are finely controlled by specific enzymatic and non-enzymatic mechanisms that protect cells against oxidative stress. The excessive generation of endogenous ROS and the imbalance between ROS and antioxidant systems, as well as the culture of stem cells with various extracellular sources of ROS, can lead to oxidative stress.

Furthermore, regulation of oxidative metabolism has been linked to stem cell aging through sirtuin family of NAD-dependent protein deacetylases, which are important regulators of oxidative stress, aging and stem cell function. For example, recent findings suggest a role for SIRT1 in maintaining mesenchymal stem cell growth and differentiation and its expression it has been found declining with aging^{104,105}. Another

member of the sirtuin family, SIRT3, is critical for the maintenance of mitochondrial metabolism and it controls ROS production¹⁰⁶.

Different pathways and genes are activated in oxidative stress conditions. For example, ataxia telangiectasia mutated (ATM) serine threonine protein kinase is a critical enzyme in the regulation of the stress response to DNA damage, specifically double-strand DNA breaks. Loss-of-function mutations in ATM are indeed associated with MSC senescence¹⁰⁷.

Another critical regulator of stress response is PI3K/Akt/mTOR/FOXO3 signalling pathway. It is reported that in presence of high levels of ROS, FOXO3 expression is activated, while its inhibition results in fewer apoptotic cells and better viability¹⁰⁸. Moreover, the p38/MAPK signalling is also responsible for establishing an irreversible ROS-induced MSC senescence, while its suppression results in partial prevention¹⁰⁹.

If all the protective mechanisms fail, the ongoing oxidative process leads to DNA damage, protein damage and mitochondrial dysfunction [Figure 1.5.2]¹.

Defects in proteostasis commonly lead to aberrant folding, toxic aggregation and accumulation of damaged proteins, which can in turn cause cellular damage and tissue dysfunction¹¹⁰. In brief, ROS accumulation in MSCs contributes to the loss of homeostasis, eventually driving to senescence¹¹¹.

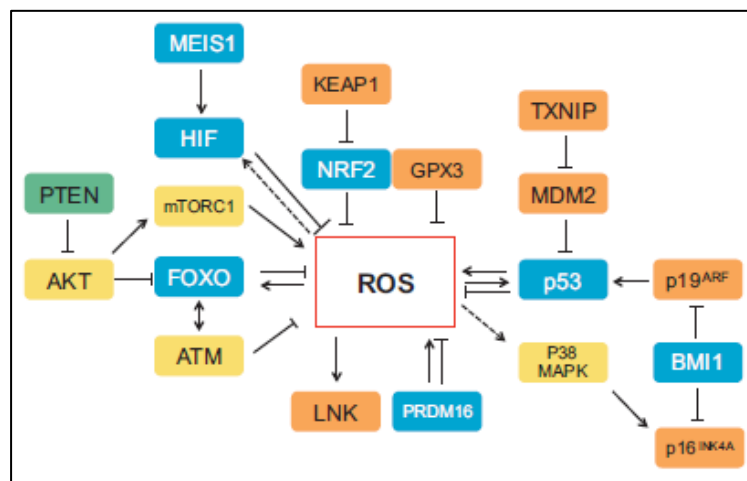


Figure 1.5.2 Redox sensor molecules

Bigarella CL, Liang R, Ghaffari S. *Development*. 2014;141(22):4206-4218

1.6. NADPH oxidase 4 (NOX4) and its role in stem cell biology

NADPH oxidase 4 (Nox4) is a membrane-associated enzyme that catalyzes the reduction of oxygen using NADPH as an electron donor producing superoxide and hydrogen peroxide through a single electron reduction. The electron travels from NADPH down an electrochemical gradient first to flavin adenine dinucleotide (FAD), then through the Nox heme groups and finally across the membrane to oxygen¹¹².

The human Nox4 gene is located on chromosome 11q14.2-q21¹¹³ and produces a protein of 66.5 kDa¹¹⁴.

Like other members of Nox family, Nox4 is composed of six α -membrane-spanning helices linked by five loops (A-E) and a dehydrogenase (DH) domain which contains the binding sites for both prosthetic groups FAD and NADPH as a relatively long cytoplasmic C-terminus^{115,116} [Figure 1.6.1]¹¹⁷.

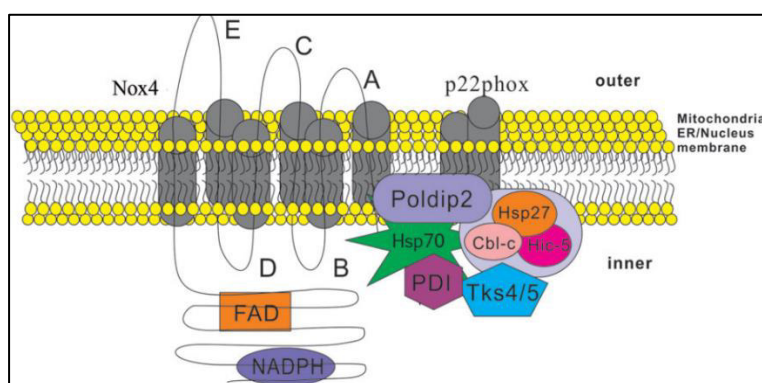


Figure 1.6.1 Schematic representation of NOX4 enzyme and its regulator partners

Guo S, Chen X. *J Drug Target*. 2015;23(10):888-896

Originally called Renox, Nox4 was discovered in the kidney¹¹⁸ but soon after it was found in focal adhesions¹¹⁹, nucleus¹²⁰, endoplasmic reticulum¹²¹, mitochondria¹²², cytoskeleton¹¹⁹, plasma membrane¹²³.

The role of Nox4 in cell proliferation has been well documented in recent observations. Nox4 regulates cell proliferation in multiple cell types such as embryonic stem cells¹²⁴, endothelial cells¹²⁵, human pulmonary artery smooth muscle cells¹²⁶, pulmonary artery adventitial fibroblasts^{127,126}, skeletal muscle precursor cells¹²⁸, preadipocytes¹²⁹, gliomas cell¹³⁰s and hepatocytes¹³¹. However, the underlying mechanisms are cell type specific.

For example, low level of Nox4-derived ROS activates mitogen-activated protein kinase (MAPK) family members including p38/MAPK, ERK and JNK/SAP kinases in endothelial cells¹¹⁷. In human pulmonary artery smooth muscle cells (HPASMC), Nox4 induces proliferation through TGF/Smad2/3 axis¹²⁶. Furthermore, there is evidence that Nox4 functionally has a role in non-small cell lung cancer (NSCLC) proliferation and invasion by interplaying with PI3K/Akt signalling¹³².

Peculiar is Nox4 role in amniotic fluid stem cells. A recent study showed that Nox4 can be found both into the cytoplasm and the nucleus of these cells, in the latter localizing with a spot distribution preferably into speckles domains¹³³. Speckles are subnuclear structures located in the interchromatin regions and enriched in both transcription factors and pre-messenger RNA splicing factors¹³⁴. It has been shown that Nox4 colocalizes with Oct4, an essential player in the maintenance of pluripotency, suggesting that this enzyme could be involved in the regulation of the transcription/pre-mRNA processing machinery by ROS production in the speckle structures. Moreover, AFSC seem to exhibit a proliferation rate inversely coupled with Nox4-derived ROS level into the nuclei accompanied by a higher DNA damage, indicating that nNox4 regulation may have important pathophysiologic effects in stem biology through modulation of nuclear signalling and DNA damage¹³³.

In fact, these data are also supported by evidences showing that inhibition of Nox4 activity reduces nuclear ROS, DNA damage and the binding between nNox4 nucleoskeleton components, improving the proliferation rate of amniotic stem cells¹³⁵. Another study investigated Nox4 role in MSCs adipocyte differentiation¹³⁶, finding that ROS scavengers or RNA interference against Nox4 impair adipocyte differentiation. In fact, it is known that CREB, an important gene induced during the adipogenesis, is activated by ROS in this differentiation pathway¹³⁷. Besides, it seems that Nox4 is downregulated after the induction of differentiation and so in mature adipocytes¹²⁹.

It is still debated the role of Nox proteins as oxygen sensors. For sure ROS take part in the hypoxia response, however the source or sources of ROS are disputed. *In vitro* studies demonstrated that Nox enzymes are less active in hypoxia¹³⁸, but *in vivo* it seems that ROS production increases in low oxygen to activate the hypoxia inducible factor-1 (HIF-1)¹³⁹ and redox sensitive K⁺ channels¹⁴⁰. Despite all, overall mechanisms are still not well understood.

Regulation of Nox4 protein expression is not clear as well. It is suggested that Nox4 is regulated by different transcriptional factors and some microRNAs such as microRNA-25¹⁴¹ and microRNA 21a-3¹⁴² more at transcriptional level rather than at protein complex assembly or by post-translational protein modifications.

Various transcription factors have been implicated in Nox4 modulation, including E2F, Nrf2, HIF-NF, Oct1, Sp3 and Sp1, c-Jun, STAT3, with a common molecular mechanism of binding to a specific position of Nox4 DNA promoter¹¹⁷.

Nevertheless, several regulatory proteins were found to regulate the enzyme. For example, protein disulfide isomerase (PDI), a chaperone of the thioredoxin superfamily, positively regulates Nox4 activity by controlling subunit traffic and assembling in VSMC¹⁴³. Polymerase- δ -interacting protein 2 (Poldip2) also can activate Nox4 by interacting with p22^{phox}, a factor which is associated to the protein complex¹⁴⁴. In addition, Tks4/5 has been reported to associate to p22^{phox} and activate Nox4¹⁴⁵. Negative regulation is achieved by Hsp70¹⁴⁶ and TGF-induced H₂O₂-inducible clone-5 (Hic-5), this one working at post-translational level by promoting the ubiquitin-proteasomal system-mediated degradation of Nox4¹⁴⁷.

For sure, we need more information on how this enzyme is targeted to different subcellular compartments and how this transport process is regulated.

Only once we will understand all the events that regulate Nox4 activation and their full impact on signalling pathways and cellular functions, it will be possible to take advantage of this knowledge to create new therapeutic tools targeting this protein.

1.7. Lamins as mediators of oxidative stress and their role in aging

The nucleus is a discrete organelle containing the genome and delimited by membranes known as nuclear envelope (NE). Different studies demonstrated that NE is a specialized cisterna of endoplasmic reticulum (ER), separating the nucleus from cytoplasm and it is made of two distinct membrane domains interconnected through nuclear pore complexes (NPC). The outer nuclear membrane (ONM) has several ER characteristics and functions (for example, ribosome-linked synthesis, post-translational processing of proteins.), while the inner nuclear membrane (INM) contains about 80 specific transmembrane proteins¹⁴⁸.

Besides nuclear genome and all the enzymatic and non-enzymatic machinery required for nuclear genome functions, the nucleoplasm contains also a protein network called nuclear matrix (NM), whose peripheral region is known as nuclear lamina¹⁴⁹. The lamina interacts with INM proteins, nucleoplasmic domains and peripheral chromatin¹⁵⁰.

Lamins are a family of nuclear proteins belonging to the V type intermediate filaments¹⁵¹. Humans have two types of lamins, types A and B. In particular, A-type lamins (lamin A and C) are produced by alternative splicing from the LMNA gene, while B-type lamins (lamins B1 and B2) are encoded by LMNB1 and LMNB2 genes respectively¹⁵². In general lamins exhibit 4 distinct structural domains^{153–155} [Figure 1.7.1]¹⁵⁶.

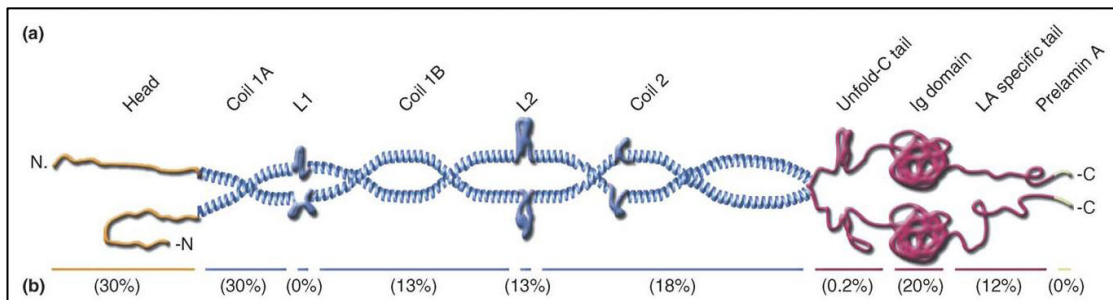


Figure 1.7.1 Schematic representation of lamin A dimer structure

Mattout A, Dechat T, Adam SA, Goldman RD, Gruenbaum Y. *Curr Opin Cell Biol.* 2006;18(3):335-341

Lamins A, B1 and B2 are produced as cytosolic precursors, prelamins, that undergo post-translational processing involving their C-terminal CAAX box, while lamin C is synthesized as a mature protein. The initial three steps are common to A- and B-type prelamins. First, the C-terminal cysteine is farnesylated by farnesyltransferase: the 15-carbon hydrophobic farnesyl group facilitates the prelamins insertion and anchoring into the cytosolic side of ER membrane (or of the ONM), thus allowing the further processing steps completed by specific ER (or ONM) enzymes. The second step requires the cutting of the AAX motif performed by one of the two proteases, FACE1/ZMPSTE24 or FACE2/Rce1. The third step is the carboxymethylation of the cysteine residue by the isoprenyl-cysteine-carboxy-methyltransferase (ICMT).

The processing of B-type lamins ends at this third stage, leading to the permanent farnesylation and carboxymethylation of mature B-type lamins. Differently, prelamins

A undergoes a fourth last proteolytic cleavage by FACE1/ZMPSTE24 that removes the 15 C-terminal aminoacids, including the farnesylated carboxymethylated cysteine residue, driving to the mature lamin A¹⁵⁷ [Figure 1.7.2]^{158,159}.

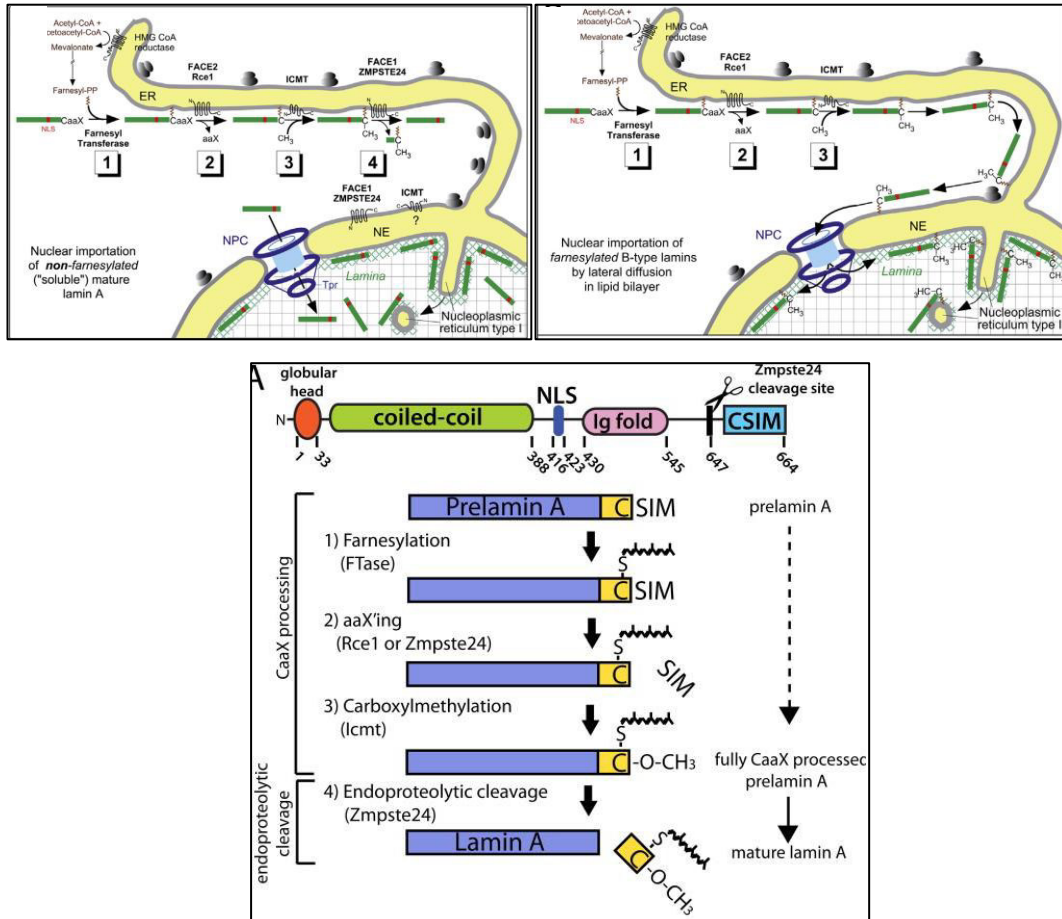


Figure 1.7.2 Lamins processing. A) Lamin A processing in 4 steps and its nuclear import. B) Lamin B processing in 3 steps and its nuclear import. C) Detailed schematic representation of processing steps and enzymes involved in the conversion of prelamins A in the mature lamin A

Cau P, Navarro C, Harhour K, et al. *Semin Cell Dev Biol.* 2014;29:125-147.

Barrowman J, Hamblet C, George CM, Michaelis S, Wente SR, ed. *Mol Biol Cell.* 2008;19(12):5398-5408

The presence or the lack of the farnesyl group influences the nucleoplasmic localization of lamins. In particular, farnesylated B-type lamins are anchored to INM in the nuclear lamina, even if they can be also detected at distance from it in the perinucleolar nucleoplasm. Lamins A and C are localized in nuclear lamina, where they interact together, with B-type lamins and with several INM and NPC proteins, but they are also distributed throughout the nucleoplasm¹⁵⁸.

In addition to this post translational processing, lamins can be interested by other modifications. For example, phosphorylation of lamins and their partners has been shown to be important for NE breakdown at the beginning of mitosis¹⁶⁰, while it has been reported that serine 301 and 404 of lamin A and C are substrates for Akt kinase¹⁶¹, activated by several signalling pathways. Furthermore, phosphorylation at position 404 leads to prelamin A autophagic degradation¹⁶².

As several other nuclear proteins such as histones, A- and B- type lamins have been shown to be acetylated on lysine residues¹⁶³ even if the significance of this modification remains unclear.

Lamin A can be also ubiquitylated on 25 lysine residue and targeted to proteasomal degradation¹⁶⁴.

In fact, it is known that the nucleus contains all the enzymatic machinery involved in regulating the fate of nuclear proteins through their balanced ubiquitylation–deubiquitylation¹⁶⁵ and sumoylation–desumoylation modifications¹⁶⁶.

In various laminopathies several ubiquitin-ligases and increase proteasomal degradation of proteins within nucleus can be activated¹⁶⁷.

Mass spectrometry experiments evidenced that A- and B-type lamins can be sumoylated, which represents another covalent and reversible lysine modification¹⁶⁸, as I will explain in detail later. In particular, binding of SUMO1 leads to mono-sumoylation, whereas binding of SUMO2 and SUMO3 results in chains of 4–7 molecules in length¹⁶⁹.

Lamins are an important component of the nucleus, because they create a framework that protects genetic material from mechanical insults, regulating at the same time shape, size and location of the nucleus. They also contribute to the correct localization of pore complexes and connect the nuclear skeleton to the of cytoskeleton.

Besides providing a structural framework to nucleoplasm¹⁵⁷, lamins play important roles in epigenetics, chromatin organization, DNA replication and repair, transcription, and their dynamics. In fact, they interact with DNA and DNA proteins, such as histones, controlling the formation of heterochromatin¹⁵⁸.

Other functions involve signal transduction, cell cycle control, apoptosis, cell differentiation, carcinogenesis, probably taking part in this way in physiological aging¹⁷⁰.

Recent data have shown a relationship between lamins mutations and altered ROS metabolism. Both A-type and B-type lamins show a double function both as sensors and inducers of oxidative stress. In particular, accumulation of the farnesylated form of prelamin A seems to induce excessive ROS and thus protein oxidation¹⁷¹. In general, reduction of mature lamin A and the presence of aberrant prelamin isoforms also alter the levels of antioxidant enzymes¹⁷¹. On the other side, oxidative stress also affects lamin structure. Oxidation of conserved cysteine residues in the tail domain of mature lamin A appears to perturb its function and promote cellular senescence and susceptibility to ROS¹⁷².

It has been suggested that lamin A can be oxidized acting as a ROS-sink inside the nucleus, protecting other more critical proteins from transient, mild oxidative damage¹⁷². This has also been reported for other abundant structural proteins inside the cytosol like actin¹⁷³. However, lamins can only buffer up to a certain critical level, while if the oxidative stress is chronic or highly acute the lamina oxidation becomes irreversible, leading to a dysfunctional lamina¹⁷² [Figure 1.7.3]¹⁷¹.

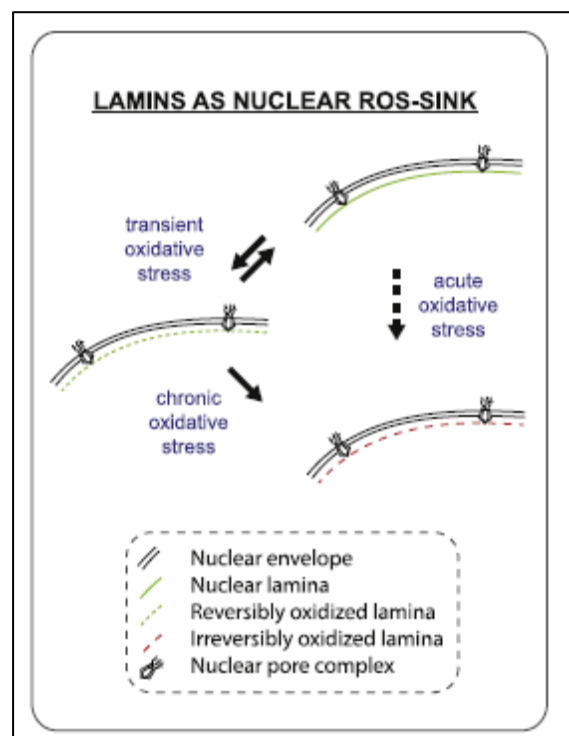


Figure 1.7.3 Lamins as nuclear ROS-sink

Sieprath T, Darwiche R, De Vos WH. *Biochem Biophys Res Commun.* 2012;421(4):635-639

Although, there are many indications for a link between a dysfunctional lamina and disturbed redox biology, the underlying pathways are still poorly understood.

A dysfunctional lamina, innate or acquired, may influence ROS in several ways. It is known that the lamina works as a docking station inside the nucleus but also as a mechanical connection between the nucleus and cytoskeleton. Into the nucleus this docking function results in gene regulation¹⁷⁴, either by direct interactions with chromatin or transcriptional complexes or indirect *via* interaction with transcription factors. As for direct interactions, lamins play a key role in intranuclear positioning and compaction of chromosomal domains¹⁷⁵. This may induce activation of repressed genes and alter DNA binding of transcription factors and regulatory proteins. For example, it has been shown that in HeLa cells expressing different disease inducing LMNA mutations, DNA damage repair is perturbed due to incorrect localization of ATR¹⁷⁶. It is thought that this mislocalization is caused by altered lamin-chromatin interactions.

Furthermore, reversible associations of lamins with a multitude of redox-responsive transcription factors including Rb, SREBP1 and Oct1 have been reported¹⁷⁷. In lamin B deficient mouse embryonic stem cells (MEFs), the transcription factor Oct1, is no longer properly sequestered at the nuclear lamina. This leads to an increase of free Oct1 inside the nucleus and higher expression of genes that are involved in oxidative stress response, like GPX3, IL-6 and SOD1¹⁷⁸. On the contrary, in LMNA knockout MEFs as well as in lamin A/C deficient patient cells (Y259X/Y259X), repetitive ruptures of the nuclear membrane cause translocation of nuclear Oct1 from nucleus to cytoplasm, resulting in opposite downstream effects compared to the lamin B deficient cells¹⁷⁹.

Recently, it has been hypothesized the presence of a nuclear shield, in which ROS antioxidant enzymes like CAT, GPX and GST are highly present, up to seven times higher than in the cytosol. The role of this shield could be the protection of the nuclear DNA against oxidative stress¹⁸⁰. Nesprin 1 and 2 seem to be essential proteins for the assembly¹⁷⁴ of this shield and it has also been reported that absence of normal and/or presence of mutant lamin A can disturb the proper localization of nesprin 2, triggering to a local decline of antioxidants around the nucleus which could result in a higher susceptibility to oxidative stress¹⁸¹.

As briefly mentioned before, next to a perturbed docking function, a dysfunctional lamina can also cause repetitive and transient disruptions of the nuclear envelope¹⁷⁹.

This determine an intermixing of cytoplasmic and nuclear components, ranging from small diffusible molecules such as transcription factors, to large macromolecular complexes, such as PML bodies and mitochondria.

Mitochondria are not the only ROS sources that could become displaced, but also NADPH oxidase 4, has been shown to colocalize with lamin A/C, especially after hepatitis C virus infection^{182,183} [Figure 1.7.4]¹⁷¹.

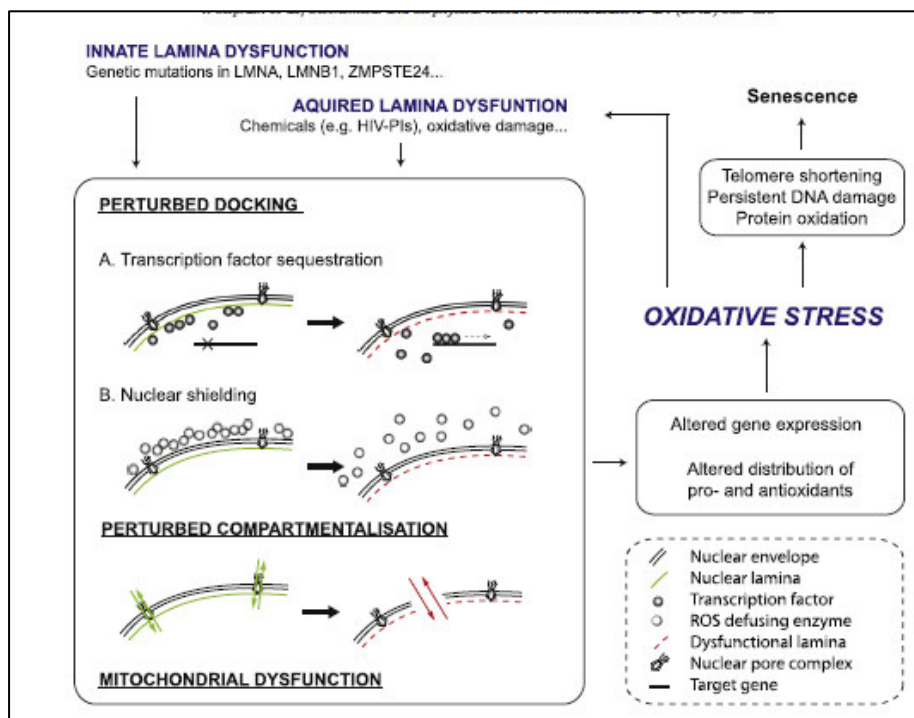


Figure 1.7.4 Cross-talk between lamins and oxidative stress

Sieprath T, Darwiche R, De Vos WH. *Biochem Biophys Res Commun.* 2012;421(4):635-639

In recent years, the composition of the nuclear envelope has become of interest for researchers involved in aging studies.

In fact, mutations in lamins and lamin-associated proteins provoke human diseases termed laminopathies¹⁸⁴. LMNA mutations can affect striated muscle, causing muscular dystrophies and dilated cardiomyopathy; muscle and neurons in Charcot-Marie-Tooth disorder; adipose tissue in lipodystrophy; adipocytes and bone in mandibuloacral dysplasia (MAD).

However, the most striking phenotypes caused by mutations in LMNA are seen in Hutchinson–Gilford progeria syndrome (HGPS), atypical Werner syndrome (WS), and

restrictive dermopathy (RD¹⁸⁵). In particular, most cases of HGPS are caused by a dominant 1824C>T mutation in LMNA that leads to the production of an incompletely processed, stably farnesylated lamin A precursor with a 50-amino-acid internal deletion (also called progerin).

Progerin accumulates in the cellular nuclei of HGPS patients resulting in premature aging. At the cellular level, accumulation of farnesylated prelamin A is associated with nuclear enlargement, heterochromatin loss and euchromatin dispersion, increase in ROS¹⁸⁶ and activation of the p53 pathway¹⁸⁷.

Recently, more interest has been developed in the analysis of prelamin A role in normal aging. In particular, it has been demonstrated that while the accumulation of either mutated or wild-type prelamin A in young or very young individuals induces deleterious effects bringing to cellular senescence and, in some cases, to serious diseases like laminopathies, on the contrary an appropriate accumulation of proper levels of prelamin A might help centenarian cells to survive at long-lasting stress stimuli through modulation of chromatin arrangement and availability of the DNA-repair machinery¹⁸⁸. In fact, as previously reported, lamin A appears to be involved both in the nuclear response to stress and in the reduction of stress stimuli¹⁸⁶ and could act in this contest as a protective structure against ROS at the nuclear level.

Further investigations are for sure necessary to clarify lamins/ prelamin A role in healthy aging and in cellular senescence.

1.8. Role of PML bodies and sumoylation in stress response and senescence

PML nuclear bodies (NBs) are discrete nuclear foci of 0.1–1.0 µm in diameter present in many tissues¹⁸⁹. They are proposed to anchor and regulate not only many nuclear functions, including DNA replication, transcription, epigenetic silencing, genome stability, but in general various cellular activities, such as resistance to oxidative stress, inhibition of proliferation, regulation of stem cell self-renewal, induction of apoptosis and cellular senescence^{189,190} [Figure 1.8.1]¹⁹¹. All these functions are probably accomplished by the numerous proteins that reside constitutively, but more often transiently, in these structures¹⁹².

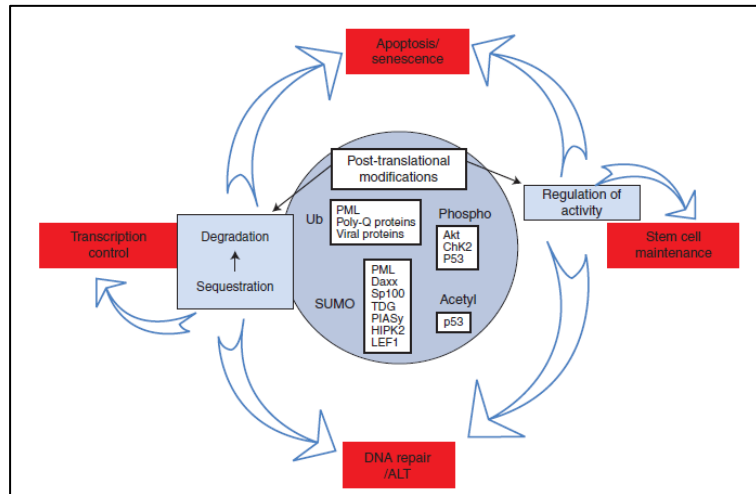


Figure 1.8.1 Mechanisms involving PML bodies

Lallemant-Breitenbach V, de Thé H. *Cold Spring Harb Perspect Biol.* 2010;2(5):a000661

Electron microscopy has displayed that PML-NBs are composed of a ring-like protein structure, which major component is the PML protein, that do not contain detectable nucleic acids inside^{193,194}. At the periphery of the ring, however, PML-NBs make extensive contacts with chromatin fibres, which contribute to maintain the integrity and position of PML-NBs inside the nucleus¹⁹⁵.

Furthermore, it has been demonstrated that some PML-NBs can also localize near other nuclear bodies, such as Cajal bodies, splicing speckles and nucleoli¹⁹⁶.

In normal tissues, the expression level of PML is dependent on the tissue and cell type, as well as the differentiation and activation stage^{197,198}.

Despite varying PML steady-state levels, in most cell types the number and size of PML-NBs increase in response to soluble factors and cellular stress¹⁹².

In fact, for example, PML promoter contains interferon (IFN) and p53 response elements and can be induced by IFN signaling¹⁹⁹ or p53 activation²⁰⁰ and become critical in senescence induction. It has also demonstrated that genotoxic drug induced-senescence increases PML transcription through JAK1/STAT1 pathway²⁰¹ and IFN production²⁰², this one known to be part of the senescence-associated secretory phenotype (SASP).

Apart from transcription regulation, in recent years new insights about post-translational modification of PML have been also revealed.

In particular, nowadays it is known that PML protein is phosphorylated on Tyr and Ser

residues²⁰³. For instance, among the kinases, the extracellular mitogen activated kinase ERK has been shown to phosphorylate PML at several residues²⁰⁴. This phosphorylation induces modification of PML by the small ubiquitin-like modifier (SUMO) and apoptosis following treatment with arsenic trioxide²⁰⁴.

Moreover, following DNA damage, PML is phosphorylated by at least two kinases, ATR²⁰⁵ and CHK2²⁰⁶. It seems that phosphorylation of PML by ATR induces PML translocation to the nucleolus followed by sequestration of MDM2, a regulator of p53 stability. Differently, phosphorylation by CHK2 is suggested to trigger PML-induced apoptosis.

As briefly mentioned above, PML proteins can be sumoylated. Indeed, not only PML sumoylation is involved in the formation of PML-NBs²⁰⁷, but also many proteins that localize to PML-NBs are sumoylated or contain a SUMO interaction motif (SIM)¹⁹² [Figure 1.8.2]¹⁹¹.

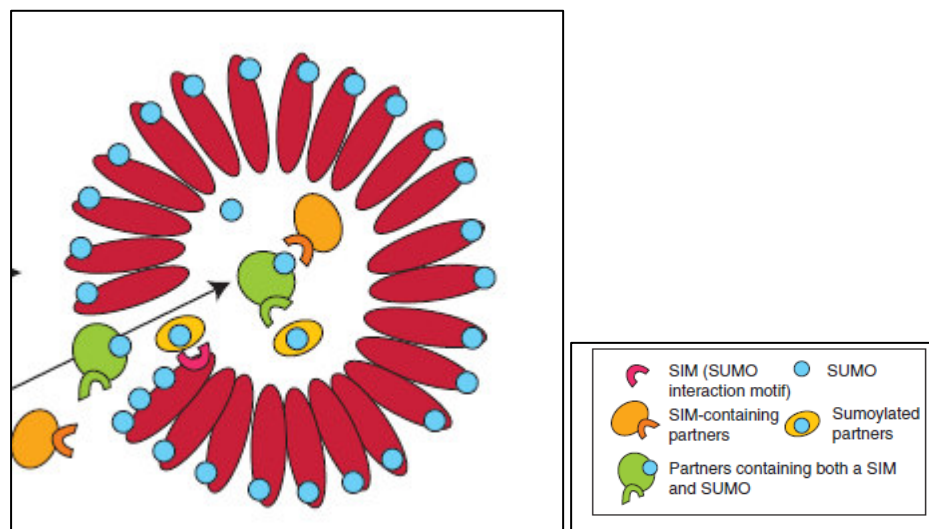


Figure 1.8.2 Schematic representation of PML bodies

Lallemand-Breitenbach V, de Thé H. *Cold Spring Harb Perspect Biol.* 2010;2(5):a000661

Sumoylation is a post-translational modification consisting of covalent binding of Small Ubiquitin related Modifier (SUMO) to a target protein. SUMO belongs to the ubiquitin-like protein (Ubl) family and in fact it has a very similar three-dimensional structure compared to ubiquitin, even if it shares only 20% of sequence.

SUMO can be found in four different isoforms, with SUMO-1 sharing 50% sequence identity with SUMO-2/3, and 86% with SUMO-4²⁰⁸.

Sumoylation is a dynamic process consisting of rapid conjugation and de-conjugation cycles, performed by specific enzymes in three steps that terminate with the bond of SUMO onto lysine residues of target proteins, within a ψ KX(D/E) consensus motif, where ψ is a large hydrophobic residue^{209,210}.

SUMO may be removed from their targets by SENP enzymes, the same family of proteases that performs SUMO maturation²¹¹ [Figure 1.8.3]²¹².

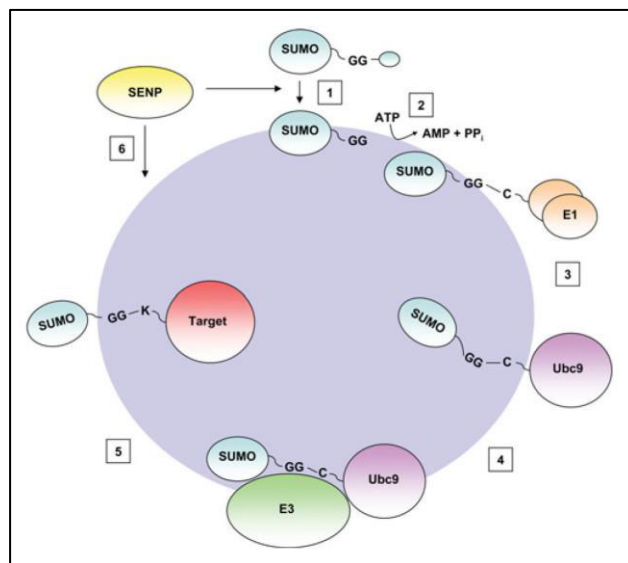


Figure 1.8.3 Sumoylation process step by step

Wilkinson KA, Henley JM. *Biochem J.* 2010;428(2):133-145

It has been shown that sumoylation can be achieved not only by covalent bonds that involved SUMO-consensus motifs present inside the target protein, but it can be also realized through non-covalent interactions that are accomplished *via* SUMO-interacting motifs (SIM)²¹³, sequences found more and more often in an increasing number of proteins. The SIMs generally comprise a hydrophobic core surrounded by acidic flanking residues or phosphorylatable serine residues²¹⁴.

Sumoylation can alter protein–protein interactions, change protein intracellular localization, or directly modify activities resulting in changes in transcription, replication, chromosome segregation and DNA repair. Importantly, SUMO conjugation has been repeatedly associated to stress response²⁰⁸.

For example, one of the main regulators of cellular senescence, p53, can be modified

by SUMO-1²¹⁵ and SUMO-2/3²¹⁶ on the same lysine residue (K386). While SUMO-1 is attached to p53 under normal conditions, SUMO-2/3 binds p53 under oxidative stress conditions, in a tissue specific manner. The interesting data is that sumoylation of p53 takes place in PML NBs, stressing the idea that PML bodies-p53 pathway-sumoylation and senescence are interconnected and cross-regulated.

Also SIRT1 can be sumoylated and interacts with PML NBs *via* its SIM, stabilizing their structure and function²¹⁷.

Finally, SUMO modification participates in cellular senescence through modulation of oxidative stress responses.

The first connection between sumoylation and ROS was established in 2008 when it was reported that the TNF-induced nuclear translocation of SENP1 is ROS dependent²¹⁸.

Nevertheless, SUMO1 is not only responsive to ROS but also it plays a role in ROS production. In fact, upon heat shock, NADPH oxidase 2 is sumoylated and downregulated, thus protecting the cell from oxidative stress-induced death²¹⁹, while another study showed that inhibition of sumoylation negatively regulates all the isoforms of NADPH oxidase (from one to five)²²⁰.

Interestingly, the fact that also PML is sensitive to oxidative stress, through the formation of disulphide bridges that induce NB biogenesis²²¹, suggests that they could contribute to stress- induced sumoylation and cooperate to promote senescence.

For example, a recent study proposes that PML-NBs might be involved in progerin accumulation and degradation, since they contain proteasome and ubiquitinated proteins. Indeed, they showed that progerin is sequestered into PML-NBs within ring-like and thread-like structures after its sumoylation. Furthermore, they demonstrated that proteasome inhibition can induce mis-localization of progerin from PML into the nucleolus, followed by degradation through an alternative autophagy pathway.

Taken together, all these evidences suggest that further investigation should be carried out to make a point about the cross-talk between PML bodies, sumoylation and senescence induction²²² [Figure 1.8.4]²⁰⁸.

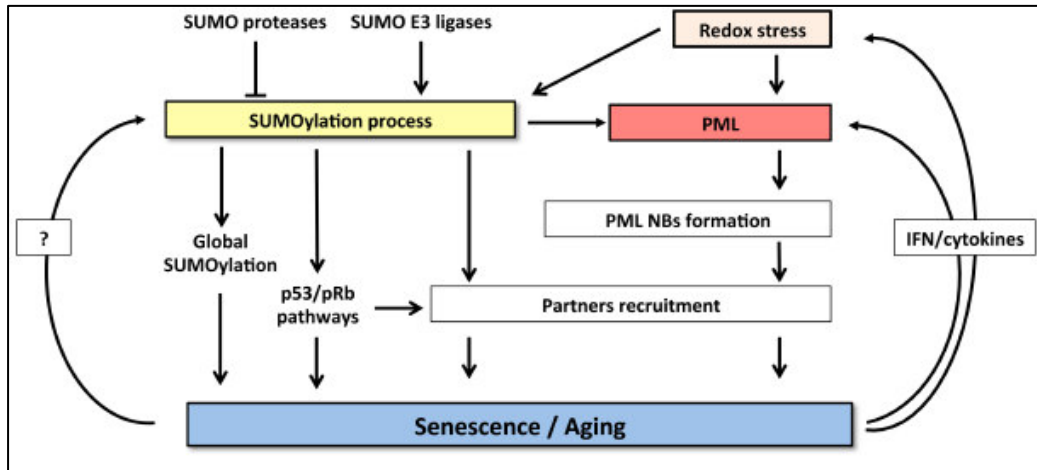


Figure 1.8.4 Cross-talk between sumoylation and PML bodies in aging
 Ivanschitz L, De Thé H, Le Bras M. *Front Oncol.* 2013;3:171

1.9. Implications of stem cells heterogeneity in *in vitro* amplification and senescence

One critical problem about MSCs research and their use in clinics regards the knowledge of their functional characteristics at the population level, which makes difficult to predict how culture expansion and exposure to extrinsic factors might alter population dynamics and function. This problem is increased by the fact that MSC populations exhibit donor-to-donor and intra-population heterogeneity²²³ [Figure 1.9.1]²²⁴.

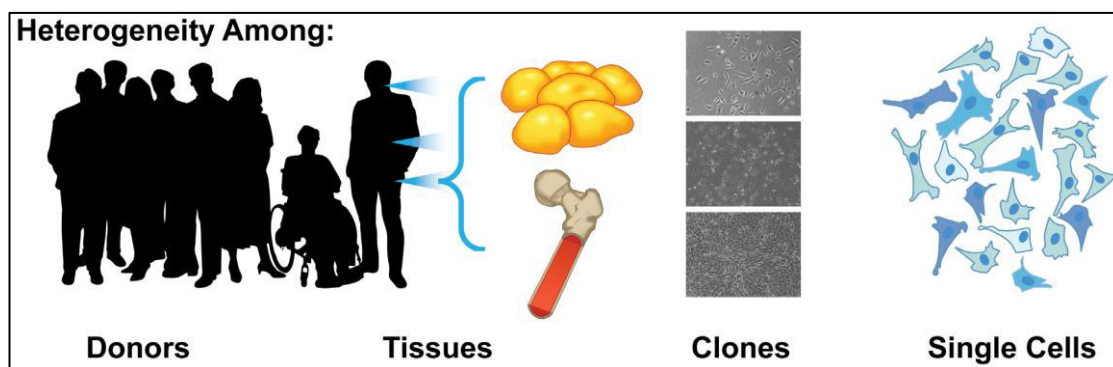


Figure 1.9.1 MSCs heterogeneity at different levels

McLeod C, Mauck R. *On the origin and impact of mesenchymal stem cell heterogeneity: new insights and emerging tools for single cell analysis.* *Eur Cells Mater.* 2017;34:217-231

In fact, even when they derive from the same tissue, MSCs show an incredible donor-to-donor variability. Of course, donors age and their health status can influence their

potential²²⁵, but surprisingly also MSCs isolated from young, healthy donors display evident differences in their proliferation rate, differentiation capacity, and in this way in their clinical utility²²⁶.

Among the other factors that could induce some inter patient variability, there are also the methods used to prepare and cultivate the samples²²³.

Moreover, various studies revealed that donor- dependent differences are in part due and explained by cell-to-cell variation within each patient population²²⁴.

In particular, cell-to-cell heterogeneity in MSC phenotype becomes evident during *in vitro* expansion where, within the same population, cells can manifest proliferative and morphological diversity, ranging from elongated spindle-like cells to large flattened cells and highly protrusive cells²²⁷.

Different processes may be responsible of culture heterogeneity. A natural inter-clonal heterogeneity is present among MSCs since their initial collection, thus faster proliferating subpopulations may overgrow others²²⁸.

Different studies have showed that fast-growing clones are usually more potent than slow-growing clones and tend to engraft better into tissues²²⁹.

In fact, for example, fast- and slow-growing MSCs differ proteomically, with differential expression of proteins including intermediate filaments (e.g. lamin A/C), calcium-binding proteins (e.g. calmodulin), and glycolytic proteins (e.g. glyceraldehyde-3-phosphate dehydrogenase)²³⁰.

Clonal heterogeneity also involves the transcriptome. Certainly, exposure to differentiation assays results in a great discrepancy in the transcriptional signature between high- and low potential clones²³¹. Similarly, undifferentiated cells display differences, in particular in the expression of genes associated with the cell cycle, cellular division²³¹, growth factors, lineage markers, self-renewal markers²²⁴, as well as in the epigenetic status of their DNA²³².

For sure by time, cultured cells can acquire mutations and stochastic defects, exacerbating this natural heterogeneity through the process of replicative senescence²²⁸. In this regard a recent study characterized senescence heterogeneity using numerous whole-transcriptome datasets showing that different transcriptome signatures are associated with different senescence programs or senescent cell type, underlining that

the senescent phenotype is dynamic and changing at varying intervals during the process²³³.

Taken together all these evidences suggest that further investigation should be conducted to better explain mechanisms causing MSC variability, in order to improve in this way their application in clinic.

1.10. Effect of hypoxia on stem cells properties

At present, most of the expansion procedures of MSCs are performed under atmospheric O₂ concentration (20% O₂), which is approximately 4–10 times higher than the concentration of O₂ in their natural niches. This higher O₂ concentration might cause environmental stress to the *in vitro* cultured MSCs, due to the increased ROS concentration⁸⁶.

In fact, following the O₂ flux into the body, the O₂ partial pressure progressively reduces from the lungs throughout the body, dropping to 1–5% when it arrives in organs and tissues²³⁴. For example, adipose stem cells have been found in a hypoxic niche with an oxygen level between 1–5%²³⁵, while the partial O₂ pressure in the amniotic cavity was measured to be around 2.3 %²³⁶.

Therefore, low oxygen tension should be considered for the culture of stem cells in scientific research, both to keep cells in their natural conditions but also to obtain more accurate data that could in this way better explain what really happens in our body.

Multiple studies have demonstrated the effect of hypoxia on different MSCs functionalities, including proliferation, differentiation, survival rate, cytokines or growth factors secretions and cell biosafety^{237–239}.

Even if it is known that generally hypoxia stimulates cell cycle arrest in mammalian cells²⁴⁰, in this case it has been shown that initially MSCs grew slower under 5% O₂ tension, acquiring a progressive growth advantage at prolonged times²⁴¹ and expressing lower levels of p21 and p53²³⁷ and higher cyclin B1²³⁴ than the normoxic condition.

Moreover, hypoxic conditions appear to increase Oct4 expression both in MSCs and in human embryonic stem cells, improving also the formation of embryoid bodies²⁴¹.

In particular, Oct4 it has been directly linked to the maintenance of stem cell properties by regulating self-renewal and reversing senescence. Oct4 achieves these functions through multiple mechanisms, as downregulating p21 by enhancing the expression of

different DNA methyltransferases²⁴². Furthermore, in embryonic stem cells it has been reported that Oct4 can bind to the promoter region of miR-302a and in this way it can induce cells in S phase cells through cyclin D1²⁴³

Also the CFU-F data support the results about proliferation observed in hypoxic hMSC constructs²⁴¹.

Several studies investigated the impact of hypoxia on MSCs differentiation, showing contrasting results^{238,244–247}. Of course, the data obtained might be influenced by different factors, such as the cellular source or the differentiation protocol used, but also for cells derived from the same tissue, results are rarely concordant. One interesting observation claims that when hypoxic-treated adipocyte stem cells are re-cultured in a normoxic condition, the inhibitory effect of hypoxia on osteogenesis and adipogenesis can be reversed²⁴⁸.

Other findings report that hypoxia (0.1–2% O₂) increases the viability of stem cells both in normal culture conditions or under the effect of stressor molecules, reducing the percentage of cells that undergo apoptosis^{239,249}. The mechanisms responsible of these results might be traced back to the activation of HIF under hypoxic conditions. In fact, HIF-1a upregulates antiapoptotic factors, as Bcl-2 and bcl-xL, downregulating the caspase-3 activation (protein involved in cell apoptosis) thus protecting MSCs from apoptosis²⁵⁰.

Furthermore, these beneficial effects could be directly modulated by the upregulated glucose metabolism through different signalling pathways, such as ERK, p38, and Akt pathways²⁵¹.

To date, hypoxic-treated bone marrow mesenchymal stem cells have been used in some clinical trials for ischemic heart disease and pulmonary emphysema²³⁴.

Based on all the available data, future work should focus on developing more defined strategies of using hypoxic-treated MSCs, also to better clarify the controversial results obtained in several research findings [Figure 1.10.1]²³⁴.

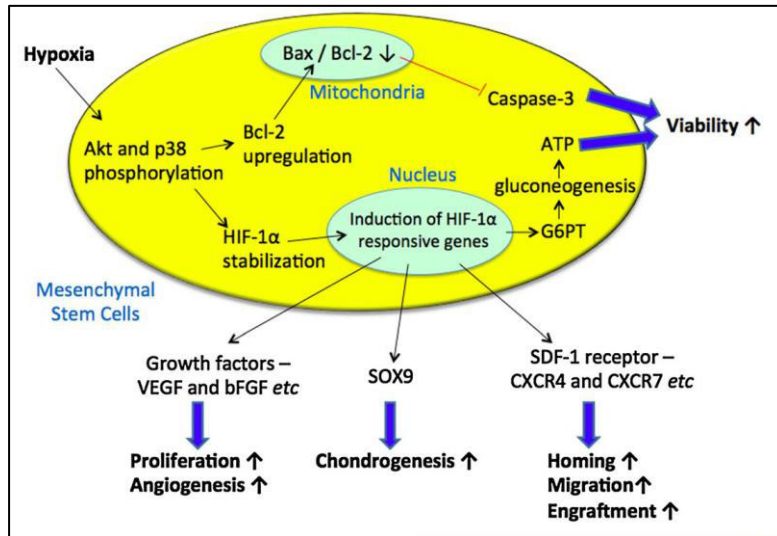


Figure 1.10.1 Possible adaptation mechanisms activated in hypoxia in mesenchymal stem cells

Choi JR, Yong KW, Wan Safwani WKZ. Cell Mol Life Sci. 2017;74(14):2587-2600

2. AIM OF THE PROJECT

Thanks to their unique properties, mesenchymal stem cells (MSCs) have emerged as a potential therapeutic approach for various disorders. The effects of MSCs treatments could be due to the combination of different factors, such as the ability to support other cell types during tissue regeneration⁵¹, the secretion of growth factors and cytokines⁵² and immunomodulation properties⁵³.

MSCs are present both in foetal and adult tissues and in the last years more interest has been developed toward amniotic fluid stem cells. What make these cells so interesting is that they show the expression of multiple pluripotent markers³⁹ and are able to differentiate into mesodermal and nonmesodermal lineages under appropriate differentiation conditions, but differently from embryonic stem cells or iPS, they do not form tumors *in vivo* and there is no evidence on their ability to form chimeras when injected into blastocysts⁴¹.

The low number of available MSCs requires their *ex vivo* expansion prior to clinical use⁸⁶. However, during their *in vitro* culture MSCs quickly reach replicative senescence⁸⁷. Cellular senescence is defined as a permanent state of cell cycle arrest that can also contribute to the decline of the regenerative potential^{88,89}.

For sure, different mechanisms are involved into stem cell aging and include the accumulation of toxic metabolites like reactive oxygen species (ROS)⁹⁵.

Among the ROS producing enzymes, NADPH oxidase 4 (Nox4) has been shown to have a peculiar role in regulating amniotic fluid stem cells biology. In fact, different evidences suggest that Nox4 could play an essential role in the maintenance of pluripotency, through modulation of both nuclear signalling and DNA damage¹³³, consequently influencing the proliferation rate and their differentiation ability¹³⁵.

Furthermore, recent data have shown a relationship among lamins mutations, altered ROS metabolism and physiological aging¹⁷⁰. Lamins are a family of nuclear proteins that provide not only a structural framework to nucleoplasm, but also play important roles in signal transduction^{151,157,158}. It has been suggested that lamin A can be oxidized acting as a ROS-sink inside the nucleus, protecting other more critical proteins from transient, mild oxidative damage¹⁷².

The principal aim of this study was to investigate the aging process occurring during *in vitro* expansion of amniotic fluid stem cells obtained at similar gestational age, focusing in particular on the redox control involving Nox4 and prelamin A, an immature form of lamin A that has been reported to accumulate both in premature aging syndromes¹⁸⁴ and in physiological aging¹⁸⁸.

At this purpose, 21 hAFSC samples were collected from healthy donors through amniocentesis, a routine diagnosis procedure, performed at 16th-17th week of pregnancy.

First, I performed different experiments to evaluate their proliferation rate, ROS levels, the expression of different stemness and senescence- related markers, including Nox4 and prelamin A. Then, I focused on the relationship between Nox4 and prelamin A in their aging process, investigating in particular which mechanisms could be involved in their interaction and degradation.

Since during my research I ran into a great inter-patient heterogeneity, I decided to study in deep this phenomenon both during my first part of the PhD but mostly in the second part.

Among the different causes, various studies have revealed that donor- dependent differences are in part due and explained by cell-to-cell variation within each patient population²²⁸. At this purpose, a fractionation protocol based on a tag-less, flow-assisted method of purifying, distinguishing and sorting MSCs^{252,253}, allowed me to define various cell subpopulations profiles contained in different samples and to collect these hAFSC subpopulations. On these subpopulations I carried out different types of analyses, both at protein and transcriptome level, in order to clarify which biological characteristics make these cells so heterogenic.

One of the other problems that could influence stem cell aging and research is that at present, most of the expansion procedures of MSCs are performed under atmospheric O₂ concentration (20% O₂), which is approximately 4–10 times higher than the concentration of O₂ in their natural niches. In fact, it is known that the partial O₂ pressure in the amniotic cavity is around 2.3 %²³⁶. This higher O₂ concentration might cause environmental stress to the *in vitro* cultured MSCs, due to the increased ROS concentration⁸⁶.

Thus, low oxygen tension should be considered for the culture of stem cells in scientific

research, both to keep cells in their natural conditions but also to obtain more accurate data that could in this way better explain what really happens in our body.

For this reason, during the last months of my PhD, I tried to clarify which is the oxygen role in stem cells aging, using, also in this case, a combination of molecular, immunofluorescence and spectrofluorimetric techniques to measure the expression of genes and proteins related to proliferation, stemness, senescence and resistance to stress. Since one of the most debated point is about the differentiation ability in these conditions^{238,244-247}, I also carried out different differentiation assays, to evaluate in particular their osteogenic and adipogenic potential.

All the results obtained during these three years could help to improve stem cell screening and manipulation prior their use in regenerative medicine, but they could also clarify some mechanisms involved into individual aging and the ability to counteract oxidative stress.

3. MATERIALS AND METHODS

3.1. Amniotic fluid collection

Human amniotic fluid stem cells were obtained from 21 amniotic fluids collected from women (average age $36.4 \pm \text{SD } 3.2$) between the 16th and 17th week of gestation during the amniocentesis procedure performed at Arcispedale S. Maria Nuova Hospital in Reggio Emilia. The informed consent was obtained in accordance with the Italian law and the guidelines of the ethics committee (protocol 2015/0004362 dated 02.24.2015). Amniocentesis was performed according to ISUOG Practice Guidelines²⁵⁴. Briefly, the woman is positioned as horizontally as possible, to allow better access to the amniotic cavity²⁵⁵. Foetal viability is confirmed by ultrasound. 20–22-G needle is inserted transabdominally under continuous ultrasound guidance^{255,256}. Firm entry is suggested to prevent tenting of the amniotic membrane. Needle insertion has four stages: abdominal skin puncture, uterine puncture, entry into amniotic cavity and advancement of the needle²⁵⁵. Once the needle has reached the amniotic cavity, the inner stylet is removed and 15 fluid (depending on the indication) is aspirated²⁵⁴.

Amniotic fluid (AF) was processed as reported by Miron²⁵⁷. AF is centrifuged, the supernatant is removed, the cellular pellet is re-suspended and cells are seeded in culture to be expanded and used for diagnostic procedures. Usually cells are expanded and divided in three F25 flasks: the third flask is used only if results are ambiguous, otherwise can be destined to research.

In particular, the flasks of amniotic fluid cells were cultured in the Laboratory of Genetics Arcispedale S. Maria Nuova for 2 weeks, then the supernumerary (unused) one was given to us and used for experiments or frozen.

3.2. Amniotic fluid stem cells selection

Human amniotic cells were expanded *in vitro* to reach at least three-five millions of cells. At this point *c-kit* (CD 117) positive cells, which represent a subpopulation with high stemness properties¹¹, were isolated using MACS technology (Miltenyi Biotec, Germany), an immunomagnetic method.

In particular, cells were harvested by trypsinization, resuspended in a phosphate buffer saline (PBS) containing 20% FBS e EDTA 2 mM (Buffer I) and filtered through cell strainer.

Then, cells were centrifuged at 1200 rpm for 6 minutes, resuspended in another PBS buffer containing this time EDTA 2mM, BSA 0.5% (g/v) (Buffer II) and c-kit microbeads antibody at 1:50 dilution and incubated at 4°C for 15 minutes. The final resuspension volume was evaluated based on the number of available cells: for example, five million cells were resuspended in 500µl.

After this incubation, cells were washed in the same buffer II, centrifuge at 1200 rpm for 5 minutes and resuspended in 500 µl of buffer II.

At this point the immunomagnetic selection of cells expressing *c-kit* started. A column from the kit was conditioned by washing with buffer II and located on the magnetic tablet. After this passage, the cellular suspension was loaded in the column but just cells that hadn't bound the magnetic antibody were elute from it. Three consecutive washings of the column with 500 µl of buffer II let the collection of all these cells. Then the column was detached from the magnetic board and *c-kit* positive cells were collected just washing it with αMEM growth medium.

3.3. Cellular culture

Amniotic stem cells were cultivated in αMEM growth medium supplemented of 20% foetal bovine serum (FBS), 2 mM L-glutamine, 100 U/ml penicillin and 100 µg/ml streptomycin (all from EuroClone Spa, Italy) and kept at 37°C 5% CO₂ at 20% oxygen. In alternative, in hypoxia experiments cells were put in incubators set at 5% or 1% oxygen, maintaining the same temperature and CO₂ concentration.

AFSC were subcultured routinely at 1:3 dilution and not allowed to expand beyond the 70% of confluence.

3.4. Evaluation of ROS levels

ROS levels were evaluated using dichlorodihydro-fluorescein diacetate (DCFH-DA) probe. This molecule is cell-permeable and is hydrolysed intracellularly to the DCFH carboxylate anion, which is retained in the cell. The oxidation of DCFH results in the formation of a fluorescent product, dichlorofluorescein (DCF), which can be monitored

by fluorescence-based techniques. It is used to measure intracellular oxygen peroxide (H_2O_2) levels²⁵⁸.

Cells were seeded at a density of 3000 cells/well in a black 96 multi well plate in 6 replicates. After 48 hours, the growth medium was replaced with PBS glucose 5 mM containing 5 μM DCFH-DA. After 30 minutes of incubation, fluorescence was detected using the Appliskan instrument (Thermo Fisher Scientific, Vantaa, Finland) at 485 nm of excitation and 535 nm of emission.

3.5. Cellular viability

Cellular viability was evaluated using MTT assay or alternatively MTS one.

As previously, cells were seeded at a density of 3000 cell/well in a black 96 well plate and were incubated with 0.5 mg/mL MTT for 4 hours at 37°C or with MTS reagent (Promega, Milan, Italy), in the same conditions following in this case the instructions of the producer.

The analysis is based on the reduction of the tetrazolium MTT or MTS by metabolically active cells, in part by the action of dehydrogenase enzymes, to generate reducing equivalents such as NADH and NADPH²⁵⁹. In the case of MTT, the resulting formazan must be solubilized prior to the quantification (using isopropanol, 0.1 M HCl). On the contrary, in the case of MTS, the derivative formazan is already dissolved into the medium and can be detected directly.

The absorbance was measured on the multi well plate reader Appliskan, (Thermo Fisher Scientific, Vantaa, Finland) at 570 nm in the case of MTT or Promega multi well plate reader (Promega, Milan, Italy) at 450 nm in the case of MTS.

3.6. Cellular proliferation

Cells were seeded in a T25 cm^2 flask at a density of 2000 cells/ cm^2 , cultured for 3.5 days then detached, counted and seeded again at 2000 cells/ cm^2 .

Cultures were performed until passage 8 and population doubling (PD) for each passage was measured applying the following formula:

$$\text{PD} = [\log_{10}\text{NH} - \log_{10}\text{NS}] / \div \log_{10}2$$

where NS is the cell number at seeding (2×10^3 cells/ cm^2) and NH is the cell number at harvest.

To calculate the cumulative number of population doublings (CPD), the PD determined for each passage was then added to the CPD of the previous passage.

The population doubling time (PDT) was calculated in the phase of exponential growth by the following formula:

$$PDT = \log_{10}(2) \times \Delta T / (\log_{10}(NH) - \log_{10}(N1d))$$

where ΔT represents the time between the cell harvesting and seeding, NH the harvested cell number and N1d the cell number at day 1.

3.7. EdU Proliferation assay

In hypoxia experiments, cellular proliferation was evaluated using EdU method. EdU (5-ethynyl-2'-deoxyuridine) is a thymidine analogue alternative to BrdU which is incorporated into newly synthesized DNA by cells. For this experiment, 8000 cells/well were seeded into coverslips put in a 24 multi well plate.

After 48 hours, 10 μ M EdU was added into the medium and cells were cultivated in these conditions for other 24 hours. The day after cells were fixed using 4% formaldehyde in PBS, kept 5 min in 100 mM Tris (pH 7.6), permeabilize 10 min in PBS + 0.1% Triton X-100, washed 3 times with PBS and incubated with a PBS label mix containing 2 mM Cu(II)SO₄, 4 μ M sulfo-Cy3-azide, 20 mg/ml sodium ascorbate for 30 minutes in the dark. After washing cells with PBS 3 times for five minutes each, coverslips were mounted with mounting media (including DAPI to visualize nuclei) onto glass slides and visualized at fluorescent microscope.

3.8. Differentiation assays

For each differentiation experiment, 50000 cells were seeded in a P60 culture dish and kept in culture medium for 4 days. Then, the medium was replaced by differentiating media.

Osteogenic differentiation was obtained after 3 weeks of culture in a medium composed by α MEM medium supplemented with 10% FBS, 2 mM L-glutamine, 100 U/ml penicillin and 100 μ g/ml streptomycin (all from EuroClone Spa, Italy) 100 μ M 2P-ascorbic acid, 100 nM dexamethasone and 10 mM β -glycerophosphate (all from Sigma-Aldrich, St Louis, MO, USA). The medium was changed twice a week.

For adipogenic differentiation, cells were incubated for 3 days in adipogenic induction medium composed by high glucose DMEM culture medium supplemented with 10 % FBS, 2 mM L-glutamine, 100 U/ml penicillin and 100 µg/ml streptomycin, 0.5 mM (all from EuroClone Spa, Italy), isobutylmethylxanthine, 1 µM dexamethasone, 10 µg/ml insulin, 0,2 mM indomethacin (all from Sigma-Aldrich, St Louis, MO, USA). After 3 days, medium was replaced with one containing only 10 % FBS, 2 mM L-glutamine, 100 U/ml penicillin and 100 µg/ml streptomycin and 10 µg/ml insulin. It was changed twice a week and cells were kept in these conditions for 3 weeks.

After 3 weeks of osteogenic or adipogenic induction, the expression of specific lineage markers was evaluated through qRT-PCR or cytofluorimetry as reported below.

3.9. Senescence assay

In order to evaluate the presence of senescent cells in AFSCs samples, 10000 cells/well were seeded in 24-well plates and after two days they were fixed and processed using a senescence β-Galactosidase staining kit (Cell Signaling, MA, USA), according to the manufacturer's instructions.

In alternative, cells were fixed for 4 minutes with 2% formaldehyde + 0.2% glutaraldehyde in PBS and incubated overnight at 37°C without CO₂ in a staining solution containing 1 mg/ml X-gal, 40 mM citric acid/Na phosphate buffer pH = 6.0, 5 mM potassium ferrocyanide, 5 mM potassium ferricyanide, 150 mM sodium chloride, 2 mM magnesium chloride. The day after, cells were washed in PBS and the positivity was directly evaluated at the optical microscope.

This analysis is based on the detection of β galactosidase, an enzyme activated at pH 6, a known characteristic of senescent cells and not found in pre-senescent, quiescent or proliferating cells²⁶⁰.

3.10. Cellular morphology

Cellular images were acquiring using EVOS XL Core Cell Imaging System (Thermo Fisher Scientific, Vantaa, Finland). Parameter and area were measuring using ImageJ using images pixels as scale. Cellular elongation was calculated using the following formula:

$$\textit{elongation} = \frac{P^2}{4\pi \cdot A}$$

3.11. Flow cytometer immune-assay

AFSCs at first passage were sub-cultured until reaching 80% confluence, then harvested by trypsin treatment, centrifuged at 1200 rpm for 5 minutes, washed in PBS and the obtained pellets fixed and incubated with 3% BSA-PBS for one hour at room temperature to block nonspecific binding sites. At this point, cells were stained with the primary reported antibodies for 30 minutes at 4°C, following datasheet indications: Rabbit-Thy-1 (CD90) and Rabbit-Endoglin (CD105) (Millipore, CA, USA), Mouse-Ssea4 (Cell Signaling Technology, MA, USA), Goat-Integrin β 1 (CD29), Rabbit-HCAM (CD44) (Santa Cruz Biotechnology, CA, USA), Mouse-5'-Nucleotidase (CD73) (Gene Tex, CA, USA).

After washing in PBS, the expression of surface markers was analysed by indirect staining using secondary fluorochrome Alexa 488-conjugated antibodies (Abcam, Cambridge, UK). Non-specific fluorescence was assessed by using the secondary antibody alone. A minimum of 5000 cells per sample was acquired and analysed using FACScan flow cytometer and Lysis II software (both from Becton Dickinson, San Jose, CA, USA).

The same cell samples were analysed for nuclear stem cell markers, such as Goat- Sox2 (Santa Cruz Biotechnology, CA, USA) and Rabbit-Nanog and Rabbit-Oct4, (Cell Signaling, MA, USA), after Fixation/Permeabilization process performed with the Staining Buffer Set (Miltenyi Biotec Inc, Auburn, CA, USA) optimized for nuclear staining.

After exposure to adipogenic differentiation medium, nuclear differentiation marker rabbit anti-PPAR (Santa Cruz, CA, USA) was analysed by using the Staining Buffer Set (Miltenyi Biotec Inc, Auburn, CA, USA).

3.12. Cells treatments

Cells were treated with 10 μ M Mevinolin (2-Methyl-1,2,3,7,8,8a-hexahydro-3,7-dimethyl-8-[2-(tetrahydro-4-hydroxy-6-oxo-2H-pyran-2-yl)ethyl]-1-naphthalenyl ester butanoic acid) for 16 hours (Sigma-Aldrich, St Louis, MO, USA), or with 50 μ M

Anacardic Acid (2-Hydroxy-6-pentadecylbenzoic acid) for 24 hours (Sigma-Aldrich, St Louis, MO, USA), or with 10 μ M MG-132 (benzyloxycarbonyl-Leu-Leu-Leu-aldehyde) for 8 hours (Selleckchem, Houston, TX, USA), or with 100 nM thapsigargin for 24 hours, or with 1 μ M sulforaphane (SF) and 10 μ M epigallocatechin gallate (EGCG) for 11 days.

3.13. Cellular extracts preparation

Cell extracts were obtained by treatment with AT lysis buffer 820 mM Tris-Cl, pH 7.0; 1% Nonidet P-40; 150 mM NaCl; 10% glycerol; 10 mM EDTA; 20 mM NaF; 5 mM sodium pyrophosphate; and 1 mM Na₃VO₄) and freshly added Sigma Aldrich Protease Inhibitor Cocktail. Lysates were sonicated, cleared by centrifugation (12700 rpm for 15 minutes at 4°C), quantified for protein content and immediately boiled in SDS sample buffer (Tris-Cl 1 M pH 6.8, SDS 10%, glycerol 30%, brome phenol blue 0.012%, dithiothreitol 0.6 M) for 5 minutes or used for immunoprecipitation experiments, as described below.

3.14. Protein quantification

Protein content was quantified using Bradford method. This assay is based on the binding of Coomassie dye to protein molecules under acidic conditions that results in a colour change from brown to blue that can be detected using spectrophotometric techniques. This method actually measures the presence of the basic amino acid residues, arginine, lysine and histidine, which contributes to formation of the protein-dye complex²⁶¹.

Briefly, 1 μ L of each sample was added into 160 μ l of MilliQ water in a 96 multi well plate. At this point, 40 μ l of Bradford reagent were added and the absorbance was immediately read at 595 nm using a multi well reader (Appliskan, Thermo Fisher Scientific, Vantaa, Finland).

3.15. Nuclei purification

Cells were harvested, counted and centrifuged at 1200 rpm for 10 minutes. The pellets were resuspended in PBS and centrifuged again at the same speed for the same amount of time. The supernatants were removed, 400 μ l of nuclear isolation buffer (10 mM Tris-HCl, pH 7.8, 1% Nonidet P-40, 10 mM β -mercaptoethanol, 0.5 mM

phenylmethylsulfonyl fluoride, 1 µg/ml aprotinin and leupeptin, and 5 mM NaF) were added to 5×10^6 cells on ice to ensure that just the cytoplasmatic membranes were lysed but not the nuclear ones. After 5 minutes, the same amount of MilliQ water was added to swell cells for 5 min. Cellular aggregates were sheared, passing the cells through a 22-gauge needle. At this point, after centrifugation at 1200 rpm for 10 minutes, the supernatants containing the cytoplasm were collected in a new tube, while the pellets containing the nuclei were resuspended in 400 µl of washing buffer (10 mM Tris-HCl, pH 7.8, and 2 mM MgCl₂, plus cocktail protease inhibitors), centrifuged at 1200 rpm for 10 minutes and the new obtained pellets were frozen or lysed as previously described to be used for experiments.

3.16. Immunoprecipitation

Equal amounts of precleared lysates, whose protein concentration was determined by the Bradford method, were incubated overnight with Rabbit-Nox4 (Santa Cruz Biotechnology, CA, USA), Rabbit-Prelamin A (Diatheva, Fano, PU, Italy), Rabbit-Farnesylated Prelamin A (Diatheva, Fano, PU, Italy) (3 µg all). The day after samples were treated with 30 µl of 50% (v/v) of protein A/G agarose slurry containing microbeads, which recognize the primary antibody used (GE Healthcare Bio-sciences, Uppsala, Sweden), at 4 °C with gentle rocking for 1 h. After this incubation cells were centrifuged at 10000 rpm for 3 minutes, washed twice with 20 mM Tris-Cl pH 7.0 containing 1% Nonidet P-40, 150 mM NaCl, 10% glycerol, 10 mM EDTA, 20 mM NaF, 5 mM sodium pyrophosphate and once with 10 mM Tris-Cl pH 7.4. Then they were boiled in SDS sample buffer to be denatured and to detach the microbeads that were removed thanks to a centrifugation. At this point samples were ready to be loaded in a SDS page gel.

3.17. SDS page and western blot

Cellular lysates were loaded in sds gels 1.55 mm thick containing a running part at 7 % or 12 % polyacrylamide and a stacking part at 4 % polyacrilamide. In this kind of electrophoresis proteins are separated based on their molecular weight. In fact, as mentioned before, prior the run the samples were treated with SDS sample buffer that denatures proteins (dithiothreitol) and makes all of them negative charged (SDS).

Protein separation was carried out first at 110V for 15 minutes a room temperature and then at 160V for 90 minutes 4°C in presence of electrolytic running buffer (Bio-rad, Hercules, CA, USA). For all the analyses at least 40 µg of proteins were loaded and 6 µl of Precision Plus Protein™ Standards Dual Color (Bio-rad, Hercules, CA, USA).

Once the separation was complete, proteins were transferred from the gel to a polyvinylidenedifluoride (PVDF) membrane using a semi- dry method working at 12 V for 90 minutes, with all components pre-treated with transfer buffer containing 25 mM Tris, 190 mM glycine, 20 % methanol.

After the transfer, the membrane was temporarily stained with Ponceau Red to verify proteins presence, blocked with Tris buffered saline solution (TBS) containing Tris 25 mM, KCl 3 mM, NaCl 140 mM pH 7.8, 3% BSA, 0.1% twin for 1 hour to block unspecific binding sites and then incubated with primary antibodies overnight.

The day after membranes were washed with 0.1% twin-TBS, incubated with secondary antibodies for 1 hour at room temperature, washed again and the luminescence signal was detected using Supersignal substrate chemiluminescence detection kit (Pierce, Rockford, IL, USA) using Kodak Image Station 440CF and Kodak 1D Image software. Primary antibodies were raised against the reported molecules, following data sheet recommended dilutions: Rabbit-p16 (Abcam, Cambridge, UK), Mouse-Tubulin (Sigma-Aldrich, St Louis, MO, USA), Mouse-SIRT1 (Cell Signaling Technology, MA, USA), Rabbit-Nox4 (Santa Cruz Biotechnology, CA, USA), Rabbit-Prelamin A (Diatheva, Fano, PU, Italy), Mouse-Lamin A/C (Santa Cruz Biotechnology, CA, USA), Rabbit-SUMO1 (Cell Signaling Technology, MA, USA), Rabbit-Actin (Sigma-Aldrich, St Louis, MO, USA), Rabbit-PARP (Santa Cruz Biotechnology, CA, USA), Goat-Akt (Santa Cruz Biotechnology, CA, USA), Rabbit-p473Akt (Cell Signaling Technology, MA, USA), Mouse-Oct4 (Santa Cruz Biotechnology, CA, USA), Rabbit-Cyclin E2 (Cell Signaling Technology, MA, USA), Rabbit-Glut1 (Millipore, CA, USA).

Secondary antibodies were used at 1:3000 dilution all from Thermo Fisher Scientific (Waltham, MA, USA).

3.18. Mass Spectrometry

Nox4- immunoprecipitated samples were separated by 10% SDS-PAGE and gels were then stained in the Coomassie brilliant blue solution (0.1% Coomassie blue in 10% acetic acid, 45% methanol) and shaken at room temperature for 1 h. The gels were destained by soaking for 2 h in destaining solution (10% acetic acid, 30% methanol). In gel digestion and mass spectrometry analysis were performed as described by Shevchenko et al²⁶². The stained bands were reduced in gel pieces and transferred into a microcentrifuge tube to be spin down and then treated with solution A (1:1 mixture of acetonitrile and 100 mM ammonium bicarbonate) for 30 min. The gel slices were subjected to reduction of disulfide bonds by 10 mM DTT at 56°C for 30 min. Alkylation step was then performed with 55 mM iodoacetamide for 20 min at room temperature in dark. Before trypsin digestion, the rehydration and dehydration steps were again performed with ammonium bicarbonate and solution A. Then samples were incubated at RT with acetonitrile until gel pieces become white. Trypsin digestion was performed by incubating the dry gel slices overnight in 1 µg of trypsin in ammonium bicarbonate (Trypsin Sigma) at 37°C. Following digestion, the tryptic digested fragments present in the supernatant were collected and lyophilized. Before mass spectrometry analysis, the lyophilized powder was dissolved in 0.1% TFA in 50% acetonitrile. The expressed proteins were identified using LC/MS/MS 6410B mass spectrometer. Protein identification against the peak list was performed in MASCOT version 2.1 with Swiss-Prot and cRAP database as the search engine. The search parameters for database search using Mascot were given as, taxonomy: human; enzyme used for digestion: trypsin with one missed cleavage allowed; fixed modification specified as carbamidomethylation (C), and oxidation (M) and deamidated (NQ) as variable modifications. The peptide mass tolerance was set as 40 ppm and 0.08 Da for MS/MS tolerance.

3.19. Immunofluorescence and confocal microscopy

For immunofluorescence analyses, 15000 cell/well were seeded in coverslips put in 24 multi well plates, fixed with 4 % paraformaldehyde after 48 hours and permeabilized with 0.1 % Triton X-100 for 4 minutes, this last step performed just if intracellular markers had to be analysed. After washed 2 times with PBS, cells were put in 3 % BSA-PBS for 1 hour to block unspecific binding sites and were incubated with the primary

antibody in a wet chamber overnight at 4°C. The day after, the samples were washed 3 times in 3 % BSA-PBS and incubated with secondary antibodies in a wet chamber at room temperature in the dark for an hour. After 2 washing with PBS, the coverslips were incubated with 4',6-diamidino-2-phenylindole (DAPI) for 5 minutes, in order to visualize the nuclei, washed again in PBS and mounted with anti-fading medium (0.21 M DABCO, 90% glycerol in 0.1 M Tris pH 8.0) on slides.

Primary antibodies were raised against Rabbit-p53 (Flarebio, MD, USA), Mouse-p21 (Novus Biologicals, CO, USA), Mouse-pH2A (Millipore, CA, USA), Rabbit-Nox4 (Santa Cruz Biotechnology, CA, USA), Mouse-Nox4 (Novus Biologicals, CO, USA), Rabbit-Prelamin A (Diatheva, Fano, PU, Italy), Rabbit-Farnesylated Prelamin A (Diatheva, Fano, PU, Italy), Mouse-PML (Santa Cruz Biotechnology, CA, USA), Mouse-SUMO1 (Novus Biologicals, CO, USA), Rabbit-Oct4 (Cell Signaling, MA, USA), Goat-Ki-67 (Santa Cruz Biotechnology, CA, USA), Goat-CD29/Integrin β 1 (Santa Cruz Biotechnology, CA, USA), Rabbit-CD44/HCAM (Santa Cruz Biotechnology, CA, USA), Mouse-CD271/NGFR (San Diego, CA, USA), Mouse-Human Mit (Millipore, CA, USA), Rabbit-Caspase 3 (Sigma-Aldrich, St Louis, MO, USA), following datasheet recommended dilutions. Confocal imaging was performed by a Nikon A1 confocal laser scanning microscope. The confocal serial sections were processed with ImageJ software to obtain three-dimensional projections. The image rendering was performed by Adobe Photoshop software.

In some cases, the cell fluorescence signal was quantified using ImageJ and applying the following formula:

$$\text{Corrected Total Cell Fluorescence (CTCF)} = \text{Integrated Density} - (\text{Area of selected cell} \times \text{Mean fluorescence of background readings})$$

In other cases, the quantification was carried out using an arbitrary scale (from 0 to 4) by two different operators that worked in an independent way.

3.20. AFSC subpopulations sorting

hAFSC subpopulations were sorted using a flow-assisted fractionation protocol through Celector® technology (Stem Sel Ltd., Italy)^{252,263}. The instrument exploits the Non-Equilibrium, Earth Gravity Assisted Dynamic Fractionation (NEEGA-DF) principles.

The instrument is composed by a capillary channel where a biocompatible buffer develops a parabolic flow profile possessing different flow speeds at heights. The mobile phase flows at a higher velocity at the centre of the channel and it is null at the channel walls.

Once cells suspension is introduced into the capillary channel, cells with different morphological features (dimension, shape, or surface properties) reach a specific position across the channel thickness due to the combined action of gravity, acting perpendicularly to the flow, and opposing lift forces that depend on the morphological features of the sample acting in the opposite direction. Cells at a specific position in the channel acquire well-defined velocities and are therefore eluted at specific times. To generalize, larger cells reach a higher position inside the capillary and, as a consequence, acquire higher velocities within the capillary device. This soft fractionation mechanism guarantees the preservation of the native physical features of the cells, as there is no contact between the eluted cells and the separation device; thus, viable, intact cells can be collected at the channel outlet.

A camera with a microscopic object is placed at the outlet of the capillary channel and it is connected to an imaging software that records live images of eluting cells and to an imaging software that plot number of counted cells related to time (sample profile). Dimension inclusion/exclusion criteria are set by the operator to refine the counting procedure. For AFSCs analysis the average diameter was set as 12-15 μm .

Every experimental day, a procedure for decontamination of the fractionation system was performed by flushing sodium hypochlorite in sterile water at 2 % as active chlorine; then it was washed copiously with sterile, demineralized water. Subsequently, in order to block unspecific interaction sites on the plastic walls, a sterile solution of bovine serum albumin (BSA) 1 % (w/v) in physiologic phosphate buffer saline (PBS) was flushed at 1 ml/min.

Finally, the fractionation system was filled with sterile mobile phase consisting of PBS added with 0.1 % (w/v) BSA and 1 % penicillin/streptomycin. All solutions were provided by Stem Sel Ltd.

In our experiments, cells were cultured to reach at least two million cells, then they were harvested by trypsinization, centrifuged at 1200 rpm for 5 minutes, resuspended in 500 μl PBS and counted.

Aliquots of 300,000 cells resuspended in 100 μ l of PBS were introduced into the system and analysed at a flow rate of 1 ml/min.

Cells collected from repeated runs were pooled and used for experiments.

3.21. RNA isolation and quantification

For hypoxia experiments cells were seeded at 2000 cells/cm² density and kept in culture for 3 days. After this time, cells were harvested, centrifuged at 1200 rpm for 5 minutes, washed 1 time in PBS and, after centrifugation at the same conditions, pellets were used for RNA isolation through ISOLATE II RNA Mini Kit (Bioline Meridian Bioscience, Paris, France), following producer instructions.

The same kit was used to isolate RNA also from pellets collected through Celector® technology.

Briefly, cells were lysed using 350 μ l of Lysis Buffer RLY with 3.5 μ l β -mercaptoethanol and in the presence of guanidinium thiocyanate, a chaotropic salt which immediately deactivates endogenous RNases to ensure purification of intact RNA. After homogenization, ethanol was added to the samples that were processed through a spin column containing a silica membrane to which the RNA binds. During the isolation procedure, genomic DNA contamination was removed by an on-column DNase I digestion at room temperature for 15 minutes. Any impurities such as salts, metabolites and cellular components were effectively removed by simple washing steps with two different buffers. Eventually, high-quality purified total RNA was eluted in RNase-free water and quantified at Nanodrop™.

3.22. cDNA retrotranscription and qRT-PCR

500 ng of RNA were reverse transcribed into cDNA using the kit High Capability cDNA Reverse Transcription (Applied Biosystems, Waltham, MA, USA). The reaction was accomplished in a T100™ Thermal Cycler (Bio-rad, Hercules, CA, USA).

The obtained cDNA samples were diluted at 5 ng/ μ l and 12 ng of each sample were loaded to perform qRT-PCR using the Universal Probe Library system (Roche, Basel, Switzerland) and SENSIFast Probe kit (Bioline Meridian Bioscience, Paris, France). The reaction was carried out using the LightCycler® 480 Instrument II (Roche, Basel,

Switzerland) in a 360 pcr multi well plate. Analysis of tubulin and actin or gapdh were used to normalize the expression of other genes CT values.

The list of primers used in my experiments is reported below.

| Gene | Sequence | RefSeq accession n |
|--------------------|---|--------------------|
| hNANOG | Fw cagtctggacactggctgaa Rv cacgtggtttccaacaaga Probe 55 | NM_024865 |
| hPOU5F1 (Oct4) | Fw tgagtagtccttcgcaagc Rv gagaaggcgaaatccgaag Probe 60 | NM_002701.5 |
| hCDKN2A (p16) | Fw gagcagcatggagccttc Rv cgtaactattcggcgttg Probe 67 | NM_000077.4 |
| hCDKN1A (p21) | Fw tcaactgtctgtacccttgtgc Rv ccgttttcgaccctgagag Probe 32 | NM_000389.4 |
| hSLC2A1 (Glut 1) | Fw tetggcatcaacgctgtc Rv gagccaatggtggcataca Probe: 66 | NM_006516.2 |
| hPDK1 | Fw tcctttgaatctaagtattgttctc Rv catttttcctttaaacatttcttagc Probe 52 | NM_001278549.1 |
| hCCNE2 (cyclin E2) | Fw cccaagaagcccagataat Rv caggtggccaacaattcct Probe 35 | NM_057749.2 |
| hPPARG | Fw gacctgaaactcaagagtacaaa Rv tgaggcttattgtagagctgagtc Probe 39 | NM_138712 |
| hCEBPA | Fw gacatcagcgcctacatcg Rv ggctgtgctggaacaggt Probe 72 | NM_001285829.1 |

| | | |
|-------------------------|---|--------------|
| hRUNX2 | Fw cagtgcacccatgtcagcaa Rv gtcacgctcgctcatttg Probe 41 | NM_001015051 |
| hSPP1 (Osteopontin) | Fw gggcttggtgtcagcag Rv tgcaattctcatggtagtgagttt Probe 63 | NM_001251830 |
| hBGLAP (Osteocalcin) | Fw tgagagccctcacactctc Rv accttgctggactctgcac Probe 81 | NM_199173 |
| hTUBULIN | Fw cttegtctccgcatcag Rv cgtgtccaggcagtagagc Probe 40 | NM_006009.3 |
| hACTB | Fw ccaaccgcgagaagatga Rv ccagaggcgtacagggatag Probe 64 | NM_001101.3 |
| hGAPDH | Fw agccacatcgctcagacac Rv gcccaatacgaccaaattcc Probe 60 | NM_002046.5 |

3.23. RNA and DNA quality check

Prior library preparation for RNA seq, RNA quality was checked using RNA 6000 Pico kit (Agilent, Santa Clara, CA, USA) following the instructions of the producer and reading the results at 2100 Bioanalyzer Instrument (Agilent, Santa Clara, CA, USA).

The procedure is based on capillary electrophoresis that takes place on special chip priming stations.

Evaluation of RNA quality control using this method results in both gel-like images, as well as electrophoretic data, making easy to detect even small degradative effects. Indications for RNA degradation are the decreasing ratio of ribosomal bands, additional peaks below the ribosomal bands, decrease in overall RNA signal, shift towards shorter fragments.

The Bioanalyzer system provides a RIN (RNA Integrity Number) value, an objective metric of total RNA quality ranging from 10 (highly intact RNA) to 1 (completely degraded RNA)²⁶⁴.

The same procedure was applied to verify both the correct fragmentation of DNA during the library preparation and to quantify the obtained fragments, using in this case the High Sensitivity DNA Kit (Agilent, Santa Clara, CA, USA).

Quantification of DNA fragments was also performed using Qubit™ 1X dsDNA HS Assay Kit (Thermo Fisher Scientific, Vantaa, Finland) at Qubit™ Fluorometer (Thermo Fisher Scientific, Vantaa, Finland), following kit instructions.

3.24. Library preparation and RNAseq

100 ng of total RNA were used to isolate mRNA using NEXTflex™ Poly(A) Beads (Bioo Scientific, Burleson Rd, Austin, TX, USA), as reported in the producer protocol. The procedure includes two bead-binding steps to ensure maximum removal of ribosomal and non-messenger RNA contaminants wherein magnetic beads were incubated with total RNA in the presence of a binding buffer. Magnetic based separation was used to retain poly(A) mRNA while removing all other transcripts. Beads were subsequently washed and 14 µl mRNA were eluted, releasing purified poly(A) mRNA. The obtained mRNA was used to prepare the RNA library using NEXTflex™ Rapid Directional qRNA-Seq™ Kit (Bioo Scientific, Burleson Rd, Austin, TX, USA), following the instructions.

This kit efficiently generates libraries equivalent to conventional directional, strand-specific RNASeq libraries, but with the added feature of Molecular Indexing™.

Briefly, the mRNA was fragmented using a cationic buffer. Fragmented RNA underwent first and second strand synthesis, followed by adenylation, ligation and PCR. Directionality is retained by adding dUTP during the second strand synthesis step and subsequent cleavage of the uridine-containing strand using Uracil DNA Glycosylase. The strand that's sequenced is the cDNA strand. This kit contains a set of 96 distinct molecular labels on the sequencing adapters. Each label consists of an 8 nucleotides barcode tag. During the ligation reaction, each cDNA fragment end independently and randomly ligated to a single label from this pool of 96 adapters to result in a total of $96 \times 96 = 9,216$ possible combinations across both ends. For every clone sequenced, paired-

end reads reveal the chosen label on each end along with adjoining cDNA sequence. This allows for differentiation between re-sampling of the same molecule and sampling of a different molecule of identical sequence. Analysis using molecular indexing information provides an absolute, digital measurement of gene expression levels, irrespective of common amplification distortions observed in many RNA-Seq experiments. In addition to encoding cDNA fragments at the molecular level, the kit also allows for the application of sample-specific barcodes during the library preparation PCR step.

After the quality check and quantification performed at the Bioanalyzer and Qubit as previously described, samples were pooled together in a unique tube at 2nM.

At this point, pooled samples were sent to the RNAseq facility of ERIBA Center (University Medical Center-Groningen) and pair end run Illumina nextseq (high output) sequencing was performed.

Quality control of all samples was performed using the FastQC software v0.11.5. Samples were aligned to the UCSC hg38 version of the human using STAR-2.5.3a aligner and a count table was directly obtained with Star. Counts for UCSC annotated genes were calculated from the aligned reads using featureCounts function of the Rsubread R package.

Differential analysis was performed using edgeR algorithm. Raw counts were normalized to obtain Counts Per Million mapped reads (CPM) and Reads Per Kilobase per Million mapped reads (RPKM). Only genes with a CPM greater than 1 in at least 1 sample were retained for differential analysis. The heterogeneity of the data was evaluated with a Principal Component Analysis (PCA)-plot of the log-transformed normalized CPM, evaluating whether they clustered with similar samples in the same dataset. Principal component analysis is used to extract the important information from a multivariate data table and to express this information as a set of few new variables called *principal components* that correspond to a linear combination of the originals. The goal of PCA is to identify directions (or principal components) along which the variation in the data is maximal. In other words, PCA reduces the dimensionality of a multivariate data to two or three principal components, that can be visualized graphically, with minimal loss of information. Sample number 36, showed into the

PCA analysis, was not considered in the following analysis due to possible experimental contaminations.

Enrichment analysis was obtained with the software Gene Set Enrichment Analysis (GSEA) (<http://software.broadinstitute.org/gsea/index.jsp>), a computational method that determines whether a priori defined set of genes shows statistically significant, concordant differences between two biological states. The gene sets are defined based on prior biological knowledge and I used the hallmark, kegg and reactome gene sets collections. To analyse stemness signature, the list “ES exp1” from publication “Ittai BP et al., nature genetics, 2008” was used. The results (FDR<0.25) were obtained both comparing individually each sample and with a paired analysis, in which F2, F3 or F4 from all patients were put together and considered as replicates, keeping in mind patient-patient variability. Investigation of the biological processes involved into each pathway was performed using the software FunRich 3.1.3.

3.25. Statistical Analysis

In vitro experiments were performed in triplicate. For quantitative comparisons, values were reported as mean \pm SD based on triplicate analysis for each sample. To test the significance of observed differences among the study groups Student’s t-test or One-way Anova with Bonferroni post hoc test were applied. A P value <0.05 was considered to be statistically significant. Statistical analysis and plot layout were obtained by using GraphPad Prism® release 6.0 software.

4. RESULTS

Throughout the course of my PhD, my research activity was focused on exploring different faces of stem cell aging, using amniotic fluid stem cells as cellular model.

During the first part, I was interested mostly in understanding the mechanisms underlining nuclear redox control of stem cell aging, showing interest in the involvement of NADPH oxidase 4 and Prelamin A.

Since during my research I ran into in a great inter-patient heterogeneity, I decided to study in deep this phenomenon both during my first part of the PhD but mostly in the second part thanks also to a collaboration with Prof. Roda Barbrara group of University of Bologna and with Dr Demaria Marco group of University Medical Center Groningen (ERIBA Center). The major aim was to comprehend if inter patient heterogeneity could be explained by cell-to-cell variation within each patient population.

During the six months I spent in Groningen, I had also the opportunity to explore what could be the oxygen role in stem cell aging and in stemness maintenance, with the purpose of clarifying what oxygen tension should be considered for the optimal culture of amniotic fluid stem cells in scientific research, both to keep cells in their natural conditions but also to obtain more accurate data about what really happens in our body.

4.1. Nuclear redox control of stem cell aging

4.1.1. Characterization of Human Amniotic Fluid Stem Cells samples

21 amniotic fluids were collected at 16th-17th week of pregnancy from foeti that did not carry genetic abnormalities. Pregnancies showed only in one case preeclampsia complication, but the Apgar score of all the new-borns was 9/10 and no one child needed assistance in neonatology. Women (average age 36.4) led healthy habits of life, except one smoker mother.

After having reached at least 1.5×10^6 cells, c-kit positive cells were selected and showed to be about 1-4% of the entire unselected population.

The first parameter to be analysed was their proliferation rate. Analysis of cumulative population doubling (CPD) during passages (up to 7th passage) established three groups of samples with different proliferation rate. A graph representative of all three samples is shown in Figure 4.1.1. The slower group (Group I), represented in blue, showed a

trendline slope around $0.96 \pm 0.02 R^2$, while the faster one (Group III), in pink, had a slope around $0.99 \pm 0.01 R^2$.

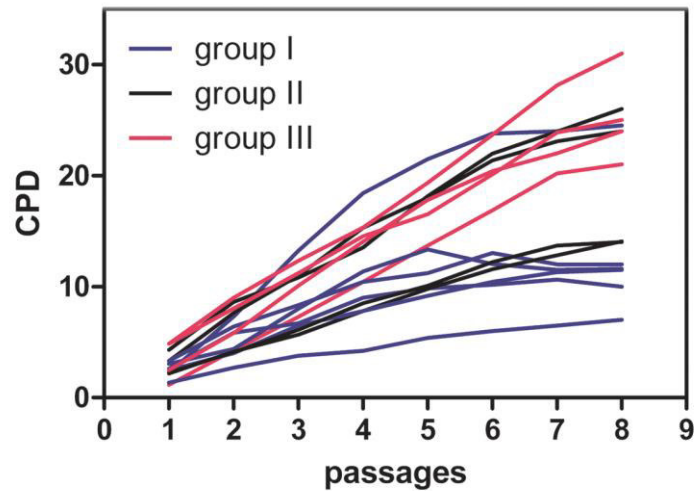


Figure 4.1.1 Cumulative population doubling (CPD). The graph shows the CPD of 21 hAFSC samples up to 7th passage in culture. Three groups can be discerned: group I (blue) represents samples that have the slowest proliferation rate; group II (black) is composed by samples that have an intermediate proliferation rate; group III (pink) gathers samples with the highest growth ability.

Analysis of Population Doubling Time (PDT) at passage 3, therefore excluding the last part of the sigmoidal curve, confirmed that hAFSC samples were distributed in three groups for the growth rate, as shown by coloured circles in Figure 4.1.2. The slowest group showed a PDT value doubled than the faster one.

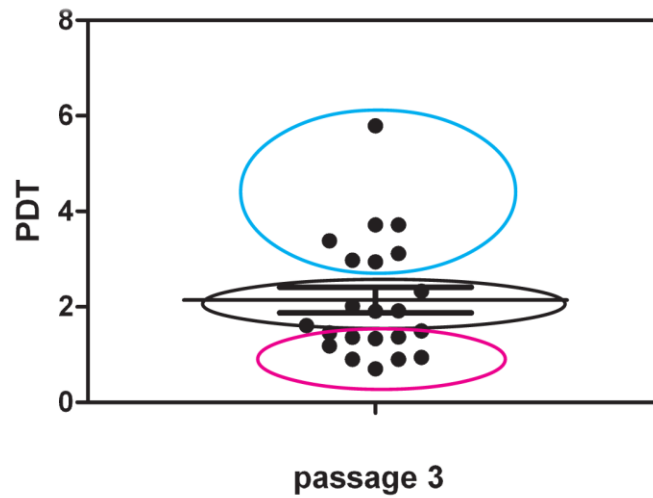


Figure 4.1.2 **Population doubling time (PDT)**. The graph shows the PDT of 21 AFSC samples evaluated at 3rd passage in culture. As in the picture above, also in this case three groups, represented by three different coloured circles (blue: slow group; black: intermediate group; pink: fast group), can be discerned.

Since, the immunophenotype still represents one of the major parameters for the characterization of MSCs cultures, flow cytometry analysis was performed to determine immunophenotype from four representative samples. As showed in Figure 4.1.3, samples at early passages (not over the 4th passage) maintained a quite similar level of cell surface markers CD29, CD44, CD73 and CD105, although CD90 seemed to be the more variable.

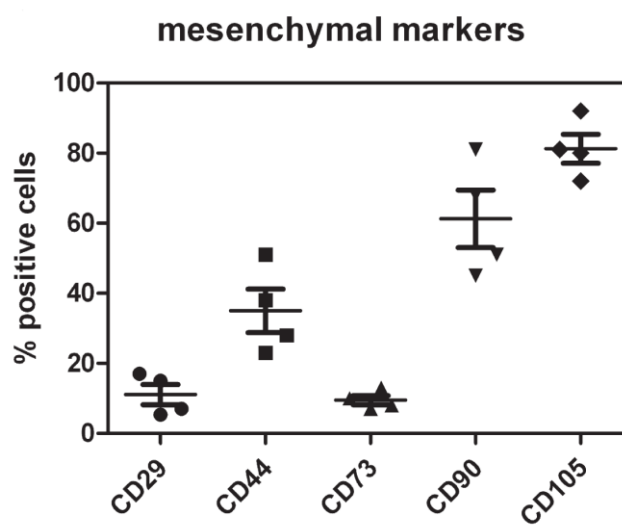
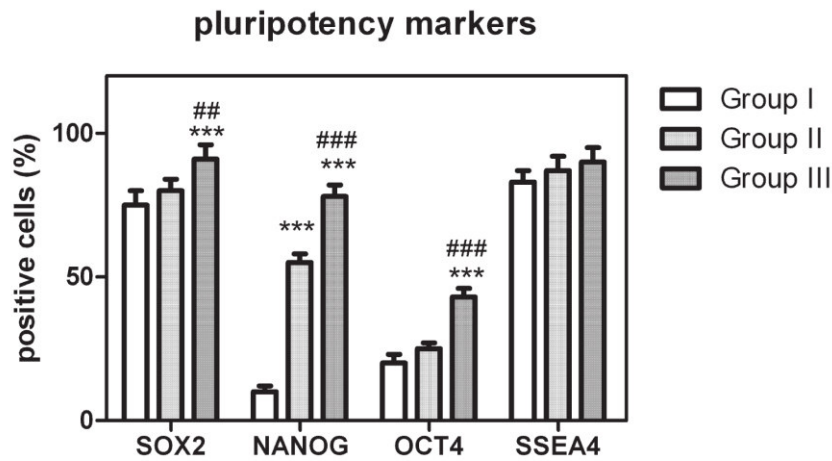


Figure 4.1.3 **Quantitative analysis of mesenchymal markers by flow cytofluorimetry**. The analysis of five different mesenchymal markers has been performed in four representative samples.

Moreover, to confirm stem cell origin of hAFSCs, cytofluorimetric analysis of the main stemness transcription factors was performed. In Figure 4.1.4 slow samples (group I) are in white, middle proliferating samples (group II) in light grey and high proliferating patients (group III) in dark grey. In all cases, three samples for each condition were analysed. As reported in the graph, the results obtained show that Sox2 and Ssea4 were expressed at a quite similar level in all hAFSC samples, while the expression of Oct4 and Nanog were much lower in slow samples (group I).

All these results confirm that a great inter patient heterogeneity exists among patients since the very early stage in culture.



*Figure 4.1.4 Cytofluorimetric analysis of stemness markers. The expression of four stemness markers was analysed in samples from the three groups. Slow samples (group I) are in white, middle proliferating samples (group II) in light grey and high proliferating patients (group III) in dark grey. Data are representative of three independent experiments. ***p value < 0.001, significantly different from group I; ##p value < 0.01; ###p value < 0.0001 significantly different from group II.*

4.1.2. Senescence-associated molecular changes in AFSCs culture

As shown above, during passaging, cells derived from different AF donors differently stop their growth during the culture. First of all, I noticed that the expression of the stem cell marker Oct4 (green) was reduced at late passages and this decrease was more evident for samples that had minor expression of it since the first days in culture [Figure 4.1.5].

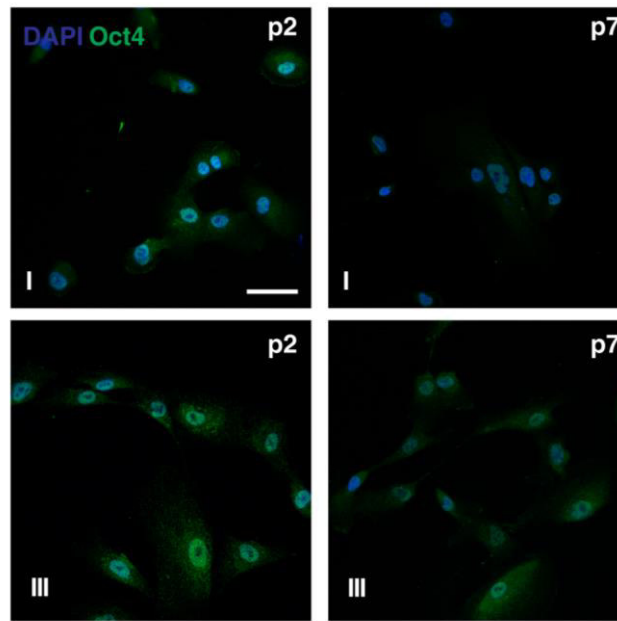
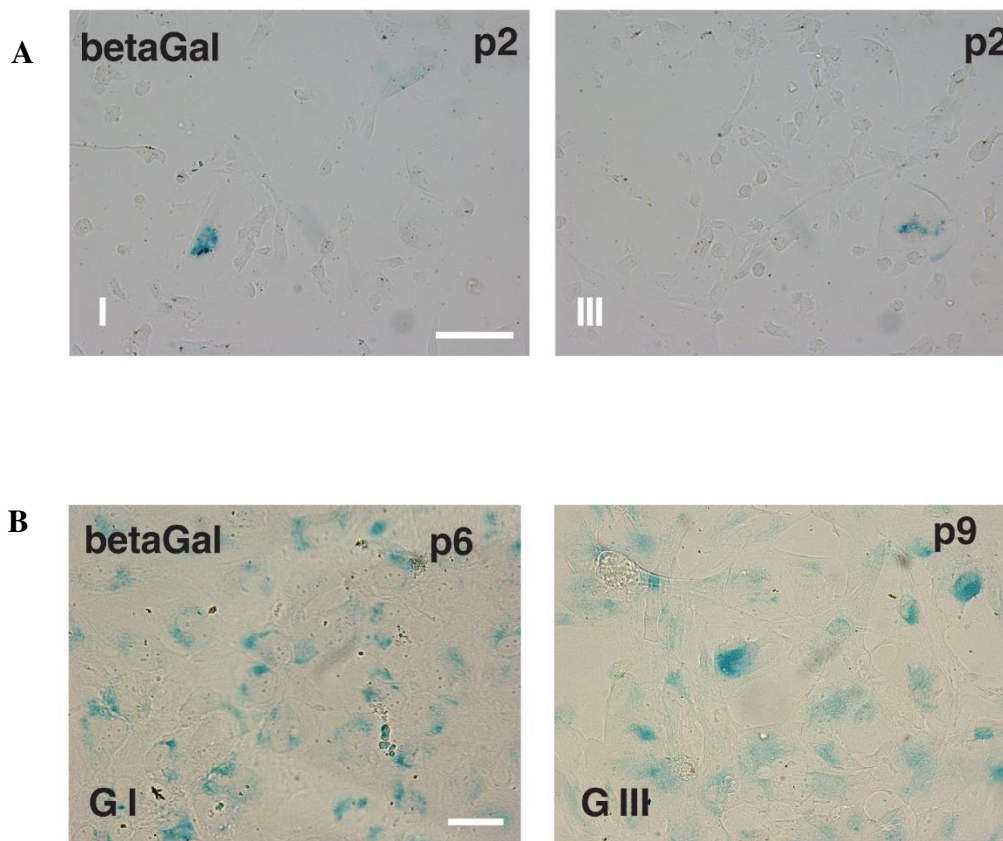


Figure 4.1.5 Oct 4 decrease during culture passage. Representative immunofluorescence of hAFSC from slowest group I (above) and faster group III (below). Cellular nuclei were stained with DAPI (blue) and with Oct4 (green). Scale bar= 10 μ m. Images are representative of analysis performed in 21 samples.

Besides, I observed that AFSCs senescence was accompanied by typical morphological changes and cells became enlarged and flattened. In particular, I noticed that these senescence-associated changes occurred later in AFSCs samples showing a relatively faster level of proliferation.

Among the biomarkers have been used for quantitative assessment of cell senescence, the increase of senescence-associated β -galactosidase (SA- $\beta\beta$ gal) activity is one of the most used. As for the morphological changes, also in this case, a slightly more intense positivity for SA- $\beta\beta$ -gal activity (blue staining) was evident for group I than group III at early passages (figure), while the same amount (about 70%) of SA- $\beta\beta$ -gal-positive cells was detected in groups I and III at different late passage, p6 and p9 respectively [Figure 4.1.6].



*Figure 4.1.6 **β -Galactosidase staining.** Representative photos of the senescence β -galactosidase assay. Cells in blue are positive for the staining. In the panel A, cells from group I (slow) and group III (fast) at second passage in culture are reported. In the panel B, it is shown as cells from the two different group reach the same amount of positivity (70%) at different culture passages. Images are representative of analysis performed in 21 samples.*

Scale bar= 30 μ M.

To gain more insight into the molecular characteristics of AFSCs senescence, I analysed also the protein level of the classical senescence-associated markers, p16INK4A (p16), p21WAF1 (p21), p53, and p14ARF (p14) as DNA damage index, in all groups of cell cultures at early and late passage. As demonstrated by western blot analysis in Figure 4.1.7, AFSCs cultures of group I showed significant higher p16 expression, as compared to group III.

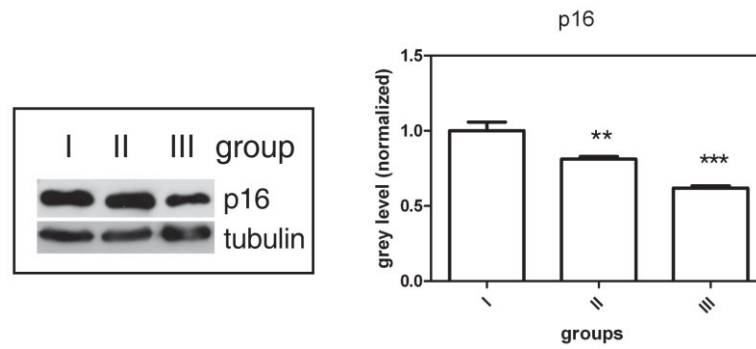
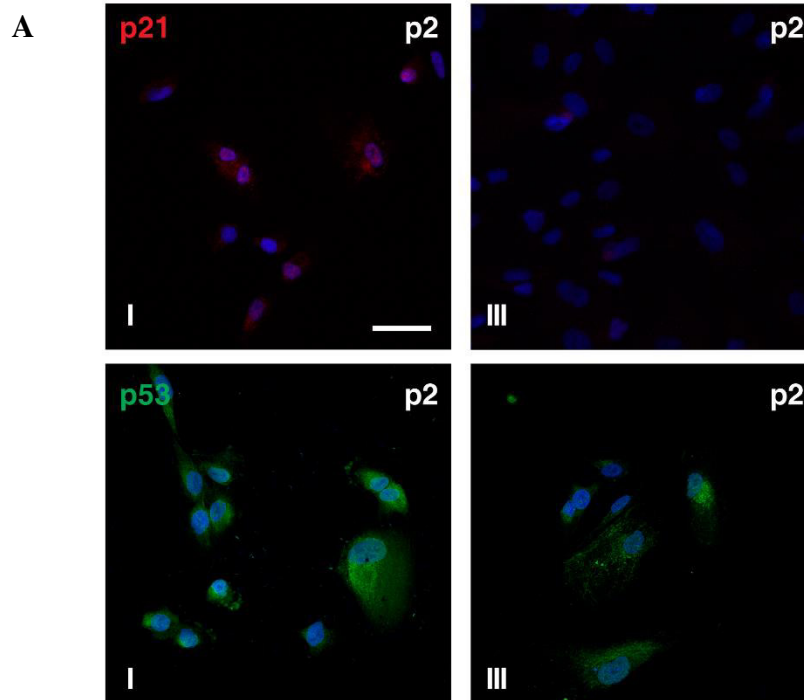


Figure 4.1.7 **p16 expression profile.** Western blot analysis of hAFSCs revealed with anti-p16 antibody. Tubulin detection was used to normalize data. In the right panel, the graph shows the densitometry analysis of the experiment. Data are representative of three independent experiments. ***p value < 0.001, ****p value < 0.0001.

Moreover, I observed more positivity for p53 (green) and p21 (red) in faster senescent cells (group I) than in group III by confocal microscopy, both in samples at late passage and at early passage, as shown in Figure 4.1.8 A and B. Also the immunofluorescence analysis of pH2A.X (Figure 4.1.8 C) showed a higher number of positive cells in group I, suggesting a correlation with the expression levels of p16 and p53/p21.



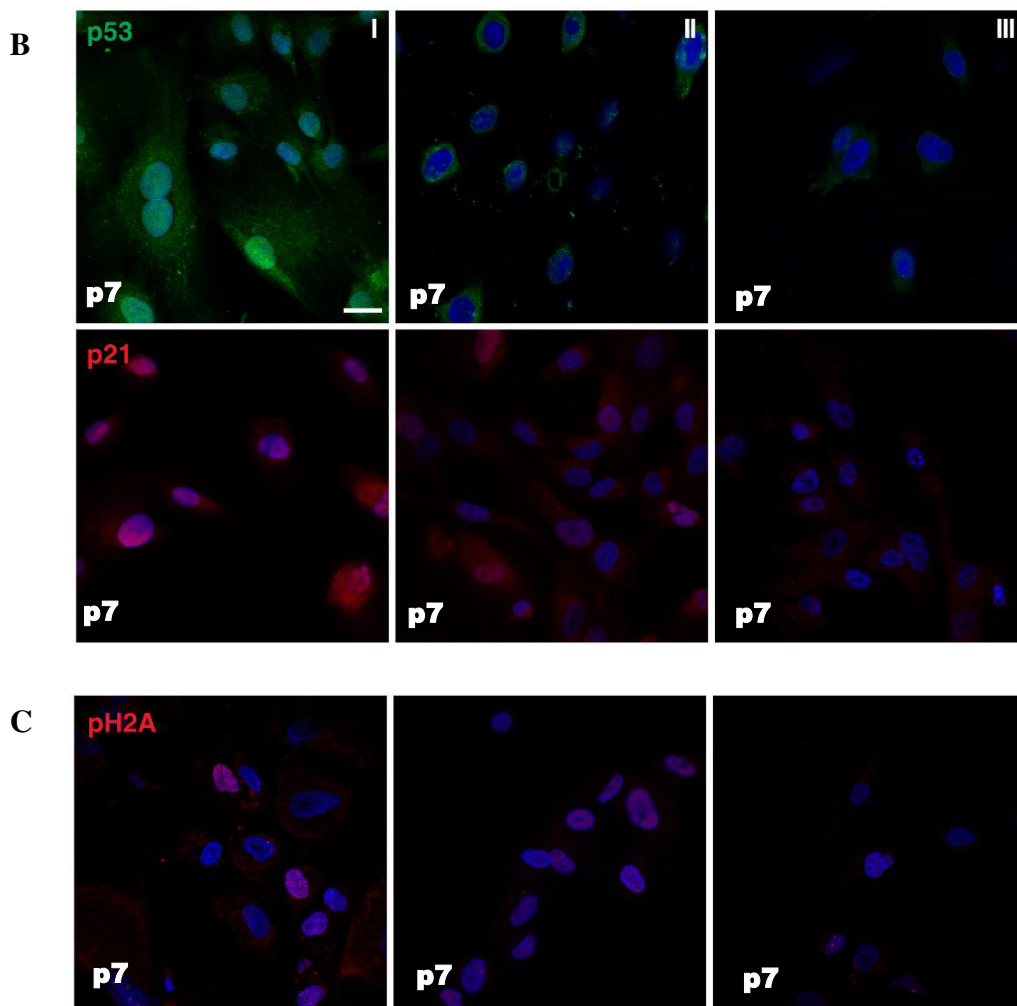


Figure 4.1.8 Senescence-associated markers. Representative confocal images of p21 (red), p53 (green) and pH2A (red) at passage two (panel A) and/or passage seven (panel B and C) in culture. I= group I (slow), II= group II (medium), III= group III (fast). Scale bare= 10 μ M. Images are representative of analysis performed in 21 samples.

All these results corroborate the idea that different patients behave differently in culture conditions and enter in a senescent program after different periods of time.

4.1.3. Differences in nuclear redox state of AFSC groups during their culture

Since oxidative stress can cause DNA damage and ROS are involved in the maintenance of stem cells homeostasis¹⁰¹, I tested total reactive oxygen species (ROS) levels in cultures at early (p1) and late passages (p7). The graph of Figure 4.1.9 shows that samples of group I (faster senescent cells, in white) have a content of ROS 10 times higher than group II (light grey), both at the first and at the seventh passage.

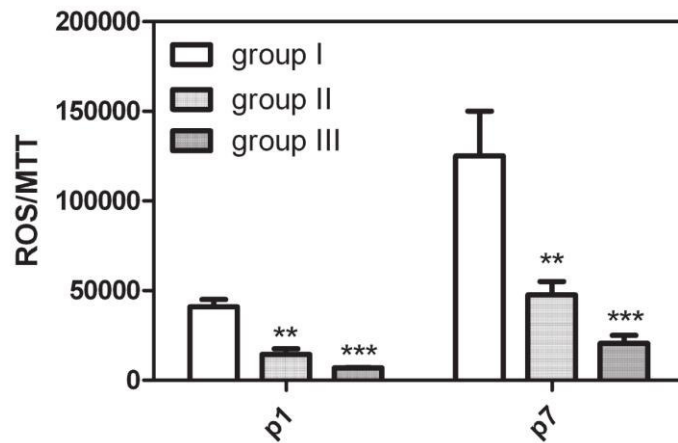


Figure 4.1.9 ROS levels. Representative graph showing fluorescence, obtained with ROS probe (DCFH-DA), normalized to MTT viability values of hAFSCs samples at 1st (left) and 7th (right) culture passage. The slowest group is in white, medium proliferating group in light grey, the fastest in dark grey. ROS were analysed in 11 different patients. *** $p < 0.0001$; ** $p < 0.01$ significantly different from group I.

Moreover, my lab has previously demonstrated that a ROS producing enzyme, the isoform 4 of NADPH oxidase (Nox4), localizes in a spot distribution into the nuclei of hAFSC, depending on their cell cycle state¹³³. Here I confirm this observation thanks to a larger cohort of samples better characterized for clinical aspects and stem cell features. Indeed, the higher Nox4 nuclear localization in group I is shown in confocal images of Figure 4.1.10. Interestingly, the nucleoplasmic Nox4 is, in some images, not only in a spot-like but also in a ring-like distribution.

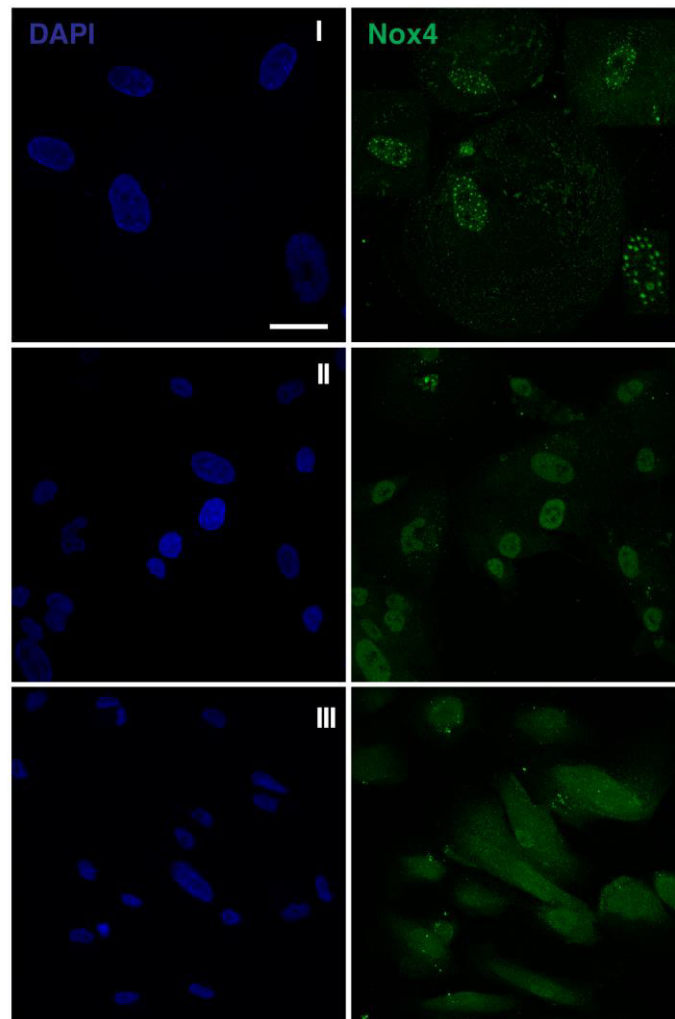
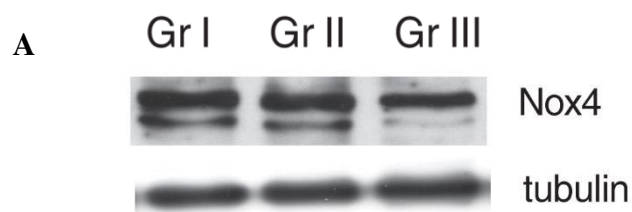


Figure 4.1.10 Nox4 distribution in hAFSC. Representative confocal images showing Nox4 distribution in the three AFSC groups. Cells were stained with DAPI for nuclei visualisation (blue) and with anti-Nox4 antibody (green). Scale bar= 10 μ M. Images are representative of analysis performed in 21 samples.

Also western blot experiments confirmed the higher expression of Nox4 enzyme in group I than group III (Figure 4.1.11 A). Moreover, the analysis of total lysates (Figure 4.1.11 B) indicates the increase, showed in this case in group II, of a double band at 74-72 kDa by time in culture.



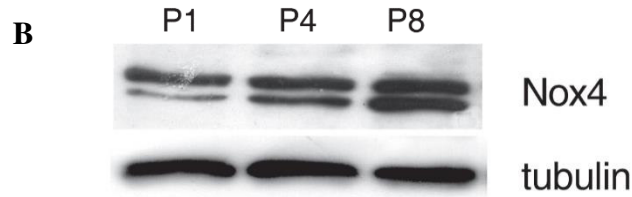


Figure 4.1.11 Nox4 expression in hAFSC. Representative western blot image of Nox4 expression in the three groups (Panel A) and during passages in culture (Panel B). Tubulin detection was used to normalize the data.

Data are representative of three independent experiments.

Since, it was found that oxidative stress can modulate sirtuins function and localization^{265,266}, I decided to test Sirtuin 1 (SIRT1) expression. In fact, sirtuins are a class of NAD⁺-dependent protein deacylases with important implications in aging²⁶⁷. In particular, the regulatory role of SIRT1 is predominantly linked to p53 activity. Interestingly, its activation in aged cells protects the cells from p53-dependent apoptosis or senescence²⁶⁸. As reported in Figure 4.1.12 A, I found that samples of group I have an expression of SIRT1 much lower than group III, moreover the effect of culture passaging decrease of SIRT1 expression, as expected (Figure 4.1.12 B).

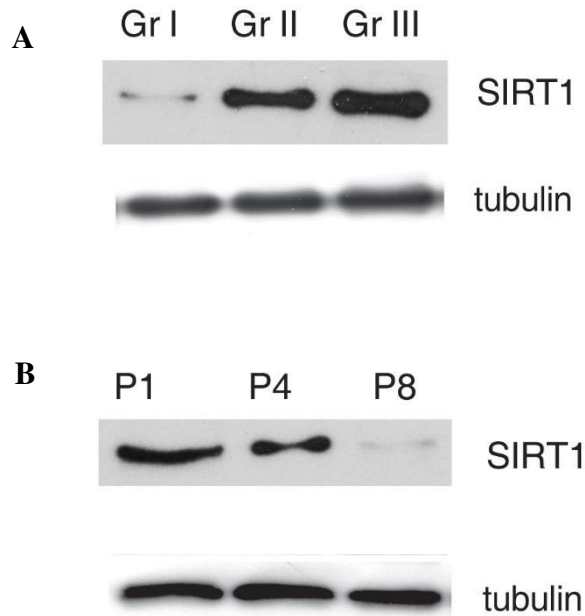


Figure 4.1.12 SIRT1 expression in hAFSC cells. Representative western blot from hAFSC lysates revealed with anti-SIRT1 antibody. Evaluation of tubulin expression was performed to normalize the data. Data are representative of three independent experiments.

4.1.4. Nox4 and prelamin A interaction in human amniotic stem cells

Since this peculiar distribution of Nox4 enzyme in AFSC nuclei, I started wondering which nuclear structure could mediate it.

Preliminary mass spectrometry analysis of proteins coimmunoprecipitating with Nox4 extracted from isolated nuclei hinted at the interaction of Nox4 with lamin A proteins (Figure 4.1.13).

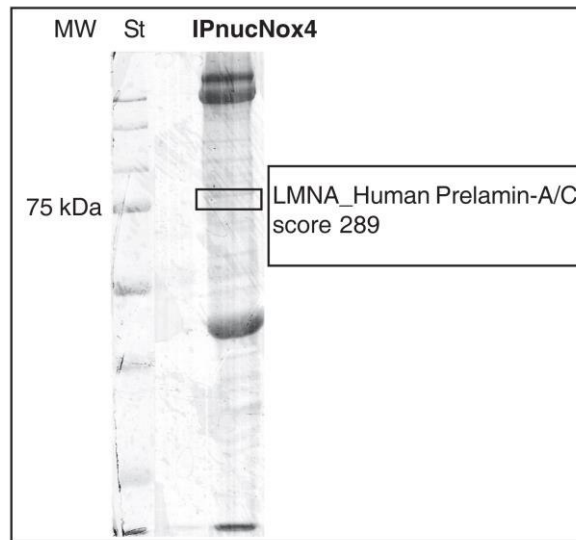


Figure 4.1.13 Mass spectrometry experiment. The picture shows the Coomassie staining of proteins immunoprecipitated with Nox4 and separated by SDS page. Black highlighted band corresponds to prelamin A/C. Data are representative of three independent experiments.

However, since nuclear Nox4 staining does not overlap neither with nuclear envelope nor with nucleoli, I wondered if this interaction could involve an immature form of lamin A, such as prelamin A.

Western blot analysis revealed the prelamin A accumulation during passaging (Figure 4.1.14 A), suggesting a positive correlation between prelamin A expression and cell aging, also parallel to Nox4 increase. Indeed, western blot of Figure 4.1.14 B probed with anti-prelamin A demonstrates the presence of a higher band (74 kDa), that is more expressed in samples from group I (faster senescent cells), although at lower intensity as compared to the positive control (cells treated with mevinolin). Moreover, the band corresponding to mature lamin A decreased: this effect is consistent with an accumulation of its immature form, prelamin A.

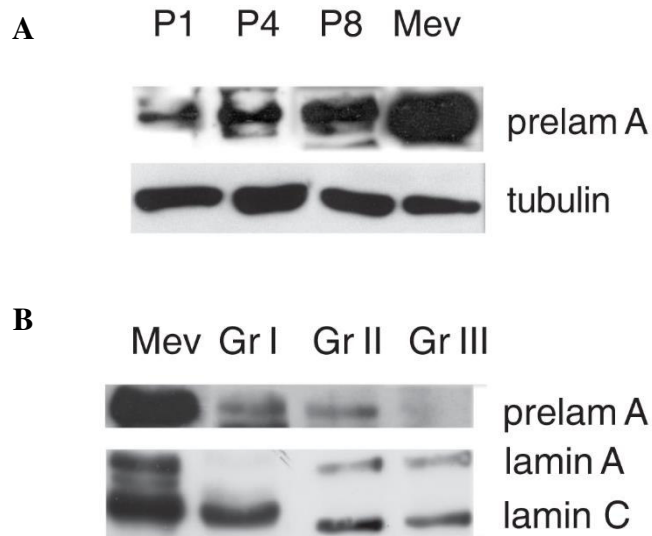


Figure 4.1.14 **Western blot analysis of hAFSC lysates.** Representative image showing the increase of prelam A expression through passages in culture (panel A) and differences in prelam A and lamin A levels among the three hAFSC groups. Data are representative of three independent experiments. Tubulin was used as loading control.

The accumulation of this protein was confirmed by immunostaining of prelam A and farnesylated prelam A in hAFSC that revealed an extensive presence of punctate dots and fibrous aggregates at later passages in group II (Figure 4.1.15), but also at early passage in group I (faster senescent cells). Interestingly, some cells from group I samples showed a drop-like staining, likely localized into the nucleoli.

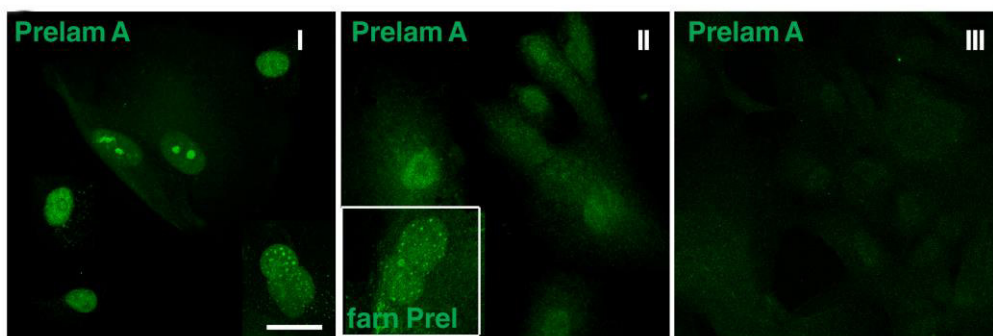


Figure 4.1.15 **Prelamin expression in hAFSC cells.** Immunofluorescence confocal images showing prelam A expression (green) in the three groups of amniotic fluid stem cells. The doubled magnification image in the white square of group II shows farnesylated prelam A (green). Scale bar= 10 μ m. Images are representative of analysis performed in 21 samples.

Double staining for prelamin A and pH2A.X revealed that the simultaneously labelling in the same cell scarcely occurs, as shown in Figure 4.1.16.

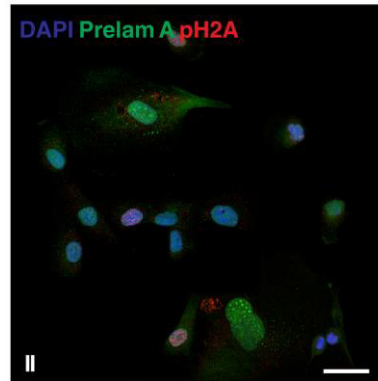


Figure 4.1.16 Co-immunostaining of prelamin A and pH2A. The figure shows prelamin A (green) and pH2A (red), a DNA damage marker, in group II hAFSC cells. Scale bar= 10 μ m. Images are representative of analysis performed in 21 samples.

Conversely, double staining for Nox4/prelamin A and Nox4/farnesylated prelamin A showed a partial colocalization of these two proteins in the nuclear spots (Figure 4.1.17).

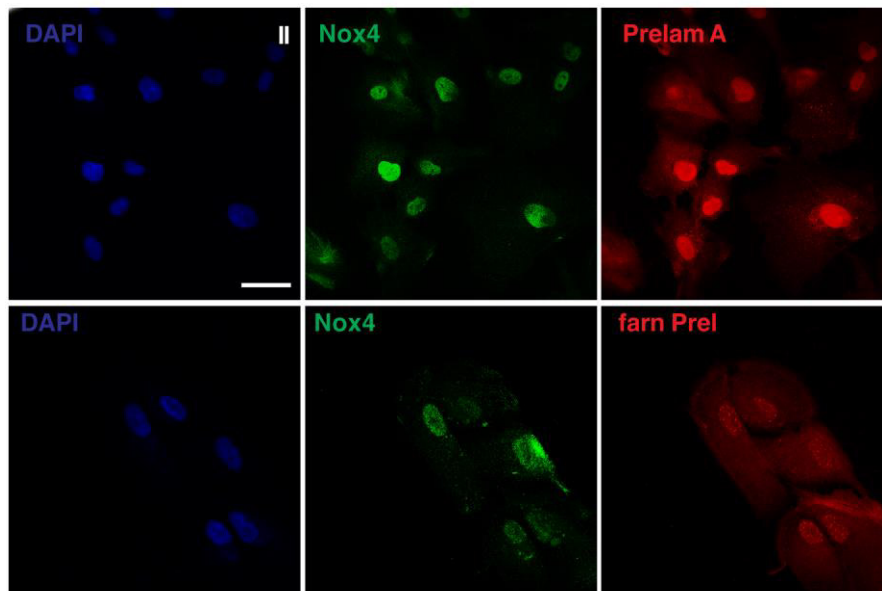


Figure 4.1.17 Co-localization between prelamin A and Nox4. Cells were stained with DAPI (blue), Nox4 (green) and prelamin A (red). Scale bar= 10 μ m. Images are representative of analysis performed in 21 samples.

This interaction was confirmed by immunoprecipitation of nuclear lysates with anti-prelamin A or farnesylated prelamin A antibody then immunoblotted with anti-Nox4, or immunoprecipitated with anti-Nox4 antibody and detected for anti-prelamin A, as shown in Figure 4.1.18.

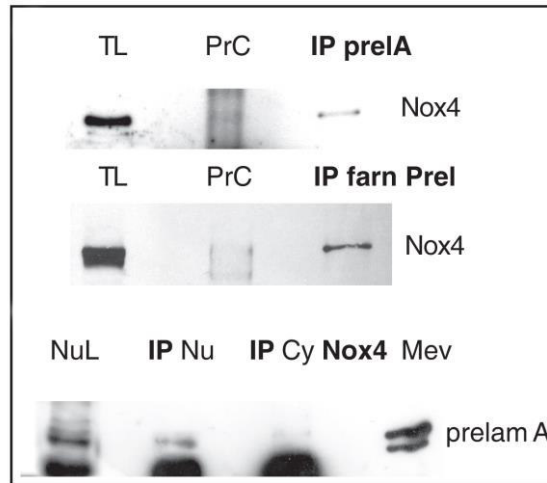


Figure 4.1.18 Nox4 and prelamin A interaction. Western blot analysis of total lysate (TL) and immunoprecipitation (IP) experiment of TL with Prelamin A (above) or farnesylated Prelamin A (in the middle) antibody then revealed with anti-Nox4. The third membrane (bottom) shows western blot analysis of nuclear lysate (NL) and immunoprecipitation experiment of nuclear lysate (IP Nu) and cytoplasmic lysate (IP Cy) with Nox4 antibody then revealed with anti-Prelamin A. Mevinolin (Mev) treatment was performed to show a prelamin A positive control. Data are representative of three independent experiments performed on patients from group I and II.

To understand the role of oxidative stress in prelamin accumulation, I treated the cells with two natural antioxidants, sulforaphane (SF) and epigallocatechin gallate (EGCG). These two phytochemicals were chosen since they possess different chemo-physical properties (EGCG is more hydrophilic than SF) and because they could modulate various cell pathways. As shown in Figure 4.1.19, the prolonged treatment (11 days) with these two molecules reduced the expression both of nuclear Nox4 (green) and prelamin A (red), supporting the idea that oxidative stress can have a role in the accumulation of this protein.

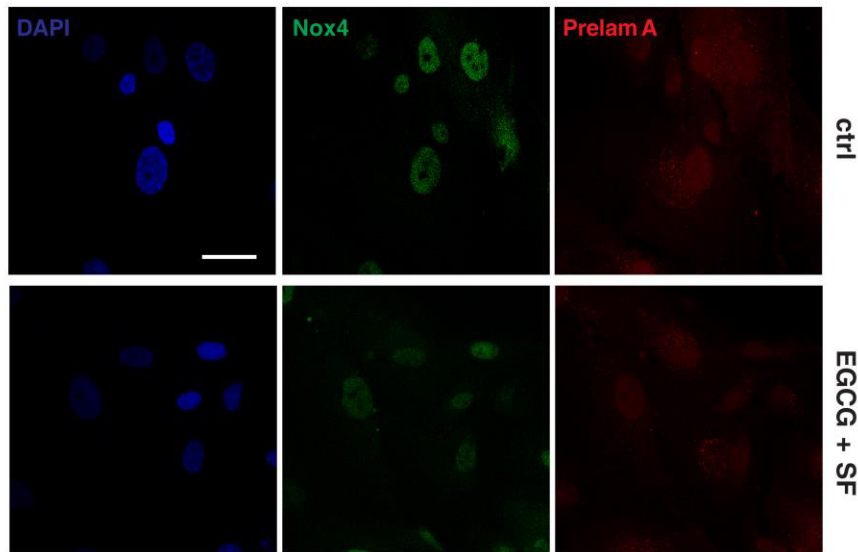


Figure 4.1.19 **Effect of ROS decrease on Nox4 and prelamin A expression.** Representative confocal images of hAFSC cells stained with DAPI (blue), Nox4 (green) and prelamin A (red) treated or not with epigallocatechin gallate (EGCG) and sulforaphane (SF). Data are representative of three independent experiments performed on patients from group II. Scale bar= 10 μ m.

Moreover, I investigated the correlation between prelamin A/ Nox4 accumulation and hAFSC functionality. In particular, I observed that the increase of prelamin and Nox4 is negatively correlated to the adipogenic differentiation capability of AFSC. In fact, Figure 4.1.20 shows that group II, which presents a medium stemness profile but accumulates prelamin A, expressed a significantly lower level of the adipogenic marker PPAR γ , compared to group III after exposure to adipogenic medium for 3 weeks. These data are in accordance with studies showing that prelamin A accumulation causes defects in the differentiation of human MSCs to adipocytes in an *in vitro* model of LMNA-lipodystrophy²⁶⁹.

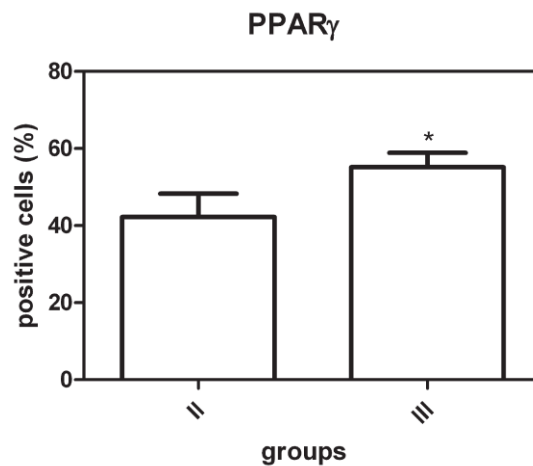


Figure 4.1.20 **Adipogenic differentiation ability.** Graph showing the cytofluorimetric analysis of PPAR γ expression in hAFSC from group II (left column) and III (right column) after exposure to adipogenic differentiation medium. Data are the result of three independent experiments. * p value < 0.05.

4.1.5. Exploring the meaning of Nox4 and prelamin A interaction

Since the peculiar distribution of Nox4 and prelamin A inside the nucleus, I started to investigate if other structures could be involved in their accumulation. Given the involvement of PML-nuclear bodies (PML-NBs) in aging and in protein sequestration/degradation²⁷⁰ and the similarity between their structure and that of Nox4/prelamin A intranuclear aggregates, I hypothesized that these compartments might have a role in their nuclear localization.

I first explored the localization of PML protein in the different hAFSC groups. As visible in Figure 4.1.21 PML-NBs morphology and number (in red) were lower in patients of group III (slower senescent cells), with PML-NBs appearing as classical punctate structures. In group I (faster senescent cells), the dimension of classical PML-NBs increased and the number of aberrant ring-like and thread-like PML-NBs appeared.

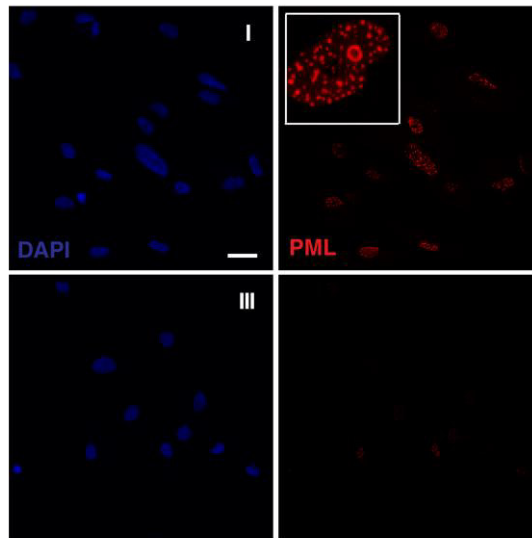


Figure 4.1.21 PML bodies morphology in hAFSC cells. Representative confocal images of PML bodies in group I (above) and group III (bottom). Cells were stained with DAPI (blue) and anti-PML protein (red). Images are representative of analysis performed in 13 different hAFSC samples. Scale bar= 10 μ m.

Then, I checked whether prelamin A colocalized with these structures, and I could observe that this was the case. Double immunostaining with anti-PML and anti-prelamin A antibodies on hAFSC group I using confocal microscopy showed that part of intranuclear farnesylated prelamin A content colocalized with the PML bodies, seeming to be sequestered inside them in some regions. A similar result was obtained for Nox4 and PML double staining Figure 4.1.22.

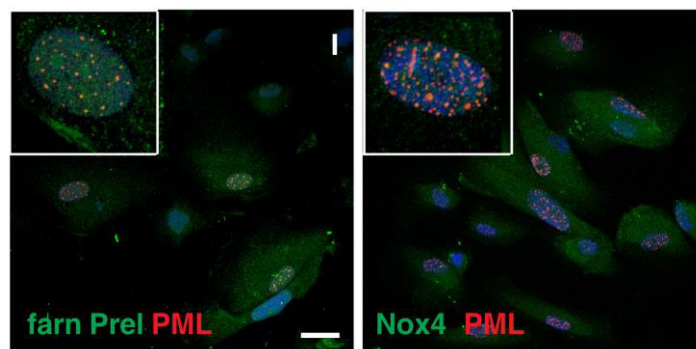


Figure 4.1.22 Colocalization between prelamin A or Nox4 and PML. Confocal images showing colocalization between prelamin A (left) or Nox4 (right) with PML bodies in AFSC. Cells were stained with DAPI to visualize the nuclei (blue), PML protein (red), farnesylated prelamin A (green) or Nox4 (green). Images are representative of analysis performed in 13 different hAFSC samples. Scale bar= 10 μ m.

As mentioned above, PML proteins can be sumoylated²⁰⁷ and most PML-associated proteins undergo SUMO-conjugation or contain a SUMO interaction motif (SIM)¹⁹². To investigate post translational modifications of nuclear Nox4, I carried out immunofluorescence experiments, using Nox4 and SUMO1 antibodies on hAFSC from group I (faster senescent cells). As shown in Figure 4.1.23, Nox4 and SUMO1 staining colocalized into PML-like intranuclear foci.

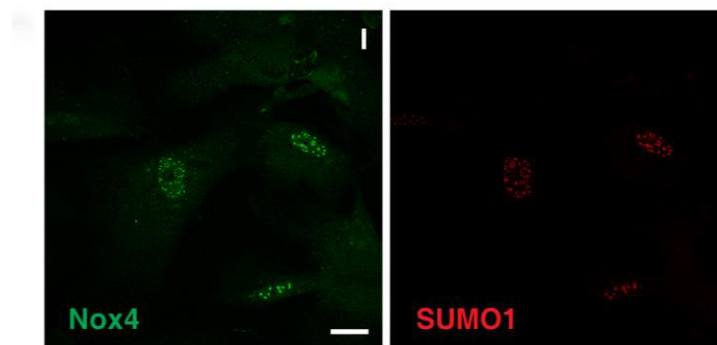


Figure 4.1.23 Colocalization between Nox4 and SUMO1. Representative images of hAFSC stained with Nox4 (green) and SUMO1 (red). Images are representative of three independent experiments performed on group I. Scale bar= 10µm.

Moreover, Western blot using SUMO1 antibody in Nox4 immunoprecipitated nuclear or cytoplasm lysates revealed that nuclear Nox4 is directly linked to SUMO1 or through another sumoylated protein with 74 kDa molecular weight, such as prelamin A, corroborating Nox4 localization within PML-NBs (Figure 4.1.24).

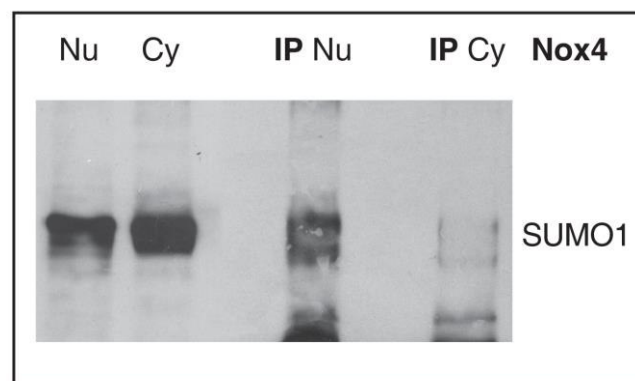


Figure 4.1.24 Interaction between Nox4 and SUMO1/sumoylated proteins. Western blot analysis of nuclear lysate (Nu), cytoplasmic lysate (Cy) and immunoprecipitation experiment of nuclei (Nu) and cytoplasm (Cy) with Nox4 antibody then revealed with anti-SUMO1. Data are representative of three independent experiments performed on patients from group I and II.

To better determine the effect of Nox4 sumoylation, I treated hAFSC of group II, since it shows intermediate features, with a membrane permeable sumoylation inhibitor (anacardic acid). Both western blot and immunofluorescence analyses (Figure 4.1.25) highlighted that SUMO inhibition induces an increase of Nox4 presence, both nuclear and cytoplasmic, suggesting that the inhibition of general sumoylation causes a block in the degradation pathway of Nox4.

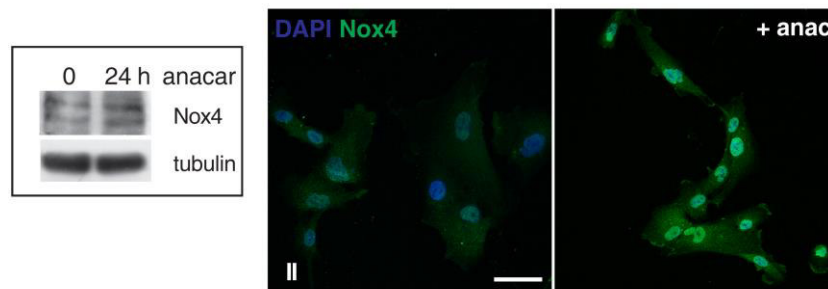


Figure 4.1.25 Effect of sumoylation inhibition on Nox4 expression. On the left, western blot of hAFSC total lysates treated or not with anacardic acid for 24 hours, then revealed for Nox4 and normalized on tubulin expression. On the right, confocal images of AFSC control or treated with anacardic acid, then stained with DAPI (blue) and Nox4 (green). Images are representative of three independent experiments performed on patients from group II. Scale bar= 10 μ m.

To determine whether proteasome inhibitors may influence the levels of nuclear Nox4, I performed treatment with MG132, an inhibitor of the proteasome pathway, and I investigated Nox4 expression by western blot and localization by immunofluorescence. Figure 4.1.26 indicates that MG132 induced an increase in Nox4 levels both in the cytoplasm but also into the PML nuclear foci.

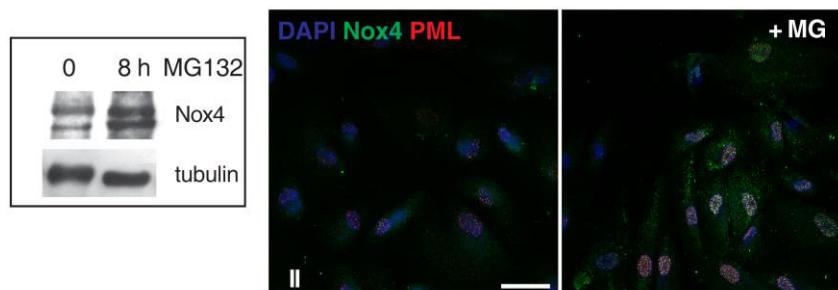


Figure 4.1.26 Effect of proteasome inhibition on Nox4 expression. Representative western blot (on the left) and confocal images (on the right) showing the effect of MG132 treatment on Nox4 expression. Tubulin was used as a loading control. Immunofluorescence was performed staining cells with DAPI (blue), Nox4 (green) and PML (red). Images are representative of three independent experiments on group II. Scale bar= 10 μ m.

Since it has been demonstrated that the effect of MG132 in Hutchinson-Gilford progeria syndrome (HGPS) fibroblasts unexpectedly resulted in a decrease of progerin staining intensity, instead of increasing progerin levels²²², I carried out immunofluorescence experiments for farnesylated prelamin A. Differently, in our case 8-hours treatment with MG132 induced the formation of large farnesylated prelamin A and PML intranuclear foci, not a decrease (Figure 4.1.27).

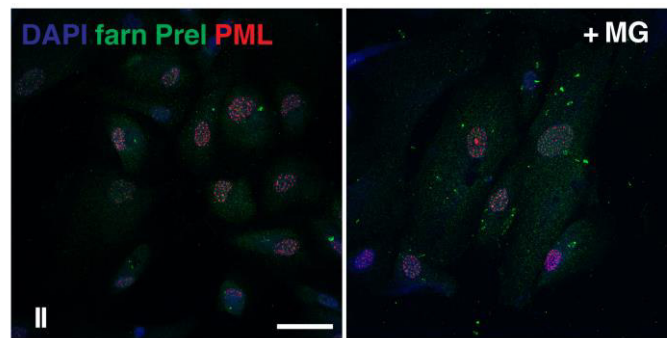


Figure 4.1.27 Effect of proteasome inhibition on prelamin A expression. Representative confocal images of hAFSC stained with DAPI (blue), farnesylated prelamin (green) and PML, in control condition or after MG132 treatment. Images are representative of three independent experiment on group II.. Scale bar= 10 μ m.

These data, also the one with the sumoylation inhibitor, confirmed that PML-NB sequestration *via* sumoylation modification may have a role in the proteasome degradation of these interacting proteins, events that could create an elimination flow of the ROS source Nox4, concentrating this protein in nuclear domains where a response to redox stress could be triggered and avoiding DNA damage maintaining the cells in a senescence state.

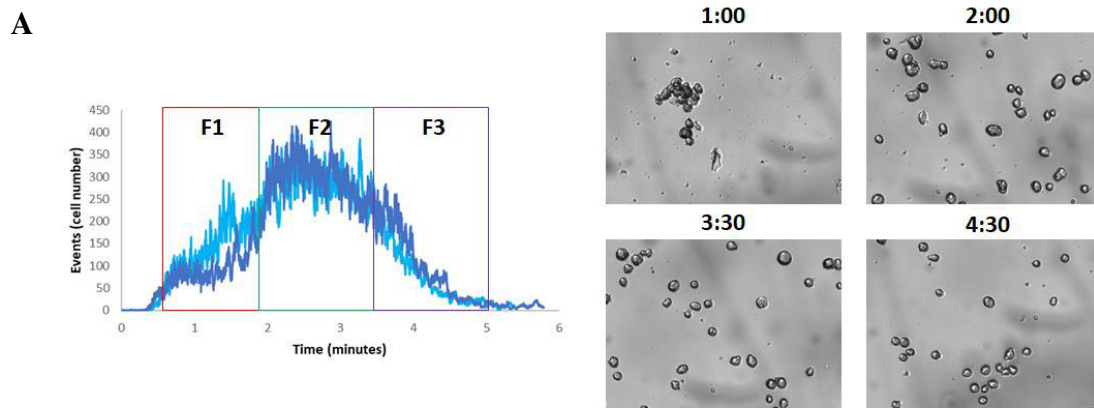
In conclusion, these data demonstrate that, also in the younger and more plastic cells of our body, like hAFSCs, differences in the capability to counteract oxidative stress exist among the individuals. Furthermore, in the more sensitive cells protective mechanisms are activated, but these are signs of poor self-renewal properties for stem cells that are not efficient for therapeutic purpose.

4.2. Investigation of c-kit⁺ hAFSC intrapopulation heterogeneity

4.2.1. hAFSC sorting

C-kit⁺ cells from 10 patients characterized in the previous part of the project, were expanded *in vitro* to reach at least two million of cells (around passage 5-6 in culture) and then sorted using the Celecator® technology. Depending on the sorting profile of each sample, three or four fractions were obtained.

In Figure 4.2.1 two sorting profile are reported. The graph of each left panel (A and B) shows the number of cells sorted as function of the time. In particular, hAFS cells were eluted between 1 minute and 8 minutes after the beginning of the run. Even if cells are in suspension, it is visible that the first sorted cells are in part aggregates and much bigger than the latest, demonstrating that this technology is able to discern different AFSC subpopulations.



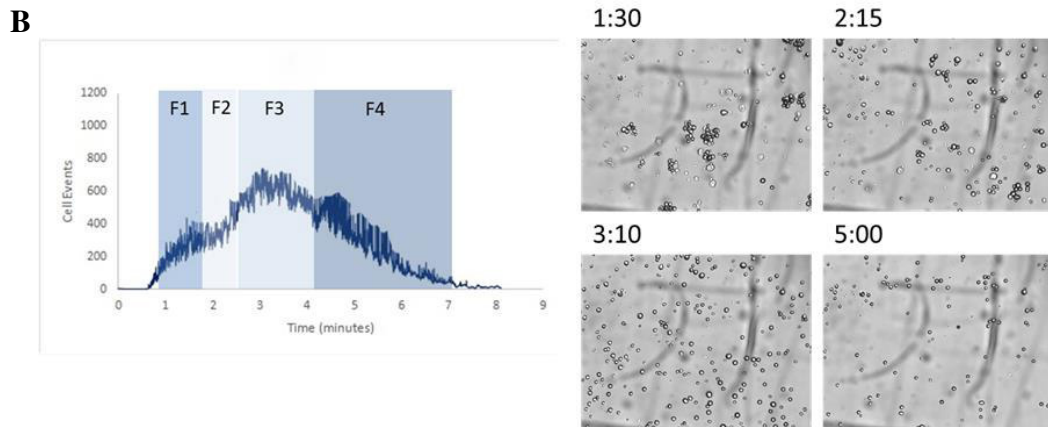
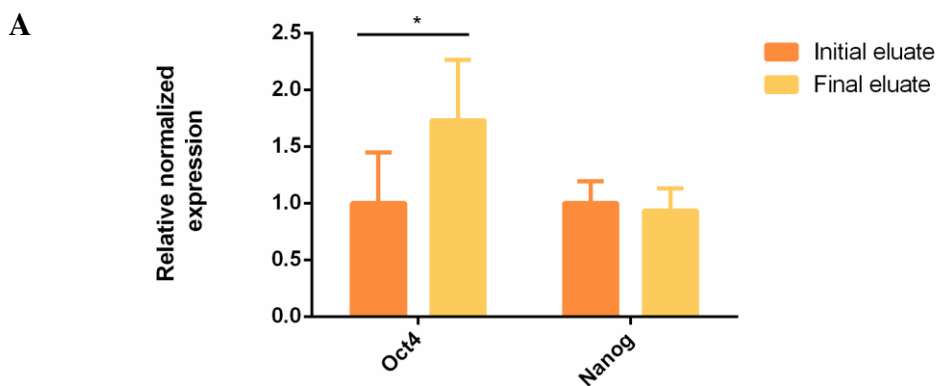


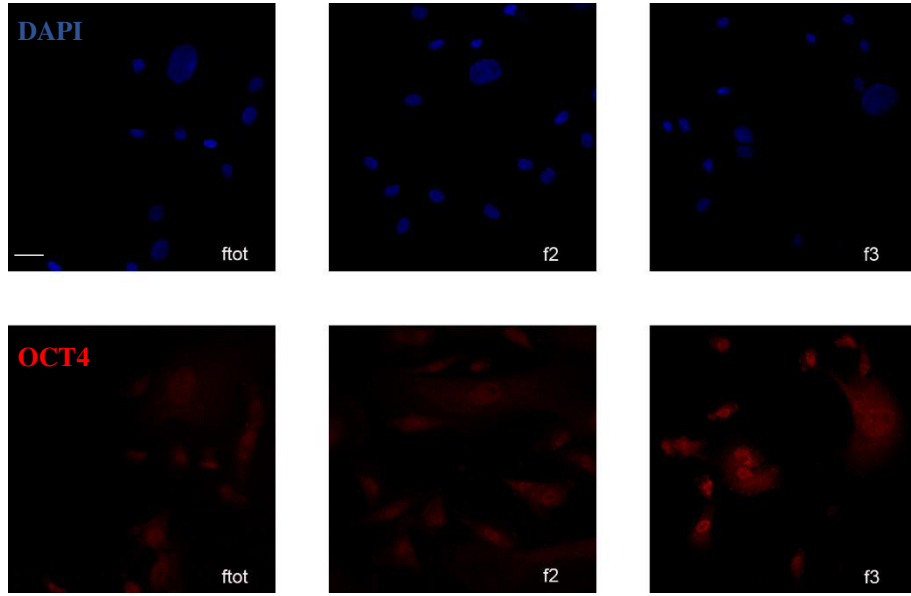
Figure 4.2.1 Celector® sorting profiles of hAFSC samples. Left panels show the number of cells sorted as function of the time. Three or four fractions can be discerned. In the right panels photos of cells swept along the channel at different time points are reported. Images are representative of analysis performed in 10 different hAFSC samples.

4.2.2. Characterization of hAFSC sorted cells

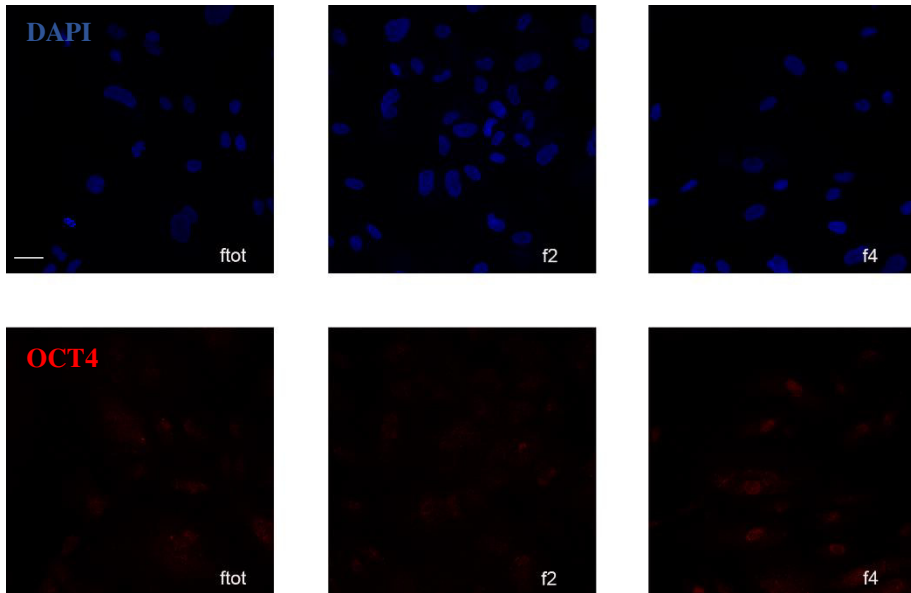
To investigate the characteristics of each eluted fraction, collected cells were first evaluated for the stemness markers Oct4 and Nanog, chosen because in our previously analysis they have showed major variability among the patients than the others. Quantitative PCR analysis revealed that only Oct4 expression was significantly higher in the last part of the eluates than the first, while no differences were observed in Nanog transcript expression (Figure 4.2.2 A). These differences in Oct4 expression were then confirmed by immunofluorescence as reported in Figure 4.2.2 B, C and D.



B



C



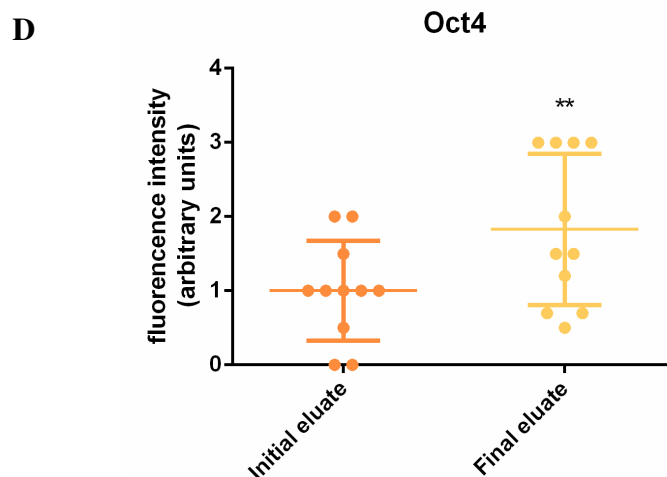
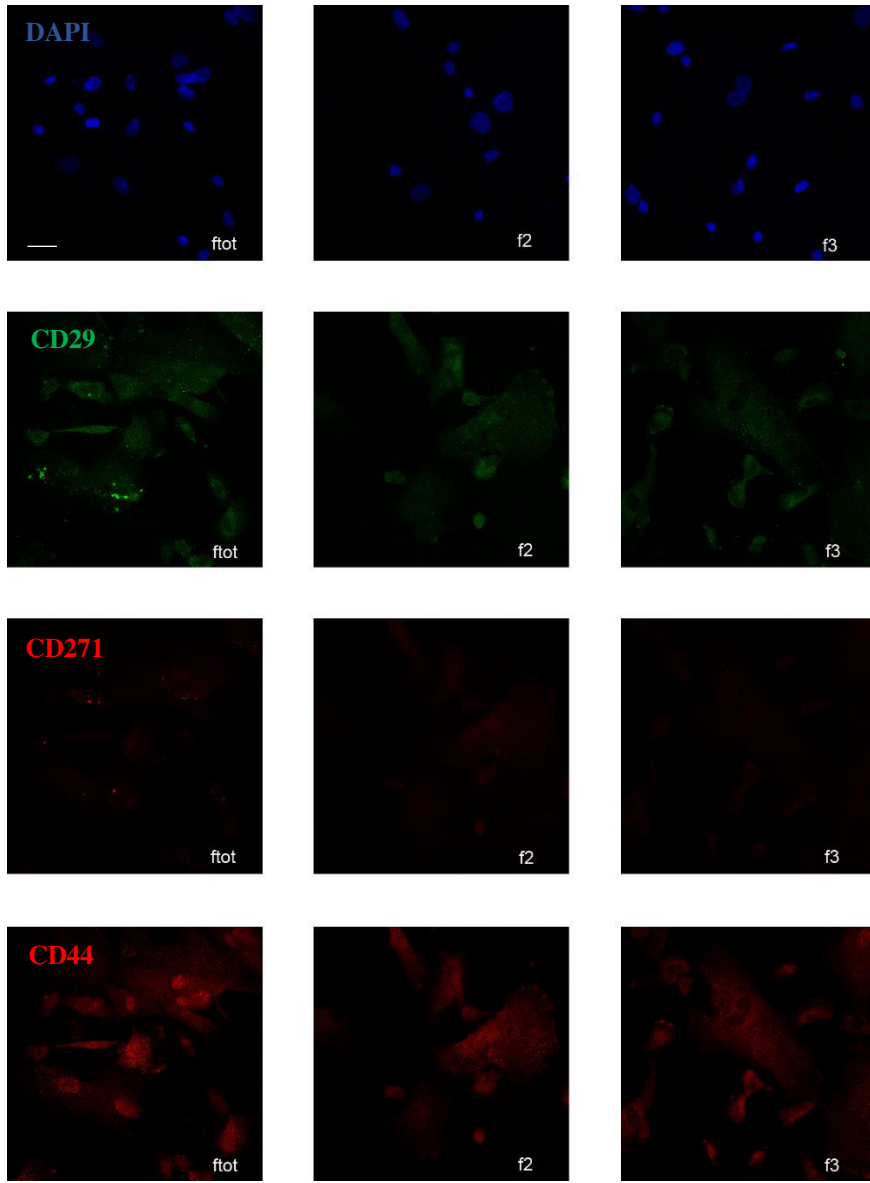


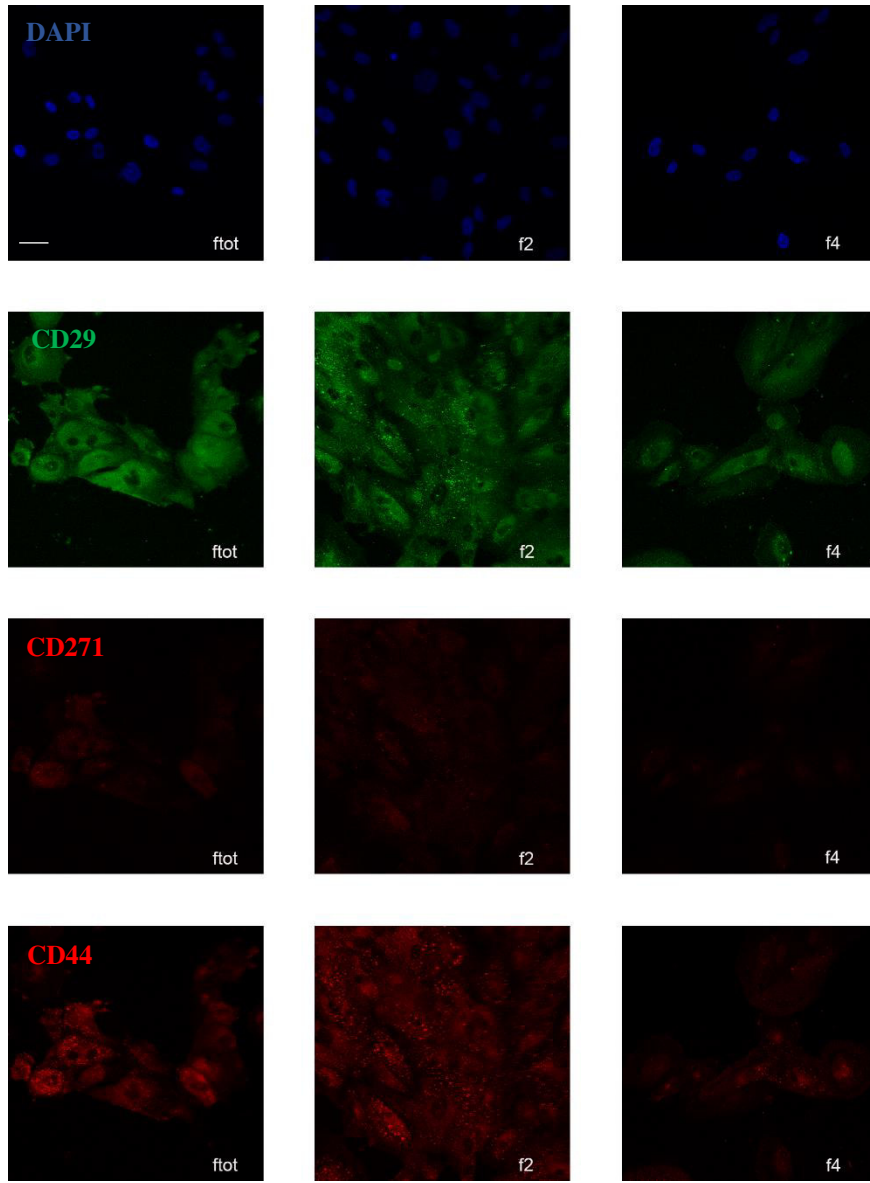
Figure 4.2.2 **Stemness markers expression in AFSC selected fractions**. In panel A, relative transcript levels of *Oct4* and *Nanog* are reported. *Tubulin* and *GAPDH* genes were used to normalized values. Six different samples were analysed * p value < 0.05. Statistical significance was obtained using a paired t -test. Panel B and C report representative confocal images of *Oct4* (red) expression in unfractionated samples (f0t), second fraction (f2), third fraction (f3) or fourth fraction (f4). DAPI (blue) was used to stain cellular nuclei. Scale bar= 10 μ m. Panel D represents the distribution plots of *Oct4* showing the cellular fluorescence intensity. The analysis was performed in 10 different hAFSC samples. A paired t test was applied. ** p value < 0.01.

Based on these results, cells were also stained for some of the mesenchymal markers CD29, CD271 and CD44. These markers were chosen not because they are always the most expressed in our cellular model²⁷¹, but because previous analysis showed that their expression is more variable among patients. As reported in the representative confocal images and relative statistical analysis of in Figure 4.2.3, in this case the last part of eluate always showed less mesenchymal markers expression then the first part, whatever was the sorting profile.

A



B



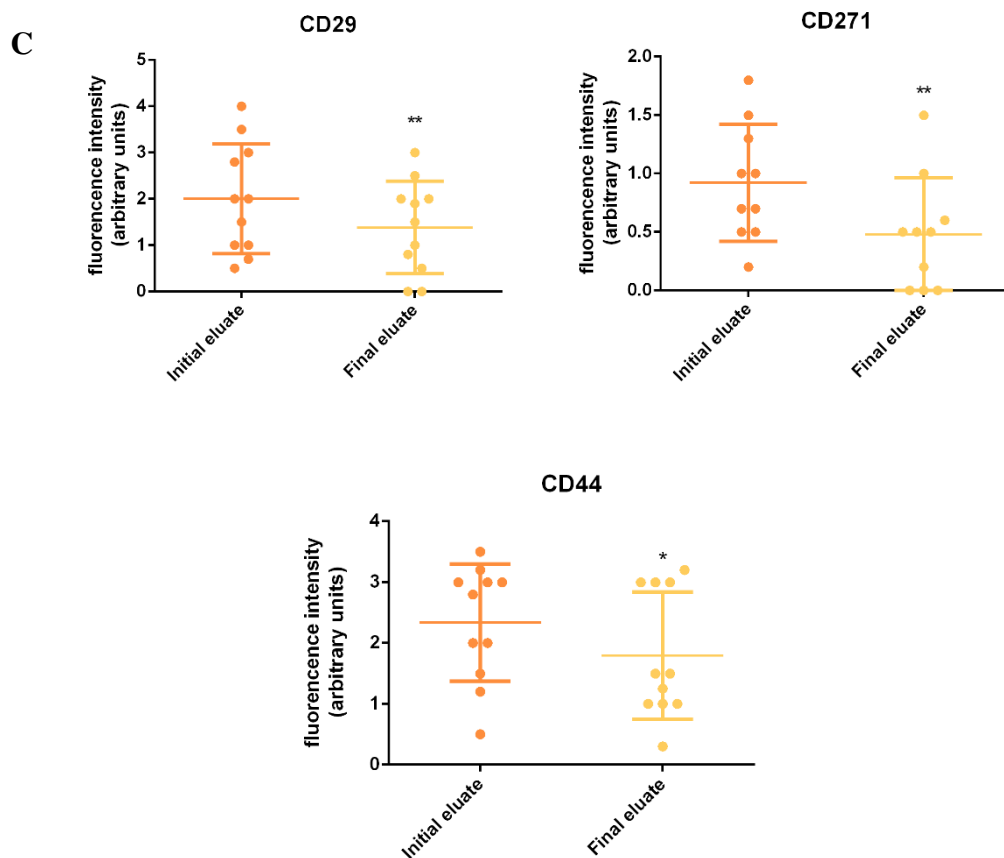


Figure 4.2.3 *Mesenchymal markers expression in AFSC sorted fractions.* A-B) Representative confocal images of hAFSC sorted fractions stained for DAPI (blue), CD29 (green), CD271 (red), CD44 (red) in unfractionated samples (f0t), second fraction (f2), third fraction (f3) or fourth fraction (f4). Scale bar= 10 μ m. C) Distribution plots of mesenchymal markers showing the cellular fluorescence intensity. A paired t test was applied. * p value < 0.05; **p value < 0.01.

All these data suggest that the last eluted cells preserved more stemness and plasticity, corroborating the idea that an enlarged and more flattened morphology is typical of cells entering in a senescent program⁹⁴.

4.2.3. Evaluation of fractions proliferation ability

Since in my initial part of PhD, I showed that a higher stemness associates with a better proliferation ability, I decided to check if this assumption occurs also among the fractions.

As the first experiments revealed that f3 and f4 had similar characteristics, I decided to ideally divide the obtained profiles in only two parts.

The analysis of the sorting plots area suggested a correlation between the distribution of cells among the fractions and the proliferation rate of each total unfractionated sample.

In fact, as reported in Figure 4.2.4 A and B, samples that showed a major distribution of cells in the first part (f1/f2) of the profile (example in Figure 4.2.1A), had a higher population doubling time (PDT) than those that presented more cells in the second part (f3/f4) of it (example of profile in Figure 4.2.1 B).

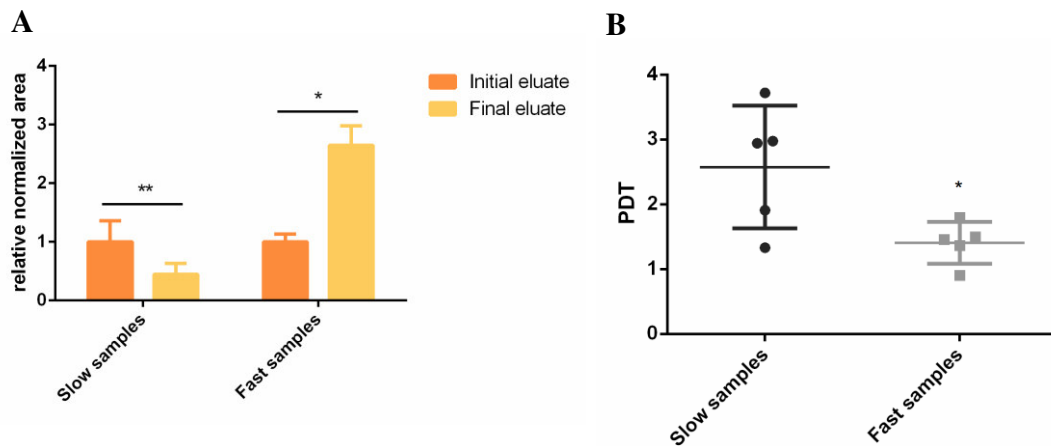
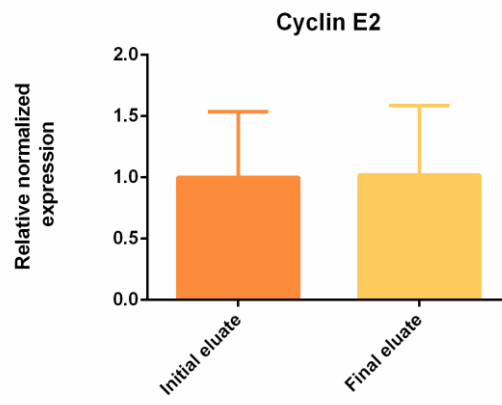


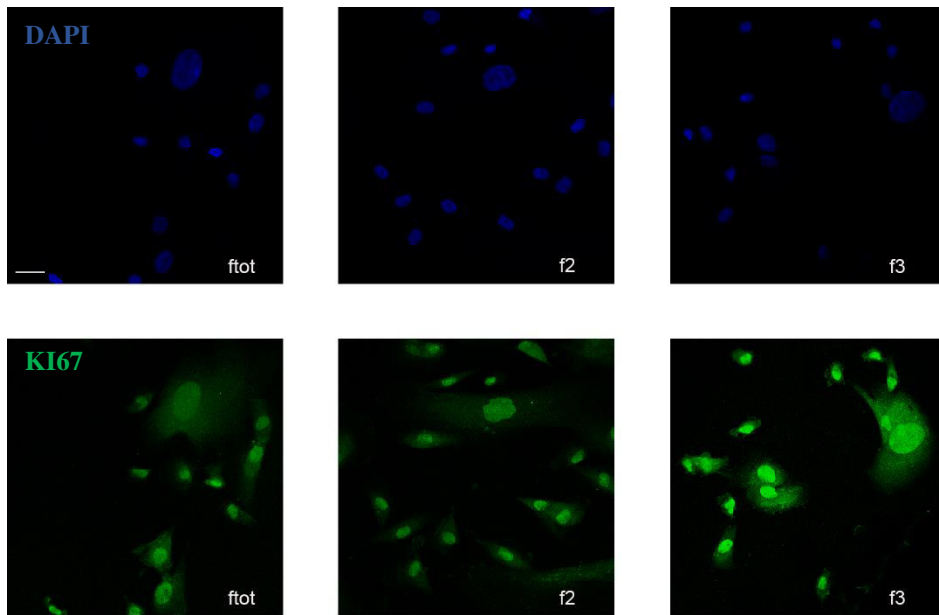
*Figure 4.2.4 Correlation between cells distribution among the fractions and population doubling time of unfractionated samples. Panel A shows the relative normalized area under each part of the Celecator® profile curve (Initial eluate= f1/f2; Final eluate= f3/f4). In panel B the doubling population time (PDT) at passage three of the two groups of samples (slow and fast) are reported. In both experiments 10 different hAFSC samples were analysed. *p value <0.05; **p value <0.001*

To better determinate if this different proliferation ability was really due to the different population composition among the samples, I checked the expression of two different cell cycle related proteins. Even if no differences were appreciated in cyclin E2 transcript levels (Figure 4.2.5 A), the expression of Ki67 protein, which reaches its maximum during the M phase²⁷², was higher in the last part of the eluate (Figure 4.2.5 B, C and D).

A



B



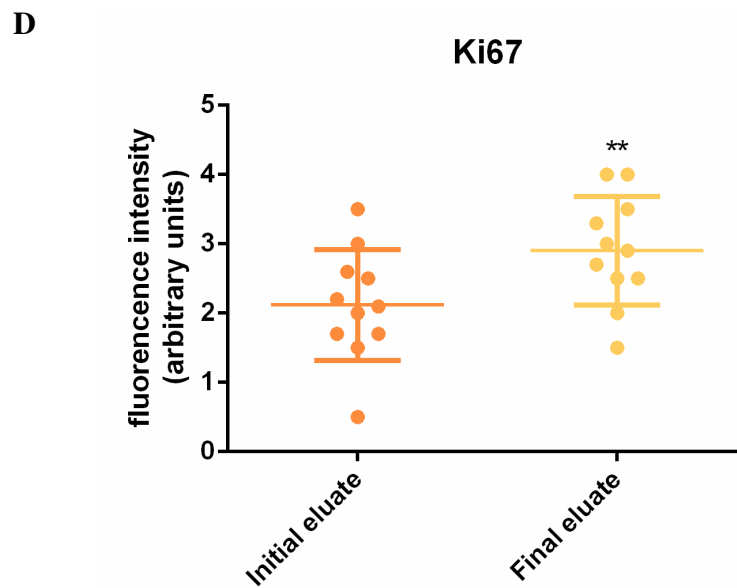
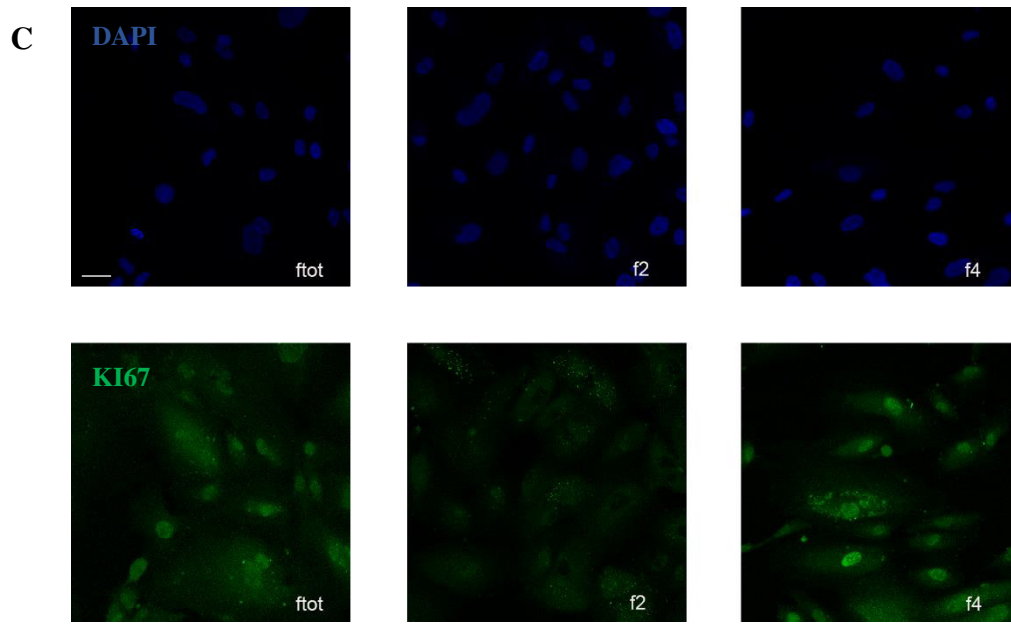


*Figure 4.2.5 Proliferation markers. A) Relative normalized expression of cyclin E2 transcript. Tubulin and GAPDH expression were used as housekeeping. Six different samples were analysed. B and C) Representative confocal images showing Ki67 expression (green) in unfractionated samples (ftot), second fraction (f2), third fraction (f3) or fourth fraction (f4). DAPI (blue) was used to stain the nuclei. Scale bar= 10 μ m. D) Distribution plots of Ki67 showing the cellular fluorescence intensity. A paired test was applied. **p value<0.01.*

These results suggest that last eluted cells are more proliferating and maybe other not evaluated factors are contributing to a faster cell cycle progression.

4.2.4. Analysis of senescence-associated molecular markers

Since an enlarged morphology and a reduced cell cycle progression are considered as hallmarks of cellular senescence⁹⁴, I evaluated some senescence associated markers. In particular, I focused on the cyclin-dependent kinase inhibitors, p16INK4A and p21WAF1, that are involved in the control of growth arrest by two major tumour suppressor pathways, p16INK4A/pRb and p53/p21WAF1. Significant differences between cells belonging to the first or the last part of the eluate were appreciated only in transcript levels of p21 (Figure 4.2.6), even if the same trend is visible also for p16.

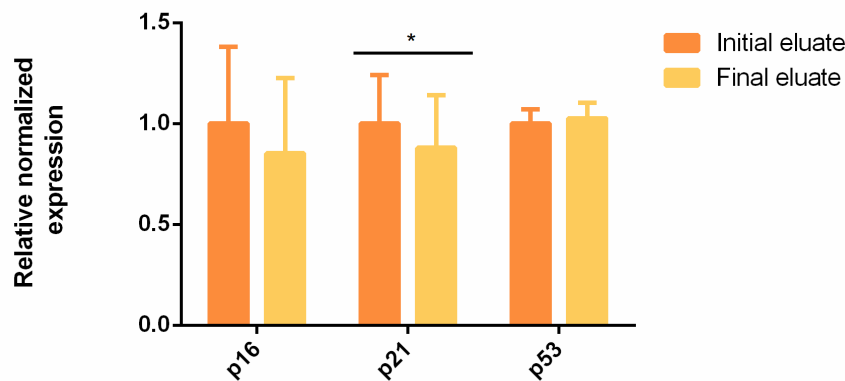


Figure 4.2.6 *Senescence-associated markers. p16, p21 and p53 relative normalized expression in the initial and in the final part of the eluate. Tubulin and GAPDH gene expression were used to normalize data. Six different samples were analysed. *p value < 0.05. Statistical analysis was performed using a paired t test.*

These data are not so clear as what found about cellular proliferation, but it should be considered that, due to technical limitations regarding the number of cells needed for the initial selection, experiments were carried out with cells at passage 7-8 in culture. As I demonstrated in my previous part of the project, in these conditions all samples showed an increase in the expression of these proteins, which can result in the flattering of differences inside the same sample, not excluding anyway that a further regulation could occur downstream these genes.

Furthermore, senescent cells undergo also metabolism alterations, resulting in an increase of the AMP:ATP and ADP:ATP ratios⁹⁴. The rise of AMP levels causes AMP kinase allosteric activation, which acts as a sensor of the reduced energetic state, further activating catabolic pathways while inhibiting biosynthetic ones, and regulating p53 and other targets²⁷³. For this reason, I measured AMPK transcript levels observing a

lower expression in the last part of eluate, demonstrating that f3/f4 cells maintain a better bioenergetic state (Figure 4.2.7).

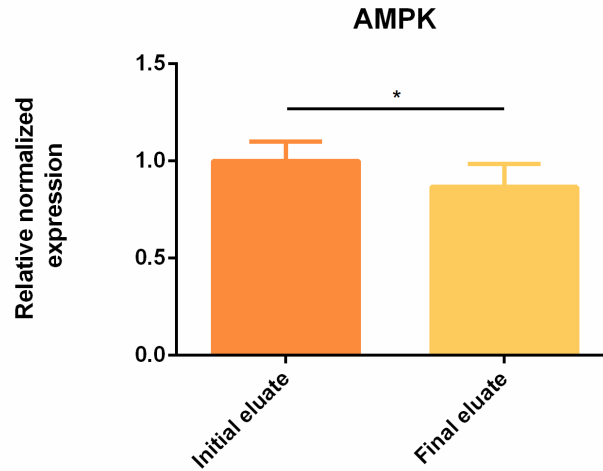


Figure 4.2.7 **AMPK expression.** Relative normalized expression in the initial and in the final part of the eluate. Tubulin and GAPDH gene expression were used to normalize data. Six different samples were analysed. * p value < 0.05. Statistical significance was obtained using a paired t-test.

4.2.5. Evaluation of overall transcriptome differences among sorted fractions

These results hinted to consider the final part of each fractioned sample as the one maintaining more pluripotent characteristics and proliferation ability also at late passages, even if only small differences were observed in the expression of the main senescence regulators.

To clarify this point, I had the opportunity to perform an RNA sequencing (RNAseq) analysis to evaluate the overall differences in the transcriptome of the fractions.

In fact, the evaluation of few genes is not always sufficient to explain the cellular behaviour, which is the result of the interplay among a huge number of genes and related proteins which can act at different levels inside multiple pathways. So, analysing the entire transcriptome gave a wider indication about each fraction behaviour.

First, RNAseq analysis allowed us to evaluate how samples clustered, if overall differences were more evident among different patients or the different fractions. The Principal Component Analysis reported in Figure 4.2.8, shows on the x axis the *principal component 1*, along which the major differences happen, while on the y axis the *principal component 2* and *3* identify differences of smaller scale.

In general, I observed that major variances tended to occur among the patients, but differences could be appreciated also inside each patient.

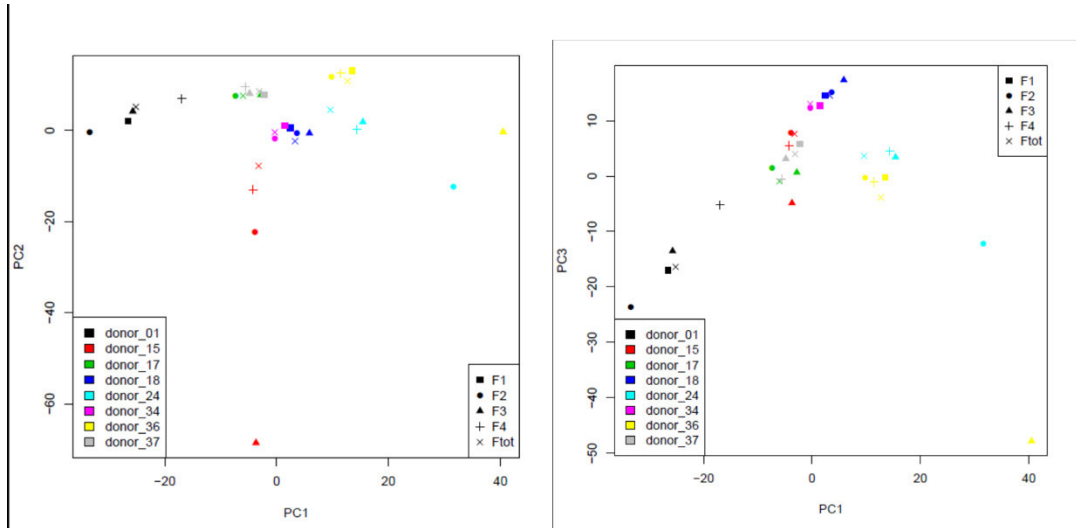
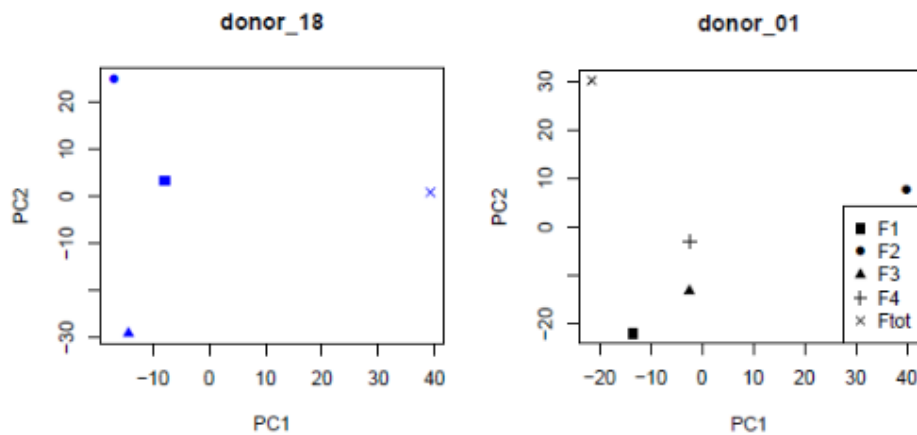


Figure 4.2.8 **Heterogeneity among patients and fractions.** Principal component analysis reporting distribution of samples along the principal component 1 (PC1), principal component 2 (PC2) and principal component 3 (PC3).

Furthermore, to emphasize differences among fractions, *Principal Component* and *Pearson correlation analyses* were performed on each sample, individually. In particular, I found out that the Pearson coefficient was always less than 1, confirming that the Celector® has been able to discern different hAFSC subpopulations. Examples of these analyses are reported in Figure 4.2.9 A and B.

A



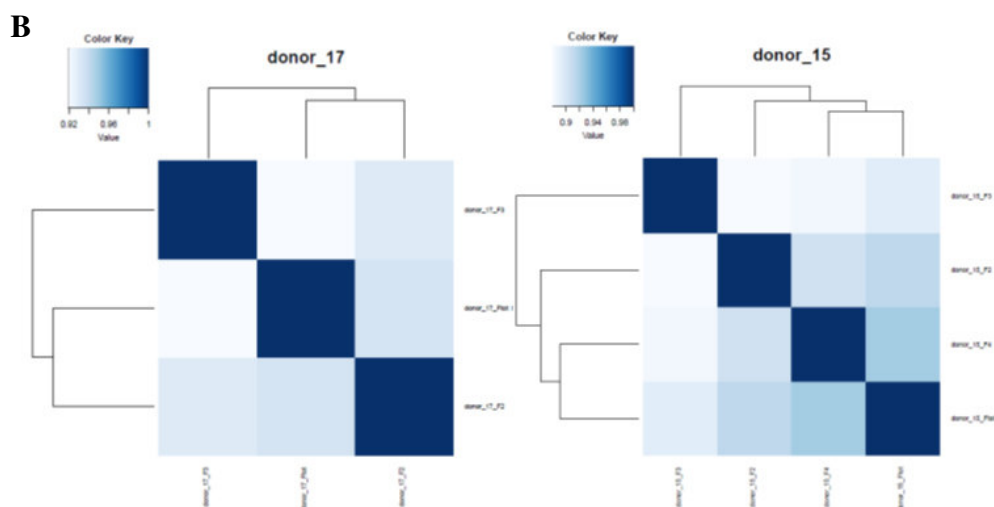


Figure 4.2.9 **Intra-population heterogeneity**. Two examples of Principal component analysis showing heterogeneity inside the samples are reported in panel A. Data are represented along principal component 1 (PC1) and principal component 2 (PC2). Two representative graphs of Pearson Correlation Analysis are reported in panel B.

After these first general evaluations, I moved on studying more in detail which transcriptional features made these fractions different using *Gene Set Enrichment Analysis*, focusing on processes of my interest, such as pathways related to proliferation and senescence. To simplify the bioinformatical analysis and to avoid confounding results deriving from the heterogeneity of f1 aggregates, I took in consideration only f2, f3 and f4.

According to Hallmark gene set database, chosen because summarizes most of the important information about biological processes²⁷⁴, seven pathways, relevant for our analyses, were found to be differently regulated in f3/f4 than f2 (Figure 4.2.10). Venn diagrams reported in Figure 4.2.11 A-G demonstrate that the majority of genes belonging to each enrichment core is preserved in both f3 and f4, supporting the idea that these two fractions have a very similar behaviour.

Hallmark

| Pathway | f3vsf2 | | f4vsf2 | |
|--|--------|-------|--------|--------|
| | NES | FDR | NES | FDR |
| HALLMARK_DNA_REPAIR | 1.81 | 0.056 | 2.13 | 0.021 |
| HALLMARK_E2F_TARGETS | 1.77 | 0.06 | 2.55 | 0.0019 |
| HALLMARK_G2M_CHECKPOINT | 1.75 | 0.058 | 1.75 | 0.047 |
| HALLMARK_HYPOXIA | 2.24 | 0.013 | 1.80 | 0.0502 |
| HALLMARK_EPITHELIAL_MESENCHYMAL_TRANSITION | -2.81 | 0 | -2.69 | 0 |
| HALLMARK_MTORC1_SIGNALING | -2.39 | 0.003 | -3.04 | 0 |
| HALLMARK_UNFOLDED_PROTEIN_RESPONSE | -2.14 | 0.007 | -2.58 | 0.001 |



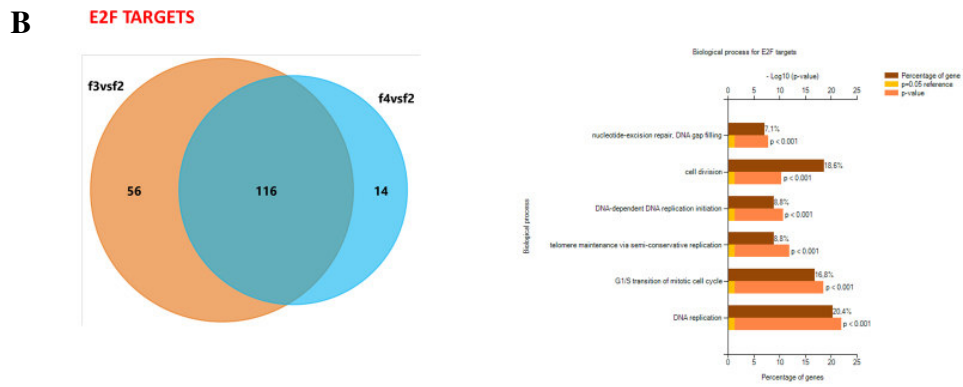
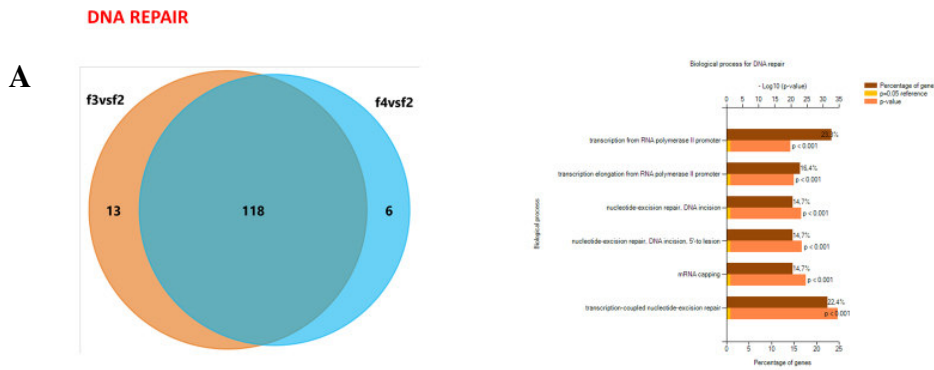
Figure 4.2.10 Pathways differently expressed in f3/f4 versus f2. Seven pathways differently expressed according to GSEA analysis and hallmark dataset performed in six different hAFSC samples. In red pathways upregulated in f3 and f4, while in green pathways downregulated in these fractions compared to f2. The table reports the Normalized Enrichment score (NES) and the False discovery rate value (FDR). FDR<0.25.

In particular, *DNA repair*, *E2F targets*, *G2M checkpoint* were found out to be upregulated in f3 and f4 than f2. As reported in Figure 4.2.11 A, B and C. All genes common to the f3 and f4 enrichment core codify for proteins directly involved in cell cycle progression, DNA quality check and transcription, corroborating the hypothesis that these two fractions proliferate more than f2 and multiple factors contribute to these characteristics.

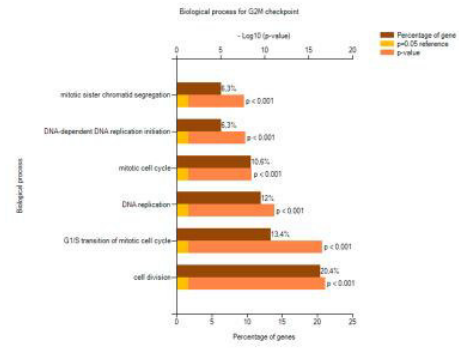
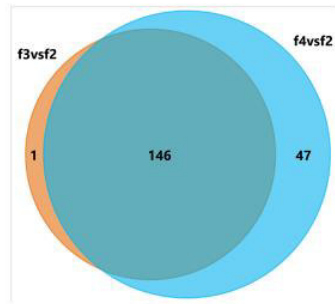
Moreover, also the *Hypoxia pathway* resulted upregulated in the last eluted fractions. This pathway describes biological processes related to glucose metabolism, which in this case was upregulated (Figure 4.2.11 D). This result was accompanied by a downregulation of *mTORC1 signalling*, that it is known to have a role in aging and in stem cell maintenance²⁷⁵, for example through metabolism regulation including an increase in mitochondrial biogenesis and activity²⁷⁶. In fact, among the biological processes that mTORC1 regulates, most of the genes are involved in the regulation of glucose metabolism, as the hypoxia pathway (Figure 4.2.11 E).

A further sign of less cellular stress in f3 and f4 is represented by the downregulation of *Unfold Protein Response (UPR)* in these fractions, pathway activated in response to an accumulation of unfolded or misfolded proteins in the lumen of the endoplasmic reticulum²⁷⁷ (Figure 4.2.11 F).

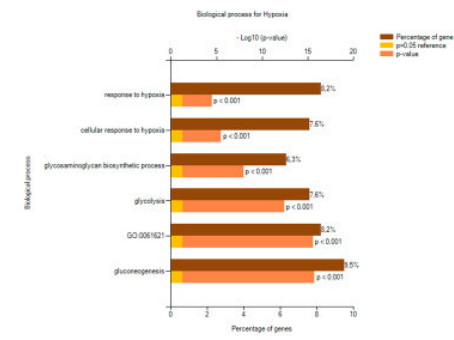
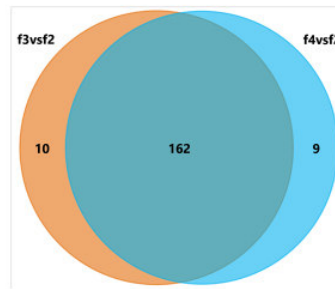
Lastly, the downregulation of *Mesenchymal Epithelial transition pathway* in f3 and f4, containing all genes involved in the extracellular matrix organization (Figure 4.2.11 G), confirmed the immunofluorescence data about the more expression of mesenchymal markers in the f2 than the last part of the eluate.



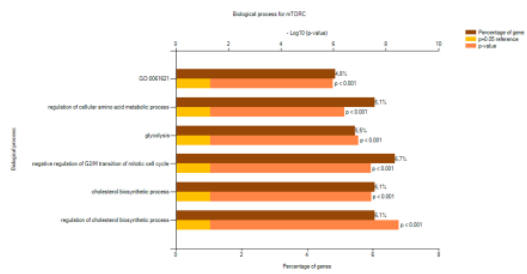
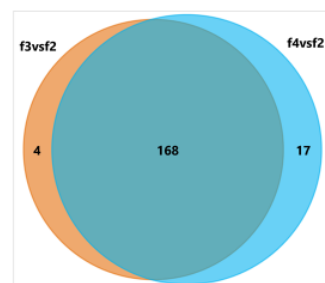
C G2M CHECKPOINT



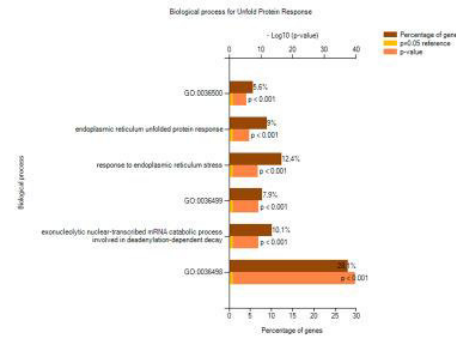
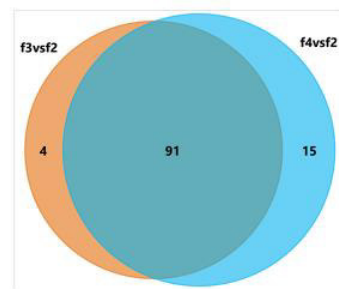
D HYPOXIA



E MTORC SIGNALING



F UNFOLD PROTEIN RESPONSE



G EPITHELIAL MESENCHYMAL TRANSITION

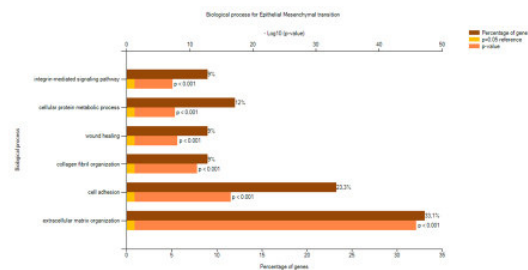
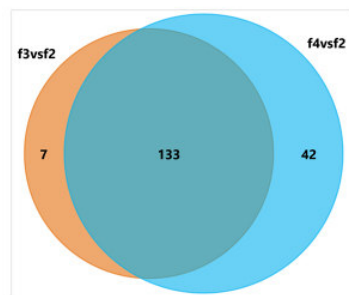


Figure 4.2.11 **Enrichment core of differently regulated pathways.** Each left panel shows the genes that contributes to the enrichment core in f3 and f4, highlighting genes that are in common. Each right panel shows at which biological processes the common genes of the enrichment core can be ascribed. In particular, the brown bar shows the percentage of genes belonging to each biological process, the yellow bar shows the reference $-\log_{10} p$ value, the orange bar reports the $-\log_{10} p$ value of each process.

Contrasting data were obtained about the p53 pathway. In fact, while in f4 it was downregulated compared to f2, opposite data were obtained for the f3. For this reason, I decided to check the results for this pathway also in other two datasets, KEGG and Reactome, finding that, according to these two public general datasets, p53 pathway was downregulated both in f3 and f4 than f2, with statistical significance in the Reactome database (Figure 4.2.12).

| Pathway | f3vsf2 | | f4vsf2 | |
|----------------------|--------|--------|--------|--------|
| | NES | FDR | NES | FDR |
| HALLMARK_P53_PATHWAY | 2.14 | 0.0208 | -2.23 | 0.0027 |



KEGG AND REACTOME

| Pathway | f3vsf2 | | f4vsf2 | |
|---|--------|--------|--------|--------|
| | NES | FDR | NES | FDR |
| KEGG_P53_SIGNALING_PATHWAY | -1.23 | 0.4088 | -1.32 | 0.2863 |
| REACTOME_P53_DEPENDENT_G1_DNA_DAMAGE_RESPONSE | -1.80 | 0.0901 | -1.81 | 0.0920 |

Figure 4.2.12 *Evaluation of p53 pathway expression in different datasets.* Differential expression of p53 pathway in f3/f4 fractions versus f2 according to Hallmark (above), Kegg and Reactome (bottom). The table reports the Normalized Enrichment score (NES) and the False discovery rate value (FDR).

To understand the causes of these divergences, I investigated the genes composition of this pathway in the three different datasets, finding out that huge differences were present in the type and number of genes. In particular Hallmark, since it describes extended biological processes, includes 200 genes involved not only in a more specific p53 function as regulator of cell cycle and senescence, but more largely in other processes such as apoptosis, which regulation in senescence is debated²⁷⁸ and mostly due to post translational processes. Only 3 genes of Hallmark dataset were found to be in common with the ones included in KEGG and Reactome datasets, these ones built including less genes, 69 and 57, respectively. In particular, Reactome focuses more on genes belonging to cell cycle regulation and also involved in NF- κ B pathway, which has been reported to interact at multiple levels with the UPR²⁷⁹ (Figure 4.2.13). For these reasons, in my opinion, Reactome better describes the processes that I was interested in.

| HALLMARK | KEGG | REACTOME |
|----------|------|----------|
| 200 | 69 | 57 |

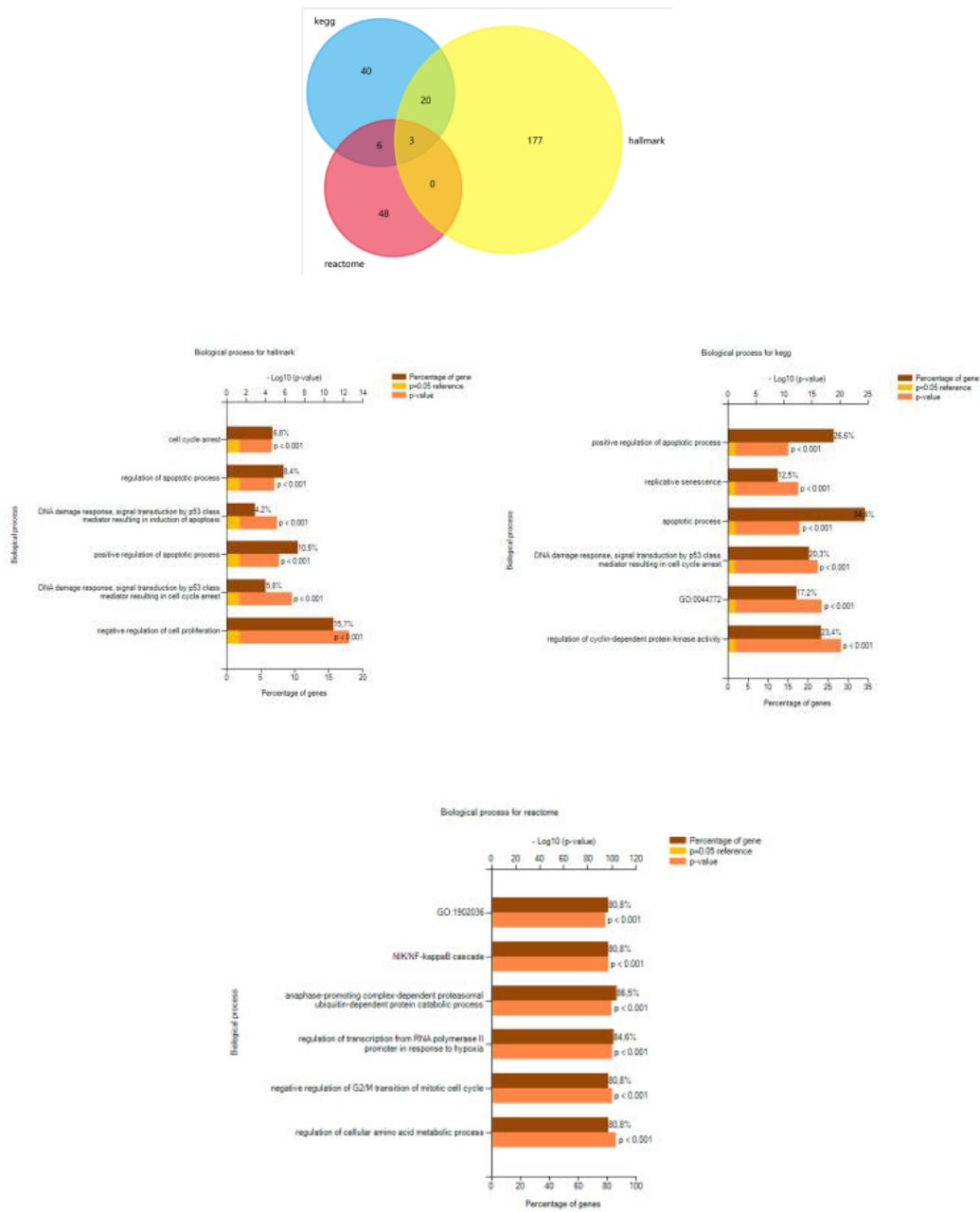


Figure 4.2.13 Comparison of three datasets on p53 pathway. In the image above the number of genes of each dataset is reported. Genes in common are highlighted. The bar graphs show at which biological processes genes composing each dataset can be ascribed. In particular, the brown bar shows the percentage of genes belonging to each biological process, the yellow bar shows the reference $-\log_{10}$ p value, the orange bar reports the $-\log_{10}$ p value of each process.

Since, no stemness signature was available in any of the three datasets used until now, I used an experimental list, as described in the methods. I chose that dataset because it contains a large number of genes (380) and all three stem cell master regulators (Oct4, Nanog and Sox2) are present. As reported in Figure 4.2.14, this stemness pathway was upregulated in the last part of the samples than in the f2, confirming in this way the qPCR and immunofluorescence data reported above.

| Pathway | f3vsf2 | | f4vsf2 | |
|----------|--------|------|--------|------|
| | NES | FDR | NES | FDR |
| ES EXP 1 | 1.46 | 0.15 | 1.95 | 0.03 |

 up

Figure 4.2.14 Evaluation of stemness signature. The table reports the Normalized Enrichment score (NES) of f3/f4 compared to f2 and the False discovery rate value (FDR).

Summarizing, all the results obtained demonstrate that the Celector® technology is able to distinguish and sort c-kit⁺ hAFSC subpopulations with different characteristics. Furthermore, my data point to indicate the last part of the eluate as the one maintaining more stemness properties, a better proliferation ability and less activation of cellular stress/ senescence pathways.

4.3. Effect of prolonged low oxygen tension on hAFSC

4.3.1. Evaluation of stemness properties of hAFSC cultured at different oxygen tensions

C-kit⁺ hAFSC cells were first expanded *in vitro* at 20% oxygen tension, then split at the same density and put at three different oxygen tension, 20%, 5% and 1%.

To verify the effect of hypoxia on stemness characteristics, Oct4 and Nanog transcript levels were evaluated at different time points, once a week for 5 weeks.

As reported in Figure 4.3.1, Oct4 levels were always significantly higher at 1% oxygen tension than the other two conditions, while no significant differences or a slight decrease were appreciated in Nanog expression. Nanog results can be explained by the fact that it is reported that its expression is finally regulated by the same Oct4 through a negative feedback mechanism. For this reason, to maintain the correct balance between differentiation and self-renewal, the upregulation of Oct4 can induce the downregulation of Nanog²⁸⁰.

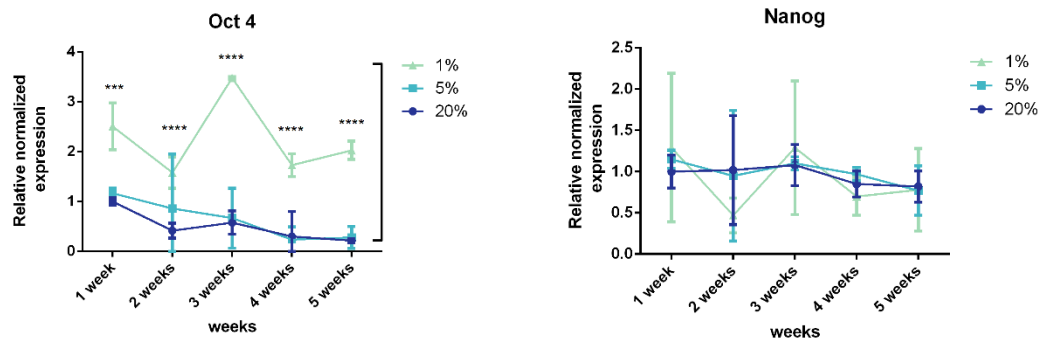
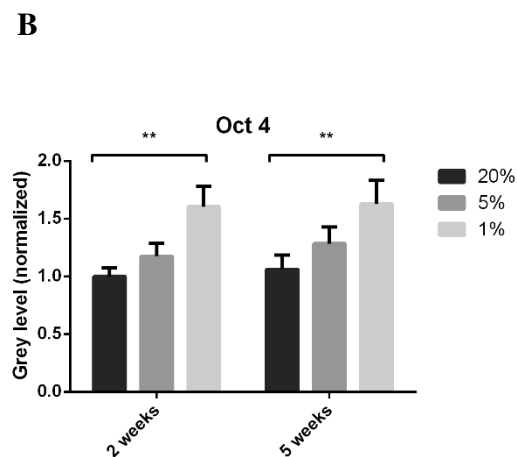
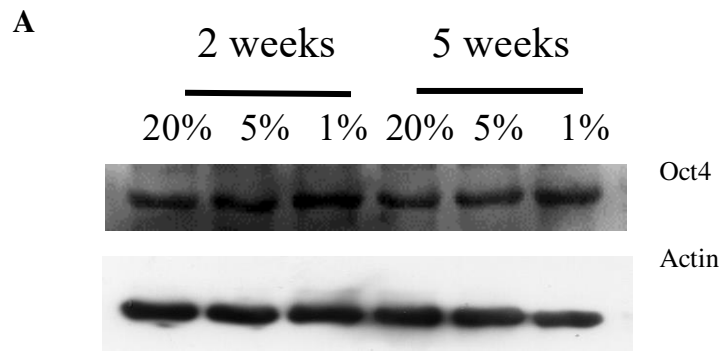


Figure 4.3.1 **hAFSC stemness markers expression.** Relative normalized expression of Oct4 and Nanog in cells exposed to 20% (dark blue), 5% (light blue), 1% (green). Tubulin and actin were used as housekeeping. *** p value < 0.001; **** p value < 0.0001 significantly different from 20%. Data are the result of quadruplicate independent measurements

Oct4 expression was also analysed by western blot, which confirmed the upregulation at 1% oxygen tension compared to 20% after 2 and 5 weeks (Figure 4.3.2).

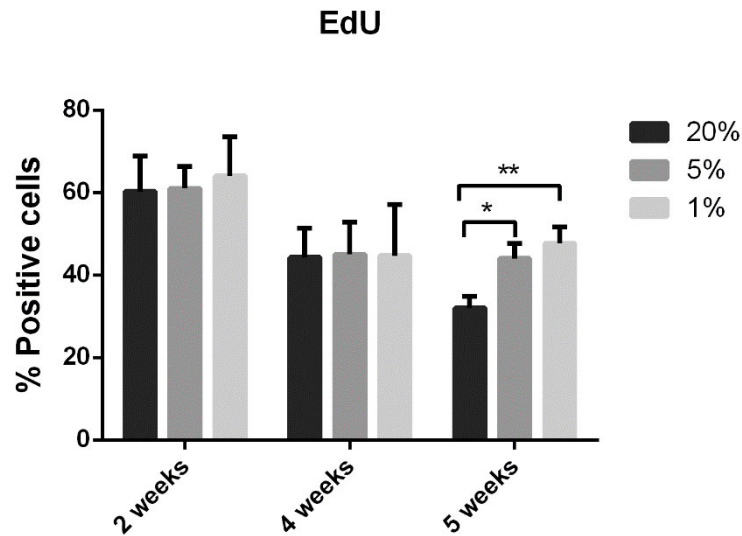
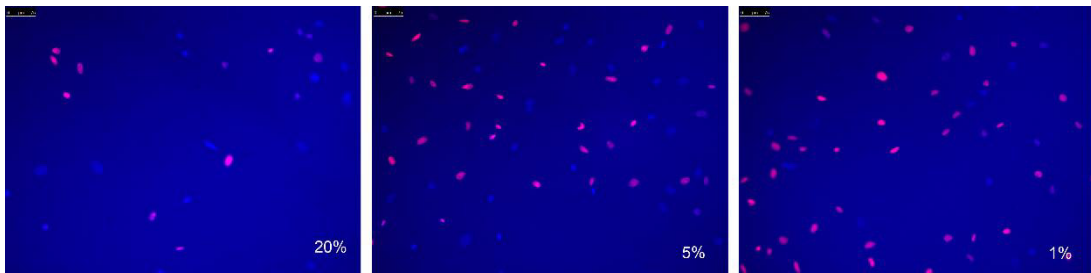


*Figure 4.3.2 Evaluation of Oct4 protein expression. A) Representative western blot showing the expression of Oct4 in hAFSC cultivated at different oxygen tensions. B) Actin detection was used to normalize data. In the right panel, the graph shows the densitometric analysis of the experiment. Data are representative of three independent experiments. **p value < 0.01; ***p value < 0.0001.*

4.3.2. Proliferation ability of AFSC at different oxygen tensions

Even if it is known that generally hypoxia stimulates cell cycle arrest in mammalian cells²⁴⁰, different studies report that first MSCs grew slower under 5% O₂ tension, then acquiring a progressive growth advantage at prolonged times²⁴¹. Moreover, in the first part of my PhD I demonstrated that a higher Oct4 expression correlates with higher proliferation.

For this reason, I decided to evaluate their proliferation ability through an EdU test, which stain cells that are synthesizing new DNA molecules. As reported in Figure 4.3.3, no differences in proliferation ability were found in the first four weeks. On the contrary, after five weeks, 20% cells decreased their EdU positivity, while 1% and 5% cells maintained a proliferation rate comparable to the week before.

A**B**

*Figure 4.3.3 Proliferation ability of hAFSC cultivated at different oxygen tensions. A) EdU test showing proliferating cells (stained in red) performed after 2 weeks, 4 weeks, and 5 weeks of culture at 20%, 5% and 1% oxygen tension. Nuclei were stained with DAPI (blue). * p value < 0.05; ** p value < 0.01.*

B) Representative immunofluorescence images of EdU test after five weeks of culture at three different oxygen tensions. Scale bar = 75 μ m.

Since, cyclin E2 is responsible of the entrance of cells in the S-phase, in which new DNA synthesis is achieved, I checked if its RNA and protein expression had been modified by hypoxia. qPCR and western blot analysis revealed that, even if no differences or a decrease of cyclin E2 expression could be observed in the first two weeks especially at 1% oxygen tension than 20%, an increase in its levels were found starting from the third week (Figure 4.3.4).

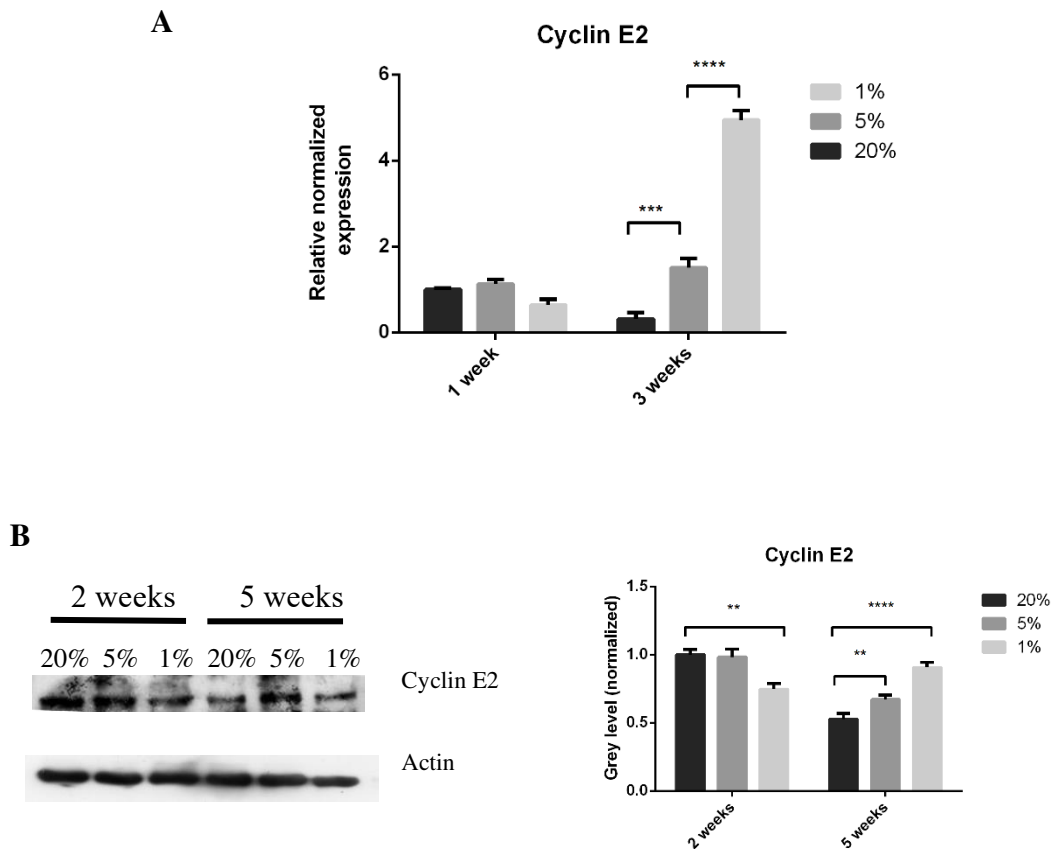


*Figure 4.3.4 Cyclin E2 expression. In panel A it is reported the normalized expression of cyclin E2 transcript. Tubulin and actin were used as housekeeping. Data were obtained in duplicated. In panel B it is shown a representative western blot image and its densitometry. Actin was used as loading control. Data are representative of three independent experiments **p value < 0.01; ***p value < 0.001; ****p value < 0.0001.*

To further confirm these data, I evaluated also Ki67 expression, which reaches its maximum during the M phase²⁷². The representative confocal images in Figure 4.3.5 show that Ki67 staining was more brilliant in 1% and 5% cells after 5 weeks.

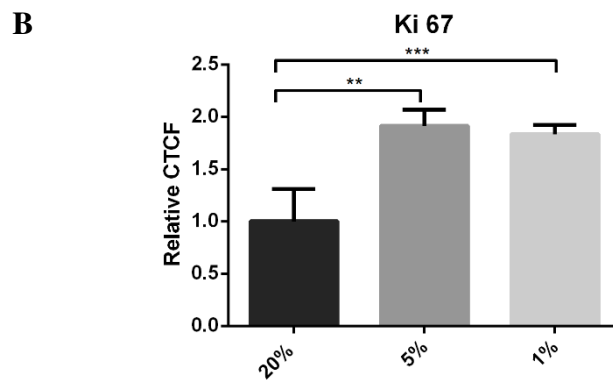
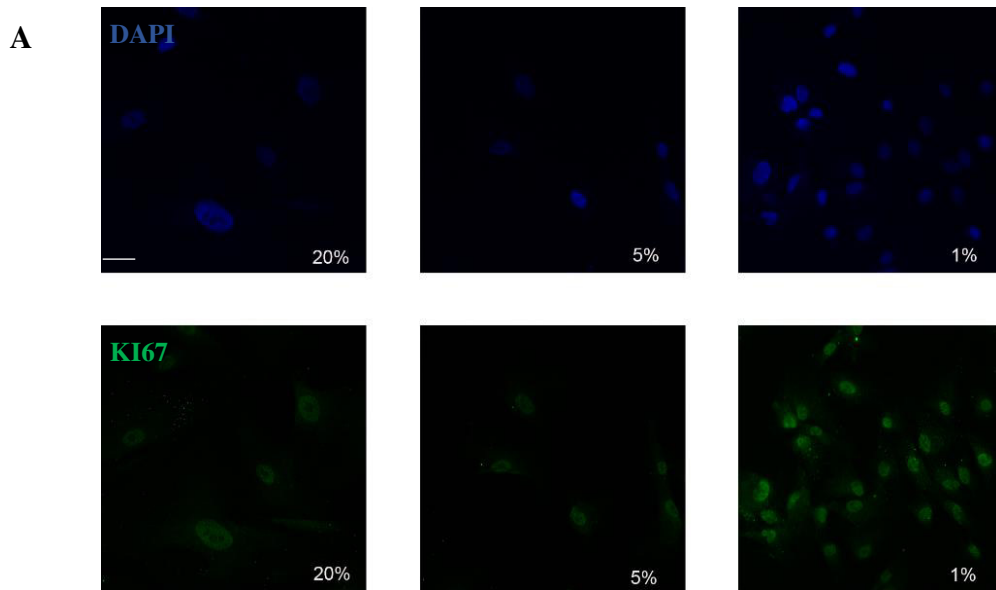


*Figure 4.3.5 Ki67 expression. A) Confocal images of hAFSC cultivated at different oxygen tension and stained with DAPI (blue) and Ki67 (green). Scale bar= 10 μ m B) Relative normalized expression of corrected total cell fluorescence of Ki67 staining. ** p value < 0.01; *** p value < 0.001*

Among the different pathways involved in the control of proliferation, one of the master regulators is represented by the PI3K/Akt axis, which it has been found to be activated in BM-MSCs cultured under hypoxic conditions²⁸¹.

For this reason, I decided to check if also in our model this pathway could be involved. I found out that the ratio of pAkt/total Akt was higher in both 1% and 5% already after 2 weeks of culture and maintained this trend also after 5 weeks (Figure 4.3.6).

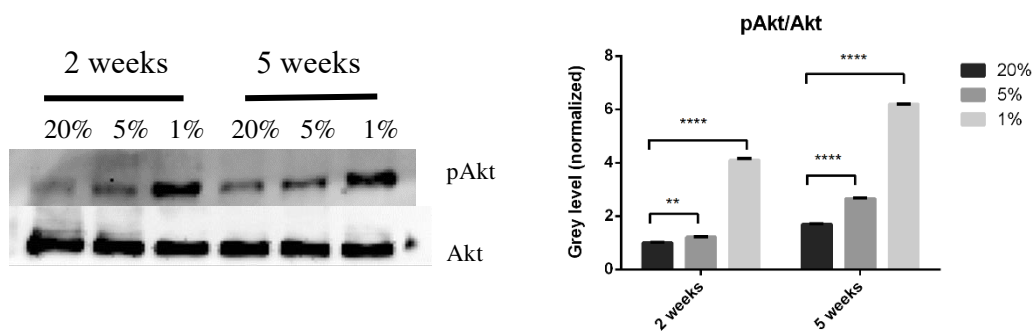


Figure 4.3.6 **Evaluation of Akt phosphorylation.** Representative western blot image and relative densitometry analysing the ratio pAkt/Akt in hAFSC cultivated at 20%, 5% and 1% oxygen tension after 2 weeks and 5 weeks.

p value < 0.01; **p value < 0.0001.

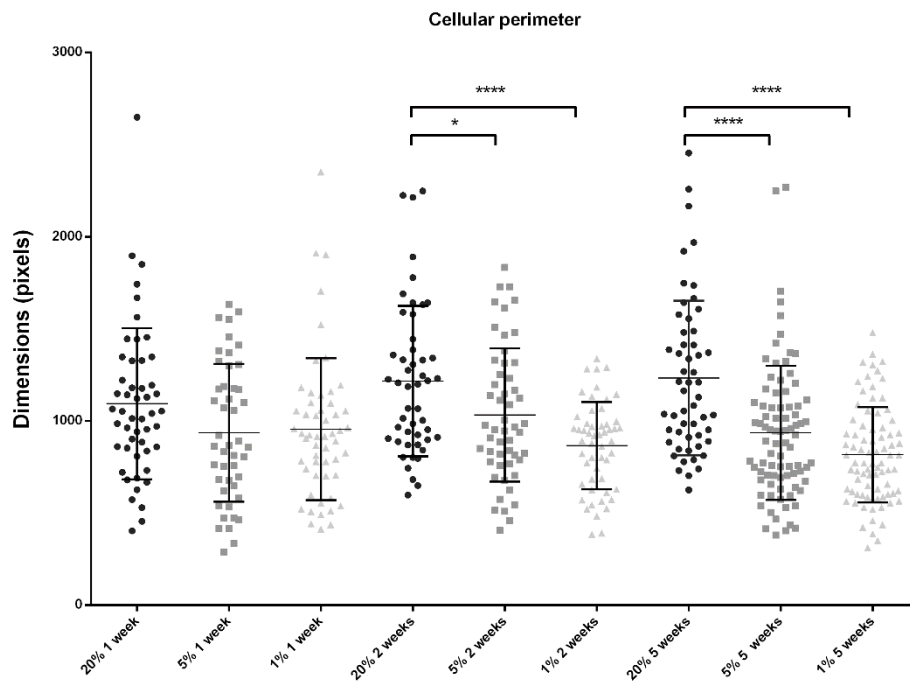
All the data obtained until now, corroborate the idea that hypoxia confers a proliferation advantage mostly at prolonged time exposure.

4.3.3. Senescence-associated markers in AFSC cultivated at different oxygen concentrations

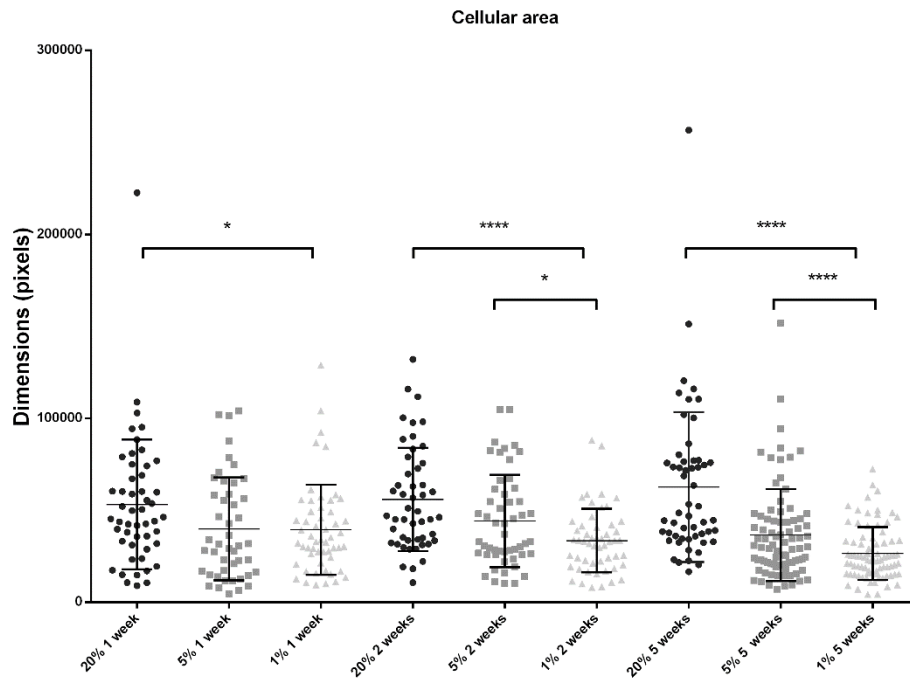
Proliferation and stemness results hinted to consider 20% cells more directed to enter in a senescent program after a month of culture than the other two conditions.

In fact, just the observation of cells under the microscope, brought to light differences in the morphology mostly after prolonged time in culture. As reported in the representative analyses of Figure 4.3.7, cells cultivated at 20% oxygen were bigger, flattened and in some cases also more elongated, strengthening the idea that 20% cells were more senescent than the other two conditions.

A



B



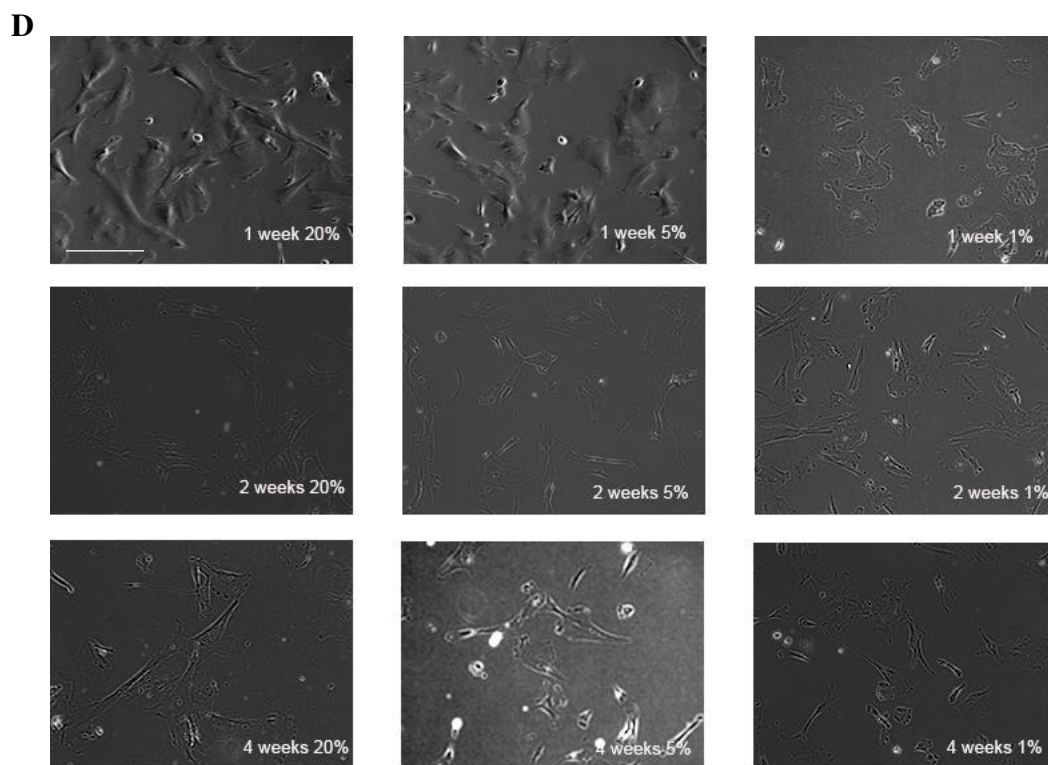
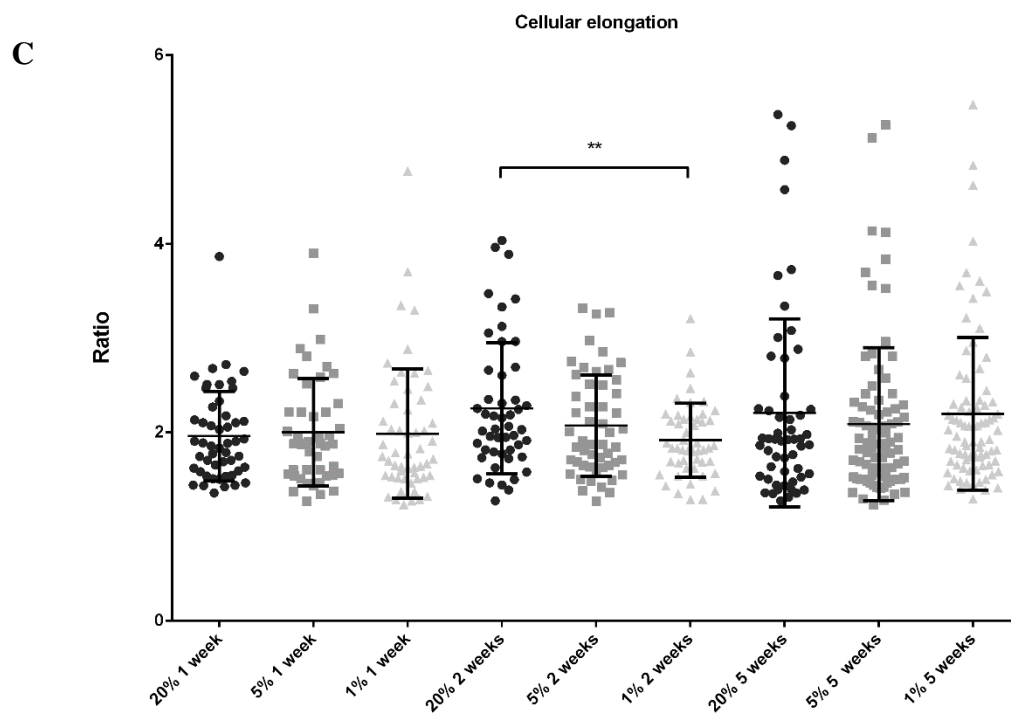


Figure 4.3.7 Morphology of hAFSC cultivated at different oxygen tensions. Analysis of cellular perimeter (A), area (B), and elongation (C) of cells cultivated at different oxygen tensions for 1 week, 2 weeks, 5 weeks. * p value < 0.05; ** p value < 0.01; **** p value < 0.0001. In panel D representative images of cells after 1 week (above), 2 weeks (middle), 4 weeks below). Scale bar=30 μ m

Evaluation of the senescence-associated β -galactosidase (SA- β gal) activity revealed that no significant differences could be appreciated until four weeks of culture as expected, while an increase in the positivity in 20% and 5% than 1% could be appreciated in the fourth and fifth week (Figure 4.3.8).

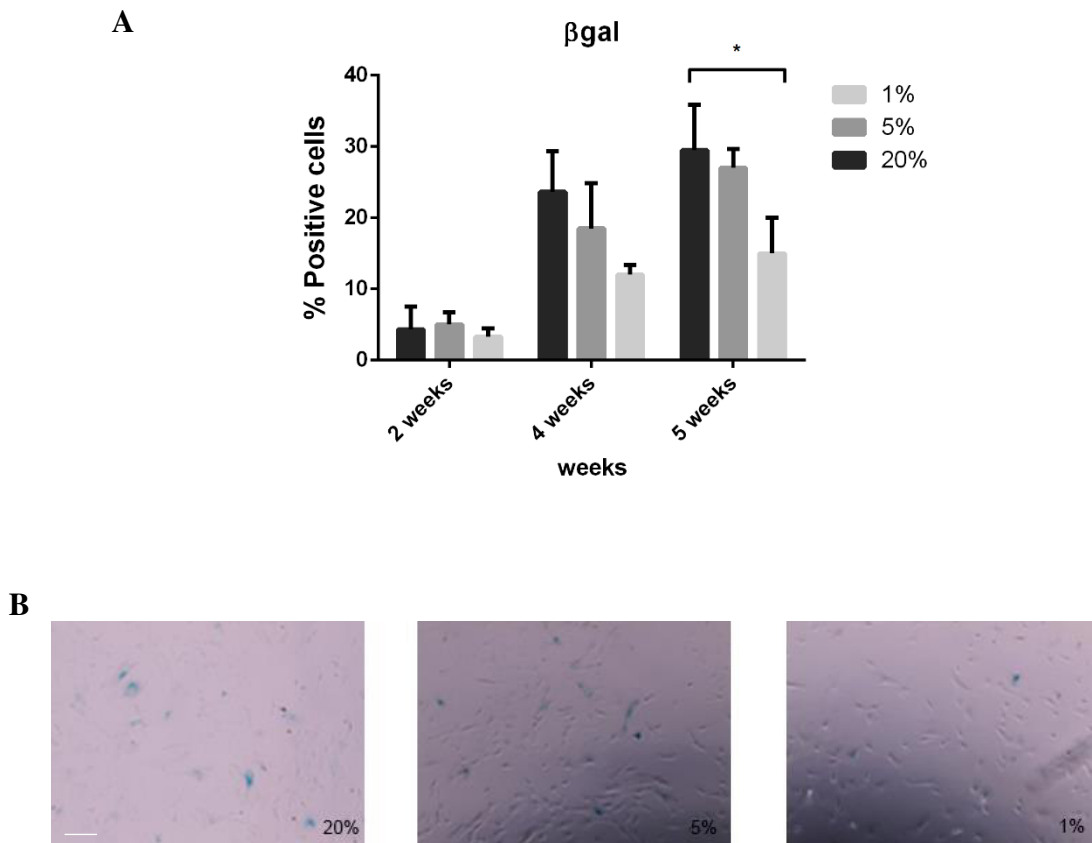
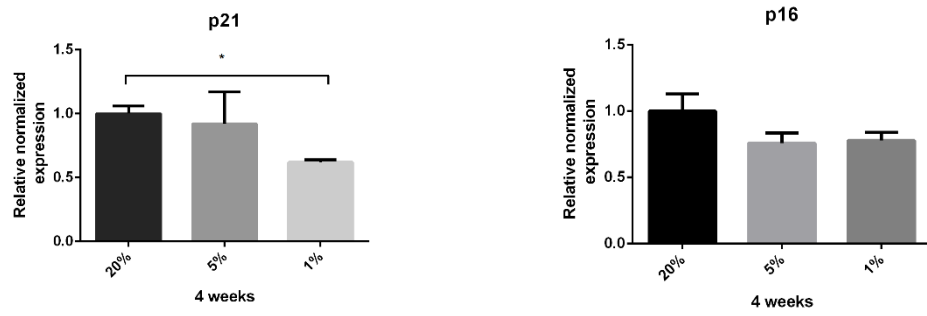
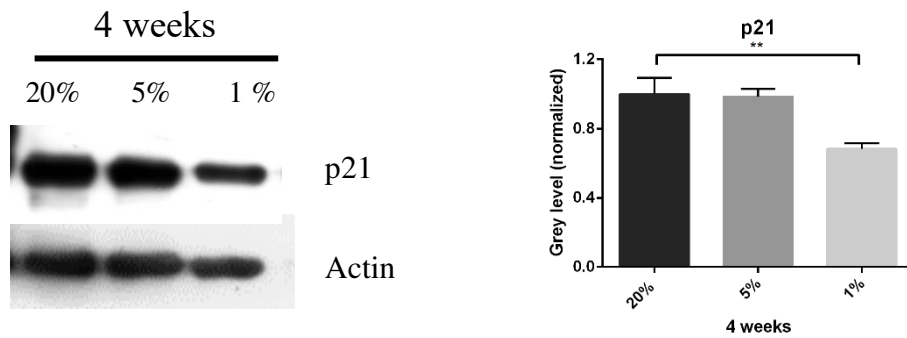


Figure 4.3.8 β -Galactosidase staining. In panel A evaluation of positive cells at β -Galactosidase staining in hAFSC cultivated at different oxygen tensions for 2,4,5 weeks. *p value<0.05. In panel B, representative images of cells stained for β -Galactosidase. Cells in blue are positive for the staining. Scale bar= 30 μ m

Based on these results, I decided to evaluate the trend of two main regulators of senescent programs, p16 and p21.

qPCR analysis showed that after 4 weeks of culture, in particular p21, but also p16, was less expressed in 1%. (Figure 4.3.9 A).

To confirm these data, I checked p21 protein expression finding that there was a decrease than the other two conditions (Figure 4.3.9 B).

A**B**

*Figure 4.3.9 Senescence-associated markers. In the superior panel qPCR analysis for p21 and p16 expression in hAFSC cultivated at 20%, 5% and 1% oxygen tension. Data are the result of quadruplicate independent measurements. Tubulin and actin were used as housekeeping. *p value<0.05; In the panel below, representative image of western blot analysis and its densitometry. Values were normalized on actin expressions. Data are representative of three independent experiments. **p value<0.01.*

Since in my first part of my PhD I demonstrated that by time hAFSC accumulate prelamin A, the immature form of lamin A, and its levels correlate with the expression of senescence characteristics, I evaluated the expression of this protein in all three conditions, finding that after four weeks it was more present in 20% cells than 1%, with intermediate levels in 5% cells (Figure 4.3.10).

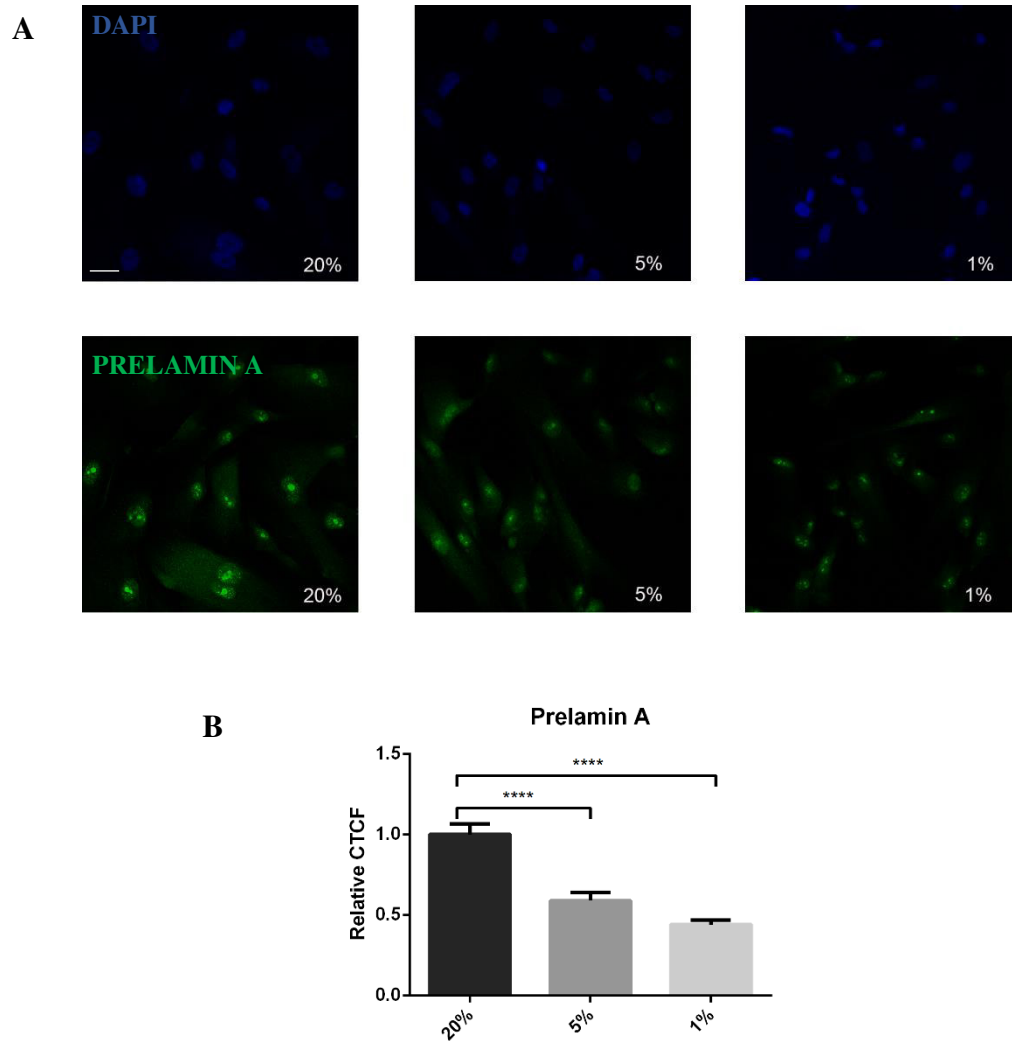
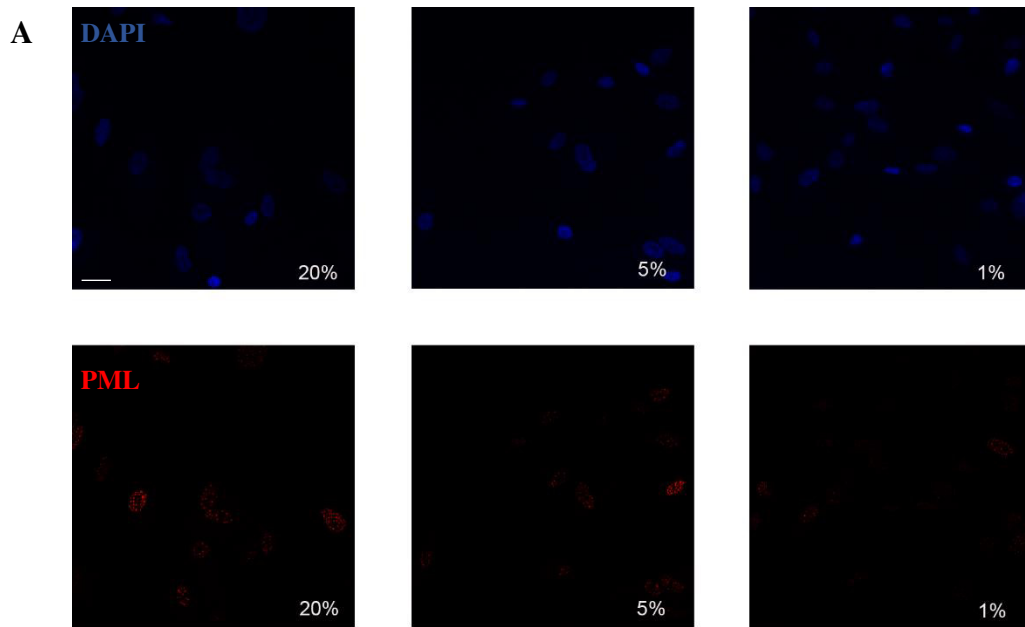


Figure 4.3.10 *Prelamin A expression in hAFSC.* A) *Prelamin A expression (green) after 4 weeks of culture at different oxygen tension. Nuclei were stained with DAPI (blue). Scale bar= 10 μ m* B) *Relative normalized expression of corrected total cell fluorescence of prelamin A staining. ****p value<0.0001.*

Moreover, since I already proved that PML bodies are involved into the aging process of hAFSC, I assessed their morphology and number. As reported in the representative confocal images of Figure 4.3.11, these structures were more and bigger in 20% than the other two conditions.



B

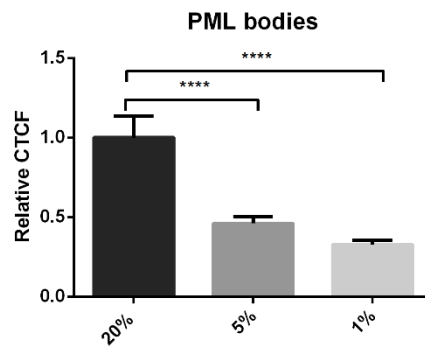


Figure 4.3.11 PML bodies morphology 4 weeks after in vitro culture A) Representative confocal images of PML bodies (red) in hAFSC cultivated at 20%, 5% and 1% oxygen tension. Nuclei were visualized with DAPI (blue). Scale bar= 10 μ m B) Relative normalized expression of corrected total cell fluorescence of PML bodies staining.

**** p value < 0.0001.*

All these results well correlate with the first data obtained on stemness and proliferation, confirming that especially cells cultivated in 1% oxygen tension maintain more pluripotent characteristics than 20%.

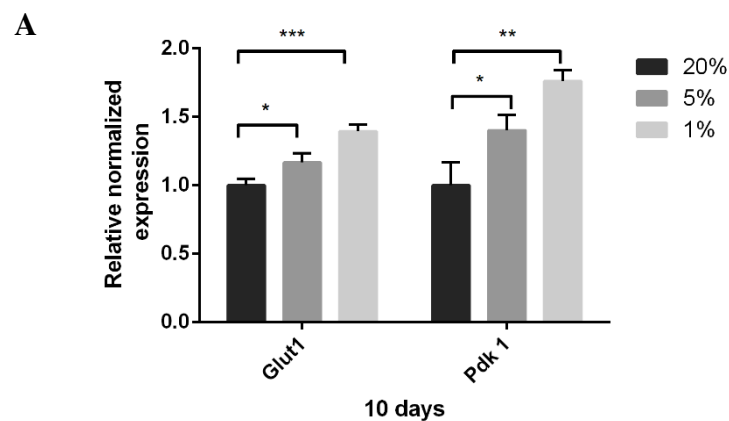
4.3.4. Metabolism variations at different oxygen tensions

It is known that lower oxygen availability induces changes in cellular metabolism. In particular, cells adapt to oxygen reduction through the stabilization of HIF factor, whose major effects on cells energy homeostasis are the activation of anaerobic glycolysis and the inhibition of the mitochondrial aerobic metabolism, the tricarboxylic acid (TCA) cycle and OXPHOS²⁸².

Furthermore, mitochondria form a highly dynamic tubular network which is regulated by frequent fission and fusion events, modulated in response to changes in the metabolic conditions of the cell²⁸².

Since different results were obtained for 5% and 1%, I decided to check if there were differences in the hypoxic adaptation at these two oxygen tensions.

qPCR performed after ten days the first exposure to these oxygen tensions, showed that both PDK1, which acts to inactivate the TCA cycle, and Glut1 (membrane channel for glucose uptake), were upregulated in both conditions but more at 1% (Figure 4.3.12 A). Glut1 upregulation was confirmed by western blot analysis, as reported in Figure 4.3.12 B.



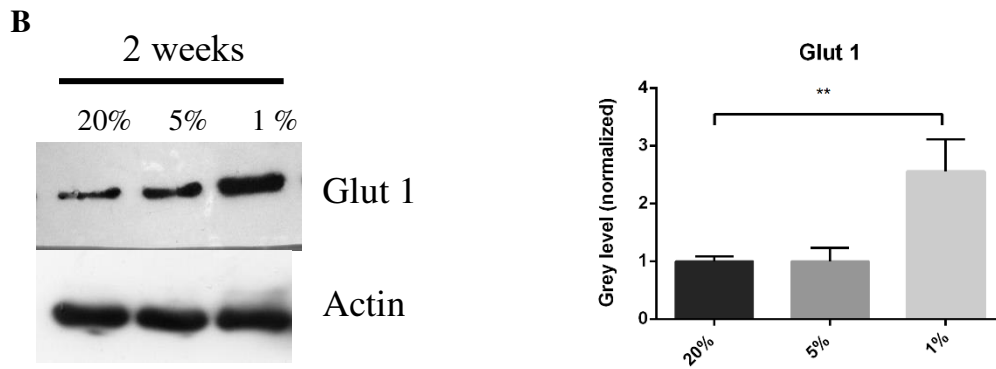


Figure 4.3.12 **Metabolism regulation in hypoxia.** A) Transcript levels of *Glut1* and *PDK1* in hAFSC cultivated at 20%, 5% and 1% oxygen tension. Actin and tubulin were used as housekeeping. Samples from two different patients were analysed B) *Glut1* protein expression after 2 weeks of in vitro culture at different oxygen tension. Actin was used as loading control. Data are representative of three independent experiments. **p* value < 0.05; ***p* value < 0.01; ****p* value < 0.001.

To evaluate if changes in mitochondrial morphology occurred, I carried out immunofluorescence analyses, which showed that at 1% mitochondria were less numerous and more fragmented compared to the 20% condition. 5% cells still presented more mitochondria and more tubular than 1% but less compared to 20% condition, confirming that 5% condition has intermediate characteristics (Figure 4.3.13).

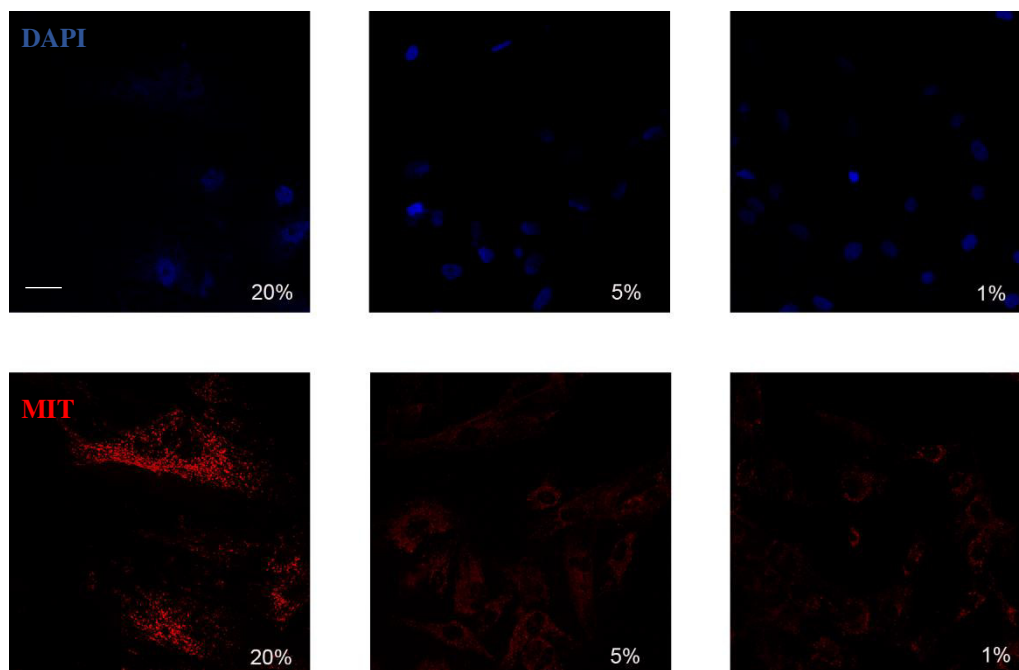


Figure 4.3.13 Mitochondrial morphology in hAFSC cultivated at different oxygen tension. hAFSC cultivated at 20%, 5% and 1% oxygen tension were stained with anti-human mit (red). Nuclei were visualized with DAPI (blue). Scale bar= 10 μ m

4.3.5. Hypoxia and resistance to stress

It has been reported that hypoxia (0.1–2% O₂) increases the viability of stem cells both in normal culture conditions or under the effect of stressor molecules, reducing the percentage of cells that undergo apoptosis^{239,249}. The mechanisms responsible of these results might be traced back to the activation of HIF under hypoxic conditions. In fact, HIF-1 α upregulates antiapoptotic factors, downregulating the caspase-3 activation (protein involved in cell apoptosis) thus protecting MSCs from apoptosis²⁵⁰.

For this reason, since starting from 4 weeks of culture 20% cells seemed to be more suffering than the other two conditions, I decided to evaluate if they were more prone to enter in an apoptosis program. First, I checked caspase-3 expression by confocal microscopy, which showed that a more brilliant punctuate staining was visible for 20% cells (Figure 4.3.14).

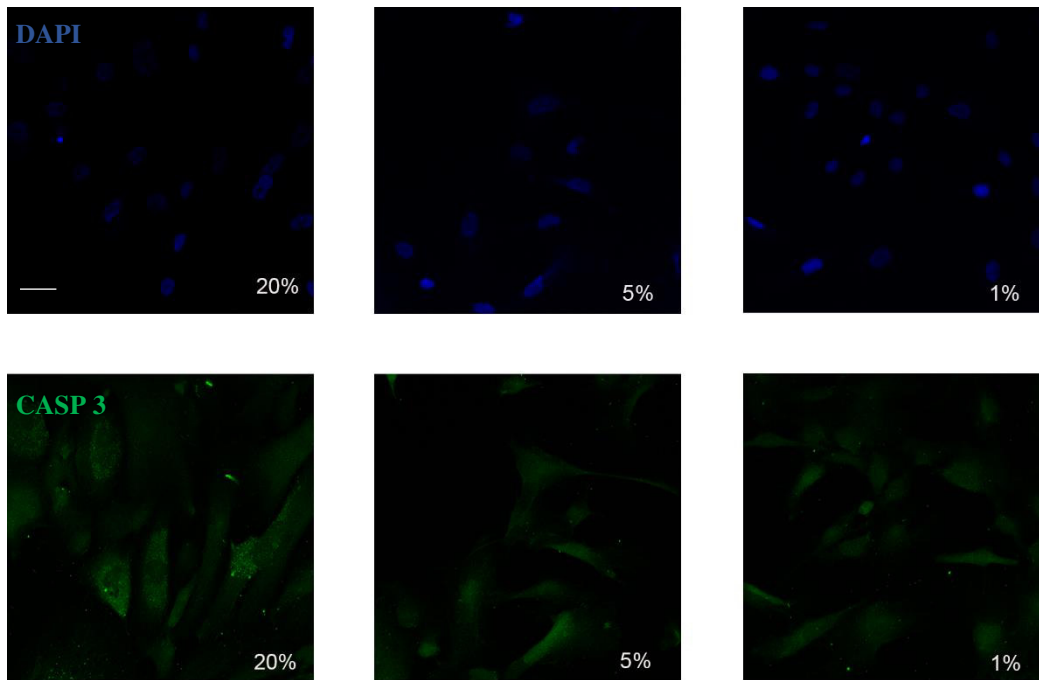


Figure 4.3.14 *Caspase-3 expression in hAFSC cultivated at different oxygen tension. Representative confocal images of cells stained with anti- active caspase 3(green) and DAPI (blue) after 4 weeks of culture. Cells were cultivated at 20%, 5% or 1% oxygen tension. Scale bar= 10μm*

Then, to understand if caspase 3 was really more activated in that condition, I evaluated the ratio cleaved PARP/ PARP, which is the main target of the caspase 3. western blot analysis revealed that this ratio was significantly higher in 20% than 5% and 1% oxygen tension (Figure 4.3.15).

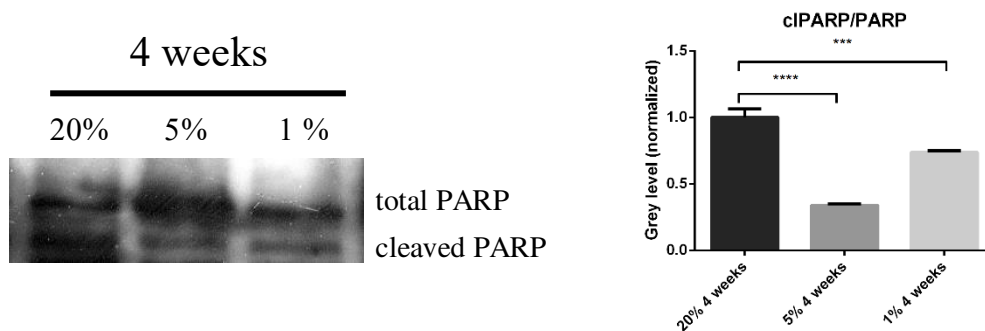
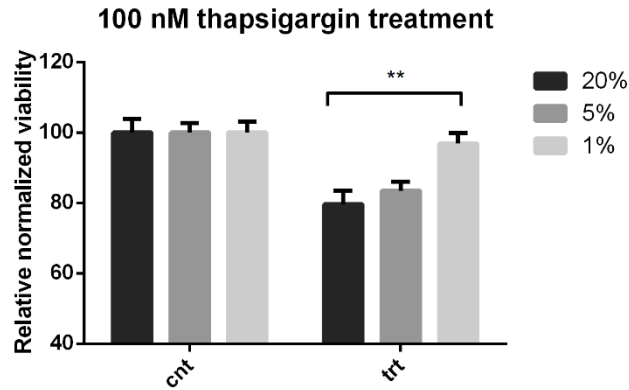


Figure 4.3.15 *Evaluation of cleaved PARP/total PARP in hAFSC. Western blot analysis reporting the ratio cleaved PARP/ total PARP in hAFSC cultivated at 20%, 5% and 1% oxygen tension. Data are representative of three independent experiments. ***p value < 0.001; ****p value < 0.0001.*

To further validate these results, I treated the cells with thapsigargin, an inducer of endoplasmic reticulum stress, chosen because its mechanism of action is independent

from oxygen tension. After 24 hour of treatment, 1% cultivated cells were significantly more viable than 20% cells, while no differences were appreciated between 20 and 5% (Figure 4.3.16).



*Figure 4.3.16 Resistance of hAFSC exposed at different oxygen tension to endoplasmic reticulum stress. Relative normalized viability of hAFSC cultivated at 20, 5 or 1% oxygen tension after thapsigargin treatment. Viability of treated samples was normalized on the corresponding control cultivated at the same oxygen tension measured through MTS test. Data are representative of three independent experiments. **p value < 0.01.*

4.3.6. Differentiation ability in hypoxia

Several studies investigated the impact of hypoxia on MSCs differentiation, showing contrasting results^{238,244–247}. For this reason and also because hypoxia seems to preserve pluripotent markers expression and the entrance in senescence, I decided to study the effect of low oxygen tension on adipogenic and osteogenic ability, which balance is finely regulated during aging process²⁸³. In fact, different studies report that unlike osteoblastogenesis, which declines with age, adipogenesis seems to accelerate with age^{284,285}.

Adipogenic process is finely regulated by CEBP α which induces an increase of PPAR γ , a receptor, necessary to regulate the deposit of fat acids and glucose metabolism in adipocytes²⁸⁶. Otherwise osteogenic process is regulated in the first phases by the upregulation of the transcription factor RUNX2, which expression is then reduced during the last phases when the matrix extracellular proteins osteopontin (encoded by the gene SPP1) and osteocalcin (encoded by the gene BGLAP) are almost deposited²⁸⁷.

So, the evaluation of adipogenic and osteogenic markers after 3 weeks exposure to the appropriate differentiation medium, displayed a reduced adipogenic (both in PPAR γ and CEBP α) but an increase of osteogenic capability of cells cultivated at 5 and 1% than 20% oxygen tension. In particular, no differences were shown in RUNX2 expression but a great increase of SPP1 and BGLAP was visible mostly in the 1% condition, supporting the idea that a terminal differentiation had been achieved (Figure 4.3.17).

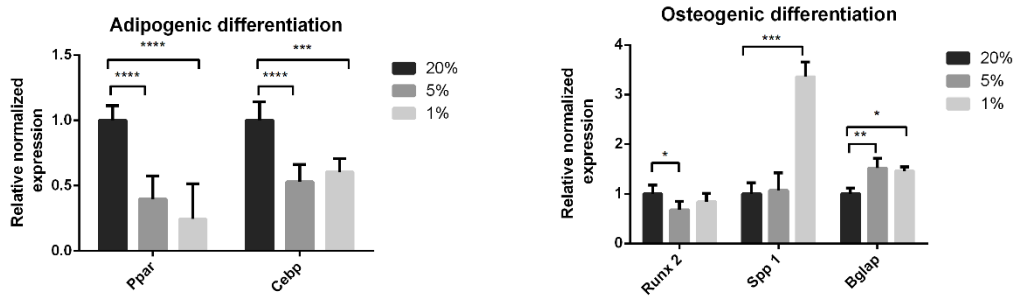


*Figure 4.3.17 Adipogenic and osteogenic differentiation of hAFSC cultivated at different oxygen tensions. qPCR analysis for adipogenic (on the left) and osteogenic (on the right) markers are reported. Actin and tubulin were used as housekeepers. Samples from two different patients were analysed. *p value < 0.05; **p value < 0.01; ***p value < 0.001; ****p value < 0.0001*

All the results obtained contribute to strengthen the idea that hypoxia preserves stemness proprieties enhancing the ability to differentiate into bone tissue, slowing down the entrance in a senescence program by increasing the resistance to stress and reducing adiopogenesis.

5. DISCUSSION AND CONCLUSIONS

In recent years mesenchymal stem cells (MSCs) have emerged as a potential therapeutic approach for various disorders since they possess different properties, such as the ability to support other cell types during tissue regeneration⁵¹, the secretion of growth factors and cytokines⁵² and immunomodulation properties⁵³.

MSCs are self-renewable, multipotent, easily accessible and culturally expandable *in vitro* with genomic stability and few ethical issues.

MSCs are present both in foetal and adult tissues and in the last years more interest has been focused toward amniotic fluid stem cells (hAFSC). hAFSC express pluripotent markers such as Oct4, Sox2, Ssea4, Ssea3, c-Myc, Klf4³⁹ and the ability to differentiate into mesodermal and nonmesodermal lineages under appropriate differentiation conditions but, unlike embryonic stem cells or iPS, they do not form tumors *in vivo* and there is no evidence on their ability to form chimeras when injected into blastocysts⁴¹.

The low number of available MSCs requires their *ex vivo* expansion prior to clinical use⁸⁶. However, during their *in vitro* culture, MSCs quickly reach replicative senescence⁸⁷. Cellular senescence is a permanent state of cell cycle arrest that can also contribute to the decline of the regenerative potential^{88,89}.

Understanding the molecular processes controlling stem cell survival, self-renewal, quiescence, proliferative expansion and commitment to specific differentiated cell lineages is essential to uncover the drivers and effectors of age-associated stem cell dysfunction.

For sure, different mechanisms are involved into stem cell aging and include the accumulation of toxic metabolites like ROS that can be responsible of DNA and proteins damage, mitochondrial dysfunction, proliferative exhaustion, extracellular signalling and epigenetic remodelling⁹⁵. In particular, oxidative stress is known to play an important role in modulating different stem cells properties, such as self-renewal, proliferation, differentiation and senescence¹⁰².

Among the ROS producing enzymes, NADPH oxidase 4 (Nox4) has been shown to have a peculiar role in regulating amniotic fluid stem cells biology. In fact, different evidences suggest that Nox4 could be crucial in the maintenance of pluripotency,

through modulation of both nuclear signalling and DNA damage¹³³, influencing consequently the proliferation rate and their differentiation ability¹³⁵.

Furthermore, recent data have shown a relationship among lamins mutations, altered ROS metabolism and physiological aging¹⁷⁰. Lamins are a family of nuclear proteins belonging to the V type intermediate filaments that provide not only a structural framework to nucleoplasm, but also play important roles in epigenetics, chromatin organization, DNA replication and repair, transcription, becoming involved in this way in signal transduction, cell cycle control, apoptosis, cell differentiation and carcinogenesis^{151,157,158}.

It has been suggested that lamin A can be oxidized acting as a ROS-sink inside the nucleus, protecting other more critical proteins from transient, mild oxidative damage¹⁷².

Various studies have revealed that ROS levels are increased in laminopathy patient cells and during prelamin A accumulation¹⁸⁶, an immature form of lamin A. Other studies observed that prelamin A accumulation in human MSCs gives rise to a premature aging phenotype that ultimately causes reduced functionality of these cells²⁶⁹.

The principal aim of this study was to investigate the aging process occurring during *in vitro* expansion of amniotic fluid stem cells, obtained at similar gestational age focusing in particular on the redox control involving Nox4 and prelamin A accumulation.

At this purpose, 21 AFSC samples were collected from healthy donors through amniocentesis, a routine diagnosis procedure, performed at 16th-17th week of pregnancy. First, I performed different experiments to evaluate proliferation rate, ROS levels, the expression of different stemness and senescence- related markers, including Nox4 and prelamin A. In particular, I observed a strong heterogeneity among samples that reflected their different behaviour in culture. In fact, at least three groups of hAFSC with different properties could be discerned. One third of hAFSC samples showed a low proliferation rate, linked to poor expression level of pluripotency markers and faster senescence occurrence, as well as higher total ROS production and an increased nuclear expression of Nox4. Interestingly, these phenomena were accompanied to the accumulation in the nucleoplasm of prelamin A, unexpected effect since these are stem cells of foetal age. Interestingly, a ROS decrease, due to antioxidant treatment, caused

a decrease on prelamin and Nox4 nuclear signals, hinting at a role for high ROS as essential drivers of cellular aging.

Furthermore, immunofluorescence analyses revealed an increased number and dimensions of PML bodies, nuclear structures involved into post translational modifications of proteins and transcriptional factors, including processes of sumoylation, ubiquitination, phosphorylation or acetylation¹⁹¹.

Since this peculiar distribution of Nox4 enzyme and prelamin A in hAFSC nuclei I decided to investigate the relationship between these two proteins in the aging process finding out that they interact, and this interaction often occurs into PML bodies.

It has been reported that this localization could be a way to sequester and favour proteasome degradation through sumoylation and/ or ubiquitination, with the possible protecting meaning to modulate ROS content, limit DNA damage and induce senescence. In fact, for example some studies have demonstrated sumoylation of lamin A at lysine 201²⁸⁸. This sumoylation site is also present in prelamin A and could be involved in its translocation to PML-NBs, therefore I focused our attention only on the possible sumoylation of Nox4. In this context, I demonstrated that nuclear Nox4 co-immunoprecipitates with SUMO1, suggesting that SUMO modifications participate in Nox4 and prelamin interactions and cellular senescence, through modulation of oxidative stress responses.

Even if PML-NBs have been proposed to function as sequestration sites of misfolded proteins targeted for proteasomal degradation¹⁹¹, some authors demonstrated that proteasome inhibition causes progerin degradation through accumulation in PML bodies and autophagic pathway, as compensatory response²²². For this reason, I tested the effect of the proteasome inhibitor MG132, on farnesylated prelamin A and Nox4. My data, also the one with the sumoylation inhibitor, confirmed that PML-NB sequestration *via* sumoylation modification may have a role in the proteasome degradation of these interacting proteins, events that could create an elimination flow of the ROS source Nox4, concentrating this protein in nuclear domains where a response to redox stress could be triggered and avoiding DNA damage maintaining the cells in a senescence state.

As I showed here, throughout my study I ran into in a great inter patient heterogeneity. In fact, even if antibody sorting for the stem cell factor CD117^{11,37} was used to isolate

a high multipotent subpopulation that represents only 1% of total amniotic fluid cells, a strong heterogeneity continued to be shown inside the population, also due to the different tissue origin that these cells can have.

For this reason, both in my first part of the PhD but mostly in the second part, I decided to study in deep this phenomenon.

Indeed, among the different causes, several studies revealed that donor- dependent differences are in part due and explained by cell-to-cell variation within each patient population²²⁴. In particular, cell-to-cell heterogeneity in MSC phenotype becomes evident during *in vitro* expansion where, within the same population, cells can manifest proliferative and morphological diversity, ranging from elongated spindle-like cells to large flattened cells and highly protrusive cells²²⁷.

At this purpose, a fractionation protocol based on a tag-less, flow-assisted method of purifying, distinguishing and sorting MSCs^{252,253}, allowed me to define various cell subpopulations profiles contained in different samples and to collect these hAFSC subpopulations. In particular, this method exploits the Non-Equilibrium Earth Gravity Assisted Field Flow Fractionation principles (NEEGA-FFF) to characterize and sub-fractionate hAFSCs based on their solely physical characteristics such as dimension, density, morphology and rigidity. Cells were injected into the capillary device and sorted at different time points, based on their characteristics^{252,263}.

On these subpopulations I carried out different types of analyses, both at protein and transcriptome level, in order to clarify which biological characteristics make these cells so heterogenic.

In particular, the analysis of stemness markers revealed that Oct4 expression was significantly higher in the last part of the eluates and it was accompanied by a less expression of mesenchymal markers compared to the first part of collected cells, suggesting that the last eluted cells maintain more pronounced plasticity.

Since in my initial part of PhD, I showed that a higher stemness associates with a better proliferation ability, I decided to check if this assumption occurs also among the fractions.

The analysis of the sorting plots area suggested a correlation between the distribution of cells among the fractions and the proliferation rate of each total unfractionated

sample. Furthermore, the analysis of cell cycle related proteins revealed that Ki67 expression, but not cyclin E2, was upregulated in the last eluted cells.

An enlarged morphology and a reduced cell cycle progression are considered as hallmarks of cellular senescence⁹⁴, but the evaluation of senescence associated markers, showed significant differences only in the transcript levels of p21, even if the same trend was visible also for p16, both resulted less expressed in the last part of eluate.

Since, the evaluation of few genes is not always sufficient to explain the cellular behaviour, which is the result of the interplay among a huge number of genes and related proteins which can act at different levels inside multiple pathways, I had the opportunity to perform a complete transcriptome analysis through RNAseq, that allowed me to have a wider indication about each cellular fraction behaviour. Differential analysis on output data showed an overall change among fractions. Furthermore, Gene Set Enrichment analysis performed using different public datasets displayed, among all significant differential expressed pathways, 5 upregulated pathways (*Stemness*, *DNA repair*, *E2F targets*, *G2M checkpoint* and *Hypoxia*) and 4 downregulated pathways (*Mesenchymal Epithelial Transition*, *mTORC1 signalling*, *Unfold Protein Response*, *p53 signalling*) in the late eluted cells (F3-F4) compared to the first sorted, which trends are consistent with the previous data obtained and confirm a different preservation of stemness properties among the fractions.

One of the other problems that could influence stem cell aging and research is that at present, most of the expansion procedures of MSCs are performed under atmospheric O₂ concentration (20% O₂), which is approximately 4–10 times higher than the concentration of O₂ in their natural niches. In fact, it is known that the partial O₂ pressure in the amniotic cavity is around 2.3 %²³⁶. This higher O₂ concentration might cause environmental stress to the *in vitro* cultured MSCs, due to the increased ROS concentration⁸⁶ and accelerates their aging process.

The influence of oxygen tension in morphology, phenotype, proliferative capacity, and functionality of adult stem cells, such as MSCs, has been increasingly studied with controversial results, in part due to for example the different cellular source or the differentiation protocols used.

For instance, preconditioning MSCs in hypoxia (1–10% oxygen) has shown improved regenerative/repairative properties in animal models of heart, brain, and lung injury^{289–291}.

In particular, several studies have shown that cultures of human stem cells over a physiological range of oxygen tensions (1–5%) improves cell growth, alters differentiation^{292–295}.

Moreover, culture at low O₂ reduced the rate of telomere shortening per cell division, indicating that the increased lifespan might reflect better maintenance of telomere length and extends lifespan²⁹⁶.

To investigate the effect of chronic exposure at low oxygen, I cultivated my hAFSC at 20%, 5% and 1% oxygen tension for a period of 5 weeks. In general, major differences were observed among 1% and the other two conditions, where cells cultivated at 5% showed intermediate characteristics. The different results between 5% and 1% could be due to the different ability of these two oxygen tensions to induce also metabolic changes. In fact, while 1% cells showed mitochondrial fragmentation accompanied by a huge increase in the expression of Glut1 and Pdk1, respectively the glucose carrier and the enzyme inhibitor of TCA cycle, cells at 5% oxygen tension maintained more mitochondria and less activation of Glut1 and Pdk1.

The analysis of stemness markers revealed that Oct4 was upregulated in cells maintained at 1% than in the other two conditions since the first week in culture, accompanied by a major proliferation ability visible at prolonged time, when 20% cells slowed down their growth while the other two conditions continued to proliferate more. It has been reported that hypoxic conditions activate PI3K/Akt axis in bone marrow derived mesenchymal stem cells, enhancing their proliferation²⁸¹. The evaluation of the ratio of pAkt/Akt revealed that it was upregulated in 1% O₂ cultivated cells, sustaining the hypothesis that it could be involved in their proliferation control.

Furthermore, 1% cells showed less expression of senescence-associated markers, such as p21, prelamin A and PML bodies, as well as β -galactosidase positivity, corroborating the idea that low oxygen tension preserves stemness proprieties.

It has been also reported that hypoxia (0.1–2% O₂) increases the viability of stem cells both in normal culture conditions or under the effect of stressor molecules, reducing the percentage of cells that undergo apoptosis^{239,249}. The mechanisms responsible of these

results might be the activation of HIF under hypoxic conditions, which could upregulate antiapoptotic factors²⁵⁰. I found out that after 5 weeks of culture pro-apoptotic factors, such as caspase 3 and PARP, were downregulated in 1% oxygen tension and continued to be more viable after treatment with stressor molecules, such as thapsigargin.

The principal aim of stem cells *in vitro* expansion is to obtain material suitable for regenerative medicine. For this reason, I investigated their osteogenic and adipogenic differentiation ability, which balance is finely regulated during aging process²⁸³.

So, the evaluation of adipogenic and osteogenic markers after 3 weeks exposure to the appropriate differentiation medium, displayed a reduced adipogenic but an increased osteogenic capability of cells cultivated at 5 and 1% than 20% oxygen tension.

Since, different studies report that unlike osteoblastogenesis, which declines with age, adipogenesis seems to accelerate with age^{284,285}, these results confirm that 1% cultivated cells continue to present younger characteristics than 20%.

Summarizing, all the results obtained during my PhD clarify different aspects of stem cell aging process and could help to improve their manipulation prior their use in regenerative medicine.

In particular, I showed a strong heterogeneity among patients that reflect their behaviour in culture and can influence their use in regenerative medicine, also demonstrating the existence of differences among individuals in the ability of counteracting oxidative stress. My results showed that the heterogeneity among samples is also accompanied by a strong intra-population heterogeneity, with cells having different dimensions and morphology. In this sense, separation of different c-kit⁺ hAFSC subpopulations from the same donor, using Celector® technology, which eluates cells with different characteristics at different times, showed that an enrichment in the last fraction could improve hAFSC application in regenerative medicine.

Furthermore, I identified three proteins, namely Nox4, prelamin A and PML, which expression increases during hAFSC aging process and could be used as new biomarkers to screen samples before their use. In particular, I found out that Nox4 degradation is regulated by sumoylation process *via* proteasome pathway and involving interactions with PML bodies and prelamin A. So, all these interactions should be studied in deep to identify new targets for pharmaceutical interventions that could slow down and ameliorate the aging process not only in stem cells but also in normal ones.

Lastly, I also showed that prolonged low oxygen tension exposure preserves stemness properties, increasing proliferation and enhancing osteogenic differentiation ability, while reducing senescence-associated markers, apoptotic pathway and adipogenic differentiation ability.

6. REFERENCES

1. Bigarella CL, Liang R, Ghaffari S. Stem cells and the impact of ROS signaling. *Development*. 2014;141(22):4206-4218. doi:10.1242/dev.107086
2. Evans MJ, Kaufman MH. Establishment in culture of pluripotential cells from mouse embryos. *Nature*. 1981;292(5819):154-156. doi:10.1038/292154a0
3. Blum B, Benvenisty N. The Tumorigenicity of Human Embryonic Stem Cells. In: ; 2008:133-158. doi:10.1016/S0065-230X(08)00005-5
4. Takahashi K, Yamanaka S. Induction of Pluripotent Stem Cells from Mouse Embryonic and Adult Fibroblast Cultures by Defined Factors. *Cell*. 2006;126(4):663-676. doi:10.1016/J.CELL.2006.07.024
5. Ullah I, Subbarao RB, Rho GJ. Human mesenchymal stem cells - current trends and future prospective. *Biosci Rep*. 2015;35(2):1-18. doi:10.1042/BSR20150025
6. Kalra K, Tomar PC. *Stem Cell: Basics, Classification and Applications*. www.ajpct.org. Accessed February 8, 2019.
7. Horwitz EM, Le Blanc K, Dominici M, et al. Clarification of the nomenclature for MSC: The International Society for Cellular Therapy position statement. *Cytotherapy*. 2005;7(5):393-395. doi:10.1080/14653240500319234
8. Pittenger MF, Mackay AM, Beck SC, et al. Multilineage Potential of Adult Human Mesenchymal Stem Cells. *Science (80-)*. 1999;284(5411):143-147. doi:10.1126/SCIENCE.284.5411.143
9. Wagner W, Wein F, Seckinger A, et al. Comparative characteristics of mesenchymal stem cells from human bone marrow, adipose tissue, and umbilical cord blood. *Exp Hematol*. 2005;33(11):1402-1416. doi:10.1016/J.EXPHEM.2005.07.003
10. Tsai M-S, Lee J, Chang Y, Hwang S. Isolation of human multipotent mesenchymal stem cells from second-trimester amniotic fluid using a novel two-stage culture protocol. *Hum Reprod*. 2004;19(6):1450-1456. doi:10.1093/humrep/deh279
11. De Coppi P, Bartsch G, Siddiqui MM, et al. Isolation of amniotic stem cell lines with potential for therapy. *Nat Biotechnol*. 2007;25(1):100-106.

doi:10.1038/nbt1274

12. Cai J, Li W, Su H, et al. Generation of human induced pluripotent stem cells from umbilical cord matrix and amniotic membrane mesenchymal cells. *J Biol Chem.* 2010;285(15):11227-11234. doi:10.1074/jbc.M109.086389
13. Huang GT-J, Gronthos S, Shi S. Mesenchymal Stem Cells Derived from Dental Tissues vs . Those from Other Sources: Their Biology and Role in Regenerative Medicine. *J Dent Res.* 2009;88(9):792-806. doi:10.1177/0022034509340867
14. Schüring AN, Schulte N, Kelsch R, Röpke A, Kiesel L, Götte M. Characterization of endometrial mesenchymal stem-like cells obtained by endometrial biopsy during routine diagnostics. *Fertil Steril.* 2011;95(1):423-426. doi:10.1016/J.FERTNSTERT.2010.08.035
15. Jiao F, Wang J, Dong Z, et al. Human Mesenchymal Stem Cells Derived From Limb Bud Can Differentiate into All Three Embryonic Germ Layers Lineages. *Cell Reprogram.* 2012;14(4):324-333. doi:10.1089/cell.2012.0004
16. Allickson JG. Recent Studies Assessing the Proliferative Capability of a Novel Adult Stem Cell Identified in Menstrual Blood. *Open Stem Cell J.* 2011;3(1):4-10. doi:10.2174/1876893801103010004
17. Ab Kadir R, Zainal Ariffin SH, Megat Abdul Wahab R, Kermani S, Senafi S. Characterization of Mononucleated Human Peripheral Blood Cells. *Sci World J.* 2012;2012:1-8. doi:10.1100/2012/843843
18. Raynaud CM, Maleki M, Lis R, et al. Comprehensive Characterization of Mesenchymal Stem Cells from Human Placenta and Fetal Membrane and Their Response to Osteoactivin Stimulation. *Stem Cells Int.* 2012;2012:1-13. doi:10.1155/2012/658356
19. Rotter N, Oder J, Schlenke P, et al. Isolation and Characterization of Adult Stem Cells from Human Salivary Glands. *Stem Cells Dev.* 2008;17(3):509-518. doi:10.1089/scd.2007.0180
20. Bartsch G, Yoo JJ, De Coppi P, et al. Propagation, Expansion, and Multilineage Differentiation of Human Somatic Stem Cells from Dermal Progenitors. *Stem Cells Dev.* 2005;14(3):337-348. doi:10.1089/scd.2005.14.337
21. Kita K, Gauglitz GG, Phan TT, Herndon DN, Jeschke MG. Isolation and Characterization of Mesenchymal Stem Cells From the Sub-Amniotic Human

- Umbilical Cord Lining Membrane. *Stem Cells Dev.* 2010;19(4):491-502. doi:10.1089/scd.2009.0192
22. Morito T, Muneta T, Hara K, et al. Synovial fluid-derived mesenchymal stem cells increase after intra-articular ligament injury in humans. *Rheumatology.* 2008;47(8):1137-1143. doi:10.1093/rheumatology/ken114
 23. Wang H-S, Hung S-C, Peng S-T, et al. Mesenchymal Stem Cells in the Wharton's Jelly of the Human Umbilical Cord. *Stem Cells.* 2004;22(7):1330-1337. doi:10.1634/stemcells.2004-0013
 24. Dominici M, Le Blanc K, Mueller I, et al. Minimal criteria for defining multipotent mesenchymal stromal cells. The International Society for Cellular Therapy position statement. 2006. doi:10.1080/14653240600855905
 25. Rasmusson I, Ringd?n O, Sundberg B, Le Blanc K. Mesenchymal stem cells inhibit the formation of cytotoxic T lymphocytes, but not activated cytotoxic T lymphocytes or natural killer cells. *Transplantation.* 2003;76(8):1208-1213. doi:10.1097/01.TP.0000082540.43730.80
 26. Ryan JM, Barry F, Murphy JM, Mahon BP. Interferon- γ does not break, but promotes the immunosuppressive capacity of adult human mesenchymal stem cells. *Clin Exp Immunol.* 2007;149(2):353-363. doi:10.1111/j.1365-2249.2007.03422.x
 27. Shi Y, Hu G, Su J, et al. Mesenchymal stem cells: a new strategy for immunosuppression and tissue repair. *Cell Res.* 2010;20(5):510-518. doi:10.1038/cr.2010.44
 28. Baraniak PR, Mcdevitt TC. Stem cell paracrine actions and tissue regeneration. *Regen Med.* 2010;5(1):121-143. doi:10.2217/rme.09.74
 29. Antonucci I, Provenzano M, Rodrigues M, et al. Amniotic Fluid Stem Cells: A Novel Source for Modeling of Human Genetic Diseases. *Int J Mol Sci.* 2016;17(4):607. doi:10.3390/ijms17040607
 30. Kim K, Doi A, Wen B, et al. Epigenetic memory in induced pluripotent stem cells. *Nature.* 2010;467(7313):285-290. doi:10.1038/nature09342
 31. Hoehn H, Bryant EM, Karp LE, Martin GM. Cultivated cells from diagnostic amniocentesis in second trimester pregnancies. II. Cytogenetic parameters as functions of clonal type and preparative technique. *Clin Genet.* 1975;7(1):29-36.

- <http://www.ncbi.nlm.nih.gov/pubmed/1167818>. Accessed June 4, 2019.
32. Loukogeorgakis SP, De Coppi P. Concise Review: Amniotic Fluid Stem Cells: The Known, the Unknown, and Potential Regenerative Medicine Applications SIGNIFICANCE STATEMENT. *Stem Cells*. 2017;35:1663-1673. doi:10.1002/stem.2553
 33. Spitzhorn L-S, Rahman MS, Schwindt L, et al. Isolation and Molecular Characterization of Amniotic Fluid-Derived Mesenchymal Stem Cells Obtained from Caesarean Sections. *Stem Cells Int*. 2017;2017:1-15. doi:10.1155/2017/5932706
 34. Murphy SV, Atala A. Amniotic Fluid Stem Cells. In: *Perinatal Stem Cells*. Hoboken, NJ, USA: John Wiley & Sons, Inc.; 2013:1-15. doi:10.1002/9781118497883.ch1
 35. Torricelli F, Brizzi L, Bernabei PA, et al. Identification of hematopoietic progenitor cells in human amniotic fluid before the 12th week of gestation. *Ital J Anat Embryol*. 98(2):119-126. <http://www.ncbi.nlm.nih.gov/pubmed/8239855>. Accessed June 4, 2019.
 36. Antonucci I, Pantalone A, Tete Stefano, et al. Amniotic Fluid Stem Cells: a Promising Therapeutic Resource for Cell-Based Regenerative Therapy. *Curr Pharm Des*. 2012;18(13):1846-1863. doi:10.2174/138161212799859602
 37. Cananzi M, De Coppi P. CD117⁺ amniotic fluid stem cells. *Organogenesis*. 2012;8(3):77-88. doi:10.4161/org.22426
 38. Anker PS, Scherjon SA, Kleijburg-van der Keur C, et al. Amniotic fluid as a novel source of mesenchymal stem cells for therapeutic transplantation. *Blood*. 2003;102(4):1548-1549. doi:10.1182/blood-2003-04-1291
 39. Antonucci I, Di Pietro R, Alfonsi M, et al. Human Second Trimester Amniotic Fluid Cells are Able to Create Embryoid Body-Like Structures in Vitro and to Show Typical Expression Profiles of Embryonic and Primordial Germ Cells. *Cell Transplant*. 2014;23(12):1501-1515. doi:10.3727/096368914X678553
 40. Schiavo AA, Franzin C, Albiero M, et al. Endothelial properties of third-trimester amniotic fluid stem cells cultured in hypoxia. *Stem Cell Res Ther*. 2015;6(1):209. doi:10.1186/s13287-015-0204-0
 41. Roubelakis MG, Pappa KI, Bitsika V, et al. Molecular and Proteomic

- Characterization of Human Mesenchymal Stem Cells Derived from Amniotic Fluid: Comparison to Bone Marrow Mesenchymal Stem Cells. *Stem Cells Dev.* 2007;16(6):931-952. doi:10.1089/scd.2007.0036
42. Valli A, Rosner M, Fuchs C, et al. Embryoid body formation of human amniotic fluid stem cells depends on mTOR. *Oncogene.* 2010;29(7):966-977. doi:10.1038/onc.2009.405
 43. Walther G, Gekas J, Bertrand OF. Amniotic stem cells for cellular cardiomyoplasty: Promises and premises. *Catheter Cardiovasc Interv.* 2009;73(7):917-924. doi:10.1002/ccd.22016
 44. Zagoura DS, Roubelakis MG, Bitsika V, et al. Therapeutic potential of a distinct population of human amniotic fluid mesenchymal stem cells and their secreted molecules in mice with acute hepatic failure. *Gut.* 2012;61(6):894-906. doi:10.1136/gutjnl-2011-300908
 45. Mirabella T, Cilli M, Carlone S, et al. Amniotic liquid derived stem cells as reservoir of secreted angiogenic factors capable of stimulating neo-arteriogenesis in an ischemic model. *Biomaterials.* 2011;32(15):3689-3699. doi:10.1016/j.biomaterials.2011.01.071
 46. Yoon BS, Moon J-H, Jun EK, et al. Secretory Profiles and Wound Healing Effects of Human Amniotic Fluid-Derived Mesenchymal Stem Cells. *Stem Cells Dev.* 2010;19(6):887-902. doi:10.1089/scd.2009.0138
 47. Maraldi T, Beretti F, Guida M, Zavatti M, De Pol A. Role of hepatocyte growth factor in the immunomodulation potential of amniotic fluid stem cells. *Stem Cells Transl Med.* 2015;4(6):539-547. doi:10.5966/sctm.2014-0266
 48. Insausti CL, Blanquer M, García-Hernández AM, Castellanos G, Moraleda JM. Amniotic membrane-derived stem cells: immunomodulatory properties and potential clinical application. *Stem Cells Cloning.* 2014;7:53-63. doi:10.2147/SCCAA.S58696
 49. Balbi C, Bollini S. Fetal and perinatal stem cells in cardiac regeneration: Moving forward to the paracrine era. *Placenta.* 2017;59:96-106. doi:10.1016/j.placenta.2017.04.008
 50. Beretti F, Zavatti M, Casciaro F, et al. Amniotic fluid stem cell exosomes: Therapeutic perspective. *BioFactors.* 2018;44(2):158-167.

doi:10.1002/biof.1407

51. Lin F, Moran A, Igarashi P. Intrarenal cells, not bone marrow–derived cells, are the major source for regeneration in postischemic kidney. *J Clin Invest.* 2005;115(7):1756-1764. doi:10.1172/JCI23015
52. Chen L, Xu Y, Zhao J, et al. Conditioned Medium from Hypoxic Bone Marrow-Derived Mesenchymal Stem Cells Enhances Wound Healing in Mice. Pesce M, ed. *PLoS One.* 2014;9(4):e96161. doi:10.1371/journal.pone.0096161
53. Le Blanc K, Tammik L, Sundberg B, Haynesworth SE, Ringdén O. Mesenchymal stem cells inhibit and stimulate mixed lymphocyte cultures and mitogenic responses independently of the major histocompatibility complex. *Scand J Immunol.* 2003;57(1):11-20. <http://www.ncbi.nlm.nih.gov/pubmed/12542793>. Accessed July 4, 2019.
54. Wang S, Qu X, Zhao R. Clinical applications of mesenchymal stem cells. *J Hematol Oncol.* 2012;5(1):19. doi:10.1186/1756-8722-5-19
55. Eberli D, Atala A, Yoo JJ. One and four layer acellular bladder matrix for fascial tissue reconstruction. *J Mater Sci Mater Med.* 2011;22(3):741-751. doi:10.1007/s10856-011-4242-6
56. Horwitz EM, Prockop DJ, Gordon PL, et al. Clinical responses to bone marrow transplantation in children with severe osteogenesis imperfecta. *Blood.* 2001;97(5):1227-1231. <http://www.ncbi.nlm.nih.gov/pubmed/11222364>. Accessed February 19, 2019.
57. Maraldi T, Riccio M, Pisciotta A, et al. Human amniotic fluid-derived and dental pulp-derived stem cells seeded into collagen scaffold repair critical-size bone defects promoting vascularization. *Stem Cell Res Ther.* 2013;4(3):53. doi:10.1186/scrt203
58. Zavatti M, Bertoni L, Maraldi T, et al. Critical-size bone defect repair using amniotic fluid stem cell/collagen constructs: Effect of oral ferutinin treatment in rats. *Life Sci.* 2015;121:174-183. doi:10.1016/j.lfs.2014.10.020
59. Kuroda R, Ishida K, Matsumoto T, et al. Treatment of a full-thickness articular cartilage defect in the femoral condyle of an athlete with autologous bone-marrow stromal cells. *Osteoarthr Cartil.* 2007;15(2):226-231. doi:10.1016/j.joca.2006.08.008

60. Wakitani S, Nawata M, Tensho K, Okabe T, Machida H, Ohgushi H. Repair of articular cartilage defects in the patello-femoral joint with autologous bone marrow mesenchymal cell transplantation: three case reports involving nine defects in five knees. *J Tissue Eng Regen Med.* 2007;1(1):74-79. doi:10.1002/term.8
61. Crisostomo PR, Wang M, Markel TA, et al. Stem cell mechanisms and paracrine effects: potential in cardiac surgery. *Shock.* 2007;28(4):375-383. doi:10.1097/shk.0b013e318058a817
62. Pedersen TO, Blois AL, Xue Y, et al. Osteogenic stimulatory conditions enhance growth and maturation of endothelial cell microvascular networks in culture with mesenchymal stem cells. *J Tissue Eng.* 2012;3(1):204173141244323. doi:10.1177/2041731412443236
63. Wise AF, Williams TM, Kiewiet MBG, et al. Human mesenchymal stem cells alter macrophage phenotype and promote regeneration via homing to the kidney following ischemia-reperfusion injury. *Am J Physiol Physiol.* 2014;306(10):F1222-F1235. doi:10.1152/ajprenal.00675.2013
64. Kuzmina LA, Petinati NA, Parovichnikova EN, et al. Multipotent Mesenchymal Stromal Cells for the Prophylaxis of Acute Graft-versus-Host Disease—A Phase II Study. *Stem Cells Int.* 2012;2012:1-8. doi:10.1155/2012/968213
65. Tyndall A. Application of autologous stem cell transplantation in various adult and pediatric rheumatic diseases. *Pediatr Res.* 2012;71(4-2):433-438. doi:10.1038/pr.2011.66
66. García-Olmo D, García-Arranz M, Herreros D, Pascual I, Peiro C, Rodríguez-Montes JA. A Phase I Clinical Trial of the Treatment of Crohn's Fistula by Adipose Mesenchymal Stem Cell Transplantation. *Dis Colon Rectum.* 2005;48(7):1416-1423. doi:10.1007/s10350-005-0052-6
67. Garcia-Olmo D, Herreros D, Pascual I, et al. Expanded Adipose-Derived Stem Cells for the Treatment of Complex Perianal Fistula. *Dis Colon Rectum.* 2009;52(1):79-86. doi:10.1007/DCR.0b013e3181973487
68. Mohyeddin Bonab M, Yazdanbakhsh S, Lotfi J, et al. Does mesenchymal stem cell therapy help multiple sclerosis patients? Report of a pilot study. *Iran J Immunol.* 2007;4(1):50-57. doi:IJIV4i1A7

69. Sun L, Zhang H, Feng X, Hou Y, Lu L, Fan L. Abnormality of bone marrow-derived mesenchymal stem cells in patients with systemic lupus erythematosus. *Lupus*. 2007;16(2):121-128. doi:10.1177/0961203306075793
70. Mao F, Xu W-R, Qian H, et al. Immunosuppressive effects of mesenchymal stem cells in collagen-induced mouse arthritis. *Inflamm Res*. 2010;59(3):219-225. doi:10.1007/s00011-009-0090-y
71. Chen B, Hu J, Liao L, et al. Flk-1⁺ mesenchymal stem cells aggravate collagen-induced arthritis by up-regulating interleukin-6. *Clin Exp Immunol*. 2010;159(3):292-302. doi:10.1111/j.1365-2249.2009.04069.x
72. Wu T, Liu Y, Wang B, Li G. The roles of mesenchymal stem cells in tissue repair and disease modification. *Curr Stem Cell Res Ther*. 2014;9(5):424-431. <http://www.ncbi.nlm.nih.gov/pubmed/24998241>. Accessed April 1, 2019.
73. Zhu W, Xu W, Jiang R, et al. Mesenchymal stem cells derived from bone marrow favor tumor cell growth in vivo. *Exp Mol Pathol*. 2006;80(3):267-274. doi:10.1016/j.yexmp.2005.07.004
74. Karnoub AE, Dash AB, Vo AP, et al. Mesenchymal stem cells within tumour stroma promote breast cancer metastasis. *Nature*. 2007;449(7162):557-563. doi:10.1038/nature06188
75. Qiao L, Xu Z, Zhao T, et al. Suppression of tumorigenesis by human mesenchymal stem cells in a hepatoma model. *Cell Res*. 2008;18(4):500-507. doi:10.1038/cr.2008.40
76. Otsu K, Das S, Houser SD, Quadri SK, Bhattacharya S, Bhattacharya J. Concentration-dependent inhibition of angiogenesis by mesenchymal stem cells. *Blood*. 2009;113(18):4197-4205. doi:10.1182/blood-2008-09-176198
77. Seo SH, Kim KS, Park SH, et al. The effects of mesenchymal stem cells injected via different routes on modified IL-12-mediated antitumor activity. *Gene Ther*. 2011;18(5):488-495. doi:10.1038/gt.2010.170
78. Gunnarsson S, Bexell D, Svensson A, Siesjö P, Darabi A, Bengzon J. Intratumoral IL-7 delivery by mesenchymal stromal cells potentiates IFN γ -transduced tumor cell immunotherapy of experimental glioma. *J Neuroimmunol*. 2010;218(1-2):140-144. doi:10.1016/j.jneuroim.2009.10.017
79. Cavarretta IT, Altanerova V, Matuskova M, Kucerova L, Culig Z, Altaner C.

- Adipose tissue-derived mesenchymal stem cells expressing prodrug-converting enzyme inhibit human prostate tumor growth. *Mol Ther.* 2010;18(1):223-231. doi:10.1038/mt.2009.237
80. Yong RL, Shinojima N, Fueyo J, et al. Human Bone Marrow-Derived Mesenchymal Stem Cells for Intravascular Delivery of Oncolytic Adenovirus 24-RGD to Human Gliomas. *Cancer Res.* 2009;69(23):8932-8940. doi:10.1158/0008-5472.CAN-08-3873
 81. Eekelen M van, Sasportas L, Kasmieh R, et al. Human stem cells expressing novel TSP-1 variant have anti-angiogenic effect on brain tumors. *Oncogene.* 2010;29(22):3185. doi:10.1038/ONC.2010.75
 82. Mueller LP, Luetzkendorf J, Widder M, Nerger K, Caysa H, Mueller T. TRAIL-transduced multipotent mesenchymal stromal cells (TRAIL-MS-C) overcome TRAIL resistance in selected CRC cell lines in vitro and in vivo. *Cancer Gene Ther.* 2011;18(4):229-239. doi:10.1038/cgt.2010.68
 83. Kanehira M, Xin H, Hoshino K, et al. Targeted delivery of NK4 to multiple lung tumors by bone marrow-derived mesenchymal stem cells. *Cancer Gene Ther.* 2007;14(11):894-903. doi:10.1038/sj.cgt.7701079
 84. Ramos CA, Asgari Z, Liu E, et al. An Inducible Caspase 9 Suicide Gene to Improve the Safety of Mesenchymal Stromal Cell Therapies. *Stem Cells.* 2010;28(6):1107-1115. doi:10.1002/stem.433
 85. Chulpanova DS, Kitaeva K V., Tazetdinova LG, James V, Rizvanov AA, Solovyeva V V. Application of Mesenchymal Stem Cells for Therapeutic Agent Delivery in Anti-tumor Treatment. *Front Pharmacol.* 2018;9:259. doi:10.3389/fphar.2018.00259
 86. Antoniou ES, Sund S, Homsy EN, Challenger LF, Rameshwar P. A theoretical simulation of hematopoietic stem cells during oxygen fluctuations: prediction of bone marrow responses during hemorrhagic shock. *Shock.* 2004;22(5):415-422. <http://www.ncbi.nlm.nih.gov/pubmed/15489633>. Accessed April 2, 2019.
 87. Sart S, Song L, Li Y. Controlling Redox Status for Stem Cell Survival, Expansion, and Differentiation. *Oxid Med Cell Longev.* 2015;2015:1-14. doi:10.1155/2015/105135
 88. Dufour E, Larsson N-G. Understanding aging: revealing order out of chaos.

- Biochim Biophys Acta - Bioenerg.* 2004;1658(1-2):122-132.
doi:10.1016/j.bbabi.2004.04.020
89. Ben-Porath I, Weinberg RA. The signals and pathways activating cellular senescence. *Int J Biochem Cell Biol.* 2005;37(5):961-976.
doi:10.1016/j.biocel.2004.10.013
 90. Hayflick L. The limited in vitro lifetime of human diploid cell strains. *Exp Cell Res.* 1965;37(3):614-636. doi:10.1016/0014-4827(65)90211-9
 91. Campisi J. The biology of replicative senescence. *Eur J Cancer.* 1997;33(5):703-709. doi:10.1016/S0959-8049(96)00058-5
 92. Toussaint O, Medrano E., von Zglinicki T. Cellular and molecular mechanisms of stress-induced premature senescence (SIPS) of human diploid fibroblasts and melanocytes. *Exp Gerontol.* 2000;35(8):927-945. doi:10.1016/S0531-5565(00)00180-7
 93. Bartkova J, Rezaei N, Linton M, et al. Oncogene-induced senescence is part of the tumorigenesis barrier imposed by DNA damage checkpoints. *Nature.* 2006;444(7119):633-637. doi:10.1038/nature05268
 94. Hernandez-Segura A, Nehme J, Demaria M. Hallmarks of Cellular Senescence. *Trends Cell Biol.* 2018;28(6):436-453. doi:10.1016/j.tcb.2018.02.001
 95. Oh J, Lee YD, Wagers AJ. Stem cell aging: mechanisms, regulators and therapeutic opportunities. *Nat Med.* 2014;20(8):870-880. doi:10.1038/nm.3651
 96. Harman D. Aging: A Theory Based on Free Radical and Radiation Chemistry. *J Gerontol.* 1956;11(3):298-300. doi:10.1093/geronj/11.3.298
 97. Poyton RO, Ball KA, Castello PR. Mitochondrial generation of free radicals and hypoxic signaling. *Trends Endocrinol Metab.* 2009;20(7):332-340. doi:10.1016/j.tem.2009.04.001
 98. Bedard K, Krause K-H. The NOX Family of ROS-Generating NADPH Oxidases: Physiology and Pathophysiology. *Physiol Rev.* 2007;87(1):245-313. doi:10.1152/physrev.00044.2005
 99. Ryu JM, Lee HJ, Jung YH, et al. Regulation of Stem Cell Fate by ROS-mediated Alteration of Metabolism. *Int J Stem Cells.* 2015;8(1):24. doi:10.15283/IJSC.2015.8.1.24
 100. Liang R, Ghaffari S. Stem Cells, Redox Signaling, and Stem Cell Aging. *Antioxid*

- Redox Signal.* 2014;20(12):1902. doi:10.1089/ARS.2013.5300
101. Holmström KM, Finkel T. Cellular mechanisms and physiological consequences of redox-dependent signalling. *Nat Rev Mol Cell Biol.* 2014;15(6):411-421. doi:10.1038/nrm3801
 102. Guo Y-L, Chakraborty S, Rajan SS, Wang R, Huang F. Effects of Oxidative Stress on Mouse Embryonic Stem Cell Proliferation, Apoptosis, Senescence, and Self-Renewal. *Stem Cells Dev.* 2010;19(9):1321-1331. doi:10.1089/scd.2009.0313
 103. Mishra BP, Zaffuto KM, Artinger EL, et al. The Histone Methyltransferase Activity of MLL1 Is Dispensable for Hematopoiesis and Leukemogenesis. *Cell Rep.* 2014;7(4):1239-1247. doi:10.1016/J.CELREP.2014.04.015
 104. Yuan H-F, Zhai C, Yan X-L, et al. SIRT1 is required for long-term growth of human mesenchymal stem cells. *J Mol Med.* 2012;90(4):389-400. doi:10.1007/s00109-011-0825-4
 105. Chen H, Liu X, Chen H, et al. Role of SIRT1 and AMPK in mesenchymal stem cells differentiation. *Ageing Res Rev.* 2014;13:55-64. doi:10.1016/j.arr.2013.12.002
 106. Kim H-S, Patel K, Muldoon-Jacobs K, et al. SIRT3 Is a Mitochondria-Localized Tumor Suppressor Required for Maintenance of Mitochondrial Integrity and Metabolism during Stress. *Cancer Cell.* 2010;17(1):41-52. doi:10.1016/j.ccr.2009.11.023
 107. Tsai W-B, Chung YM, Takahashi Y, Xu Z, Hu MC-T. Functional interaction between FOXO3a and ATM regulates DNA damage response. *Nat Cell Biol.* 2008;10(4):460-467. doi:10.1038/ncb1709
 108. Zhang F, Cui J, Liu X, et al. Roles of microRNA-34a targeting SIRT1 in mesenchymal stem cells. *Stem Cell Res Ther.* 2015;6:195. doi:10.1186/s13287-015-0187-x
 109. Li Y, Wu Q, Wang Y, Li L, Bu H, Bao J. Senescence of mesenchymal stem cells (Review). *Int J Mol Med.* 2017;39(4):775-782. doi:10.3892/ijmm.2017.2912
 110. Bucciantini M, Giannoni E, Chiti F, et al. Inherent toxicity of aggregates implies a common mechanism for protein misfolding diseases. *Nature.* 2002;416(6880):507-511. doi:10.1038/416507a

111. Passos JF, Saretzki G, Ahmed S, et al. Mitochondrial Dysfunction Accounts for the Stochastic Heterogeneity in Telomere-Dependent Senescence. De Lange T, ed. *PLoS Biol.* 2007;5(5):e110. doi:10.1371/journal.pbio.0050110
112. Brown DI, Griendling KK. Nox proteins in signal transduction. *Free Radic Biol Med.* 2009;47(9):1239-1253. doi:10.1016/j.freeradbiomed.2009.07.023
113. Shiose A, Kuroda J, Tsuruya K, et al. A Novel Superoxide-producing NAD(P)H Oxidase in Kidney. *J Biol Chem.* 2001;276(2):1417-1423. doi:10.1074/jbc.M007597200
114. Wingler K, Wünsch S, Kreutz R, Rothermund L, Paul M, Schmidt HH. Upregulation of the vascular NAD(P)H-oxidase isoforms Nox1 and Nox4 by the renin-angiotensin system in vitro and in vivo. *Free Radic Biol Med.* 2001;31(11):1456-1464. <http://www.ncbi.nlm.nih.gov/pubmed/11728818>. Accessed April 5, 2019.
115. Jackson HM, Kawahara T, Nisimoto Y, Smith SME, Lambeth JD. Nox4 B-loop Creates an Interface between the Transmembrane and Dehydrogenase Domains. *J Biol Chem.* 2010;285(14):10281-10290. doi:10.1074/jbc.M109.084939
116. Takac I, Schröder K, Zhang L, et al. The E-loop Is Involved in Hydrogen Peroxide Formation by the NADPH Oxidase Nox4. *J Biol Chem.* 2011;286(15):13304-13313. doi:10.1074/jbc.M110.192138
117. Guo S, Chen X. The human Nox4: gene, structure, physiological function and pathological significance. *J Drug Target.* 2015;23(10):888-896. doi:10.3109/1061186X.2015.1036276
118. Geiszt M, Kopp JB, Varnai P, Leto TL. Identification of Renox, an NAD(P)H oxidase in kidney. *Proc Natl Acad Sci.* 2000;97(14):8010-8014. doi:10.1073/pnas.130135897
119. Hilenski LL, Clempus RE, Quinn MT, Lambeth JD, Griendling KK. Distinct Subcellular Localizations of Nox1 and Nox4 in Vascular Smooth Muscle Cells. *Arterioscler Thromb Vasc Biol.* 2004;24(4):677-683. doi:10.1161/01.ATV.0000112024.13727.2c
120. Kuroda J, Nakagawa K, Yamasaki T, et al. The superoxide-producing NAD(P)H oxidase Nox4 in the nucleus of human vascular endothelial cells. *Genes to Cells.* 2005;10(12):1139-1151. doi:10.1111/j.1365-2443.2005.00907.x

121. Chen K, Kirber MT, Xiao H, Yang Y, Keaney JF. Regulation of ROS signal transduction by NADPH oxidase 4 localization. *J Cell Biol.* 2008;181(7):1129-1139. doi:10.1083/jcb.200709049
122. Block K, Gorin Y, Abboud HE. Subcellular localization of Nox4 and regulation in diabetes. *Proc Natl Acad Sci.* 2009;106(34):14385-14390. doi:10.1073/pnas.0906805106
123. Lee Y-M, Kim B-J, Chun Y-S, et al. NOX4 as an oxygen sensor to regulate TASK-1 activity. *Cell Signal.* 2006;18(4):499-507. doi:10.1016/j.cellsig.2005.05.025
124. Ateghang B, Wartenberg M, Gassmann M, Sauer H. Regulation of cardiotrophin-1 expression in mouse embryonic stem cells by HIF-1 and intracellular reactive oxygen species. *J Cell Sci.* 2006;119(6):1043-1052. doi:10.1242/jcs.02798
125. Peshavariya H, Dusting GJ, Jiang F, et al. NADPH oxidase isoform selective regulation of endothelial cell proliferation and survival. *Naunyn Schmiedebergs Arch Pharmacol.* 2009;380(2):193-204. doi:10.1007/s00210-009-0413-0
126. Sturrock A, Cahill B, Norman K, et al. Transforming growth factor- β 1 induces Nox4 NAD(P)H oxidase and reactive oxygen species-dependent proliferation in human pulmonary artery smooth muscle cells. *Am J Physiol Cell Mol Physiol.* 2006;290(4):L661-L673. doi:10.1152/ajplung.00269.2005
127. Li S, Tabar SS, Malec V, et al. NOX4 Regulates ROS Levels Under Normoxic and Hypoxic Conditions, Triggers Proliferation, and Inhibits Apoptosis in Pulmonary Artery Adventitial Fibroblasts. *Antioxid Redox Signal.* 2008;10(10):1687-1698. doi:10.1089/ars.2008.2035
128. Mofarrahi M, Brandes RP, Gorchach A, et al. Regulation of Proliferation of Skeletal Muscle Precursor Cells By NADPH Oxidase. *Antioxid Redox Signal.* 2008;10(3):559-574. doi:10.1089/ars.2007.1792
129. Schröder K, Wandzioch K, Helmcke I, Brandes RP. Nox4 Acts as a Switch Between Differentiation and Proliferation in Preadipocytes. *Arterioscler Thromb Vasc Biol.* 2009;29(2):239-245. doi:10.1161/ATVBAHA.108.174219
130. Shono T, Yokoyama N, Uesaka T, et al. Enhanced expression of NADPH oxidase Nox4 in human gliomas and its roles in cell proliferation and survival. *Int J Cancer.* 2008;123(4):787-792. doi:10.1002/ijc.23569

131. Crosas-Molist E, Bertran E, Sancho P, et al. The NADPH oxidase NOX4 inhibits hepatocyte proliferation and liver cancer progression. *Free Radic Biol Med*. 2014;69:338-347. doi:10.1016/j.freeradbiomed.2014.01.040
132. Zhang C, Lan T, Hou J, et al. NOX4 promotes non-small cell lung cancer cell proliferation and metastasis through positive feedback regulation of PI3K/Akt signaling. *Oncotarget*. 2014;5(12):4392-4405. doi:10.18632/oncotarget.2025
133. Maraldi T, Guida M, Zavatti M, et al. Nuclear Nox4 Role in Stemness Power of Human Amniotic Fluid Stem Cells. *Oxid Med Cell Longev*. 2015;2015:1-11. doi:10.1155/2015/101304
134. Lamond AI, Spector DL. Nuclear speckles: a model for nuclear organelles. *Nat Rev Mol Cell Biol*. 2003;4(8):605-612. doi:10.1038/nrm1172
135. Guida M, Maraldi T, Resca E, et al. Inhibition of Nuclear Nox4 Activity by Plumbagin: Effect on Proliferative Capacity in Human Amniotic Stem Cells. *Oxid Med Cell Longev*. 2013;2013:1-12. doi:10.1155/2013/680816
136. Kanda Y, Hinata T, Kang SW, Watanabe Y. Reactive oxygen species mediate adipocyte differentiation in mesenchymal stem cells. *Life Sci*. 2011;89(7-8):250-258. doi:10.1016/j.lfs.2011.06.007
137. Chaudhari P, Ye Z, Jang Y-Y. Roles of Reactive Oxygen Species in the Fate of Stem Cells. *Antioxid Redox Signal*. 2014;20(12):1881-1890. doi:10.1089/ars.2012.4963
138. Gabig TG, Bearman SI, Babior BM. Effects of oxygen tension and pH on the respiratory burst of human neutrophils. *Blood*. 1979;53(6):1133-1139. <http://www.ncbi.nlm.nih.gov/pubmed/36182>. Accessed April 5, 2019.
139. Chandel NS, McClintock DS, Feliciano CE, et al. Reactive Oxygen Species Generated at Mitochondrial Complex III Stabilize Hypoxia-inducible Factor-1 α during Hypoxia. *J Biol Chem*. 2000;275(33):25130-25138. doi:10.1074/jbc.M001914200
140. Miera EV-S de, Rudy B. Modulation of K⁺ channels by hydrogen peroxide. *Biochem Biophys Res Commun*. 1992;186(3):1681-1687. doi:10.1016/S0006-291X(05)81602-X
141. Varga Z V., Kupai K, Szűcs G, et al. MicroRNA-25-dependent up-regulation of NADPH oxidase 4 (NOX4) mediates hypercholesterolemia-induced

- oxidative/nitrative stress and subsequent dysfunction in the heart. *J Mol Cell Cardiol.* 2013;62:111-121. doi:10.1016/j.yjmcc.2013.05.009
142. Gordillo GM, Biswas A, Khanna S, et al. Dicer Knockdown Inhibits Endothelial Cell Tumor Growth via MicroRNA 21a-3p Targeting of Nox-4. *J Biol Chem.* 2014;289(13):9027-9038. doi:10.1074/jbc.M113.519264
143. Laurindo FRM, Fernandes DC, Amanso AM, Lopes LR, Santos CXC. Novel role of protein disulfide isomerase in the regulation of NADPH oxidase activity: pathophysiological implications in vascular diseases. *Antioxid Redox Signal.* 2008;10(6):1101-1113. doi:10.1089/ars.2007.2011
144. Lyle AN, Deshpande NN, Taniyama Y, et al. Poldip2, a Novel Regulator of Nox4 and Cytoskeletal Integrity in Vascular Smooth Muscle Cells. *Circ Res.* 2009;105(3):249-259. doi:10.1161/CIRCRESAHA.109.193722
145. Diaz B, Shani G, Pass I, Anderson D, Quintavalle M, Courtneidge SA. Tks5-Dependent, Nox-Mediated Generation of Reactive Oxygen Species Is Necessary for Invadopodia Formation. *Sci Signal.* 2009;2(88):ra53-ra53. doi:10.1126/scisignal.2000368
146. Gil Lorenzo AF, Bocanegra V, Benardon ME, Cacciamani V, Vallés PG. Hsp70 regulation on Nox4/p22phox and cytoskeletal integrity as an effect of losartan in vascular smooth muscle cells. *Cell Stress Chaperones.* 2014;19(1):115-134. doi:10.1007/s12192-013-0439-6
147. Desai LP, Zhou Y, Estrada A V., et al. Negative Regulation of NADPH Oxidase 4 by Hydrogen Peroxide-inducible Clone 5 (Hic-5) Protein. *J Biol Chem.* 2014;289(26):18270-18278. doi:10.1074/jbc.M114.562249
148. Hetzer MW. The Nuclear Envelope. *Cold Spring Harb Perspect Biol.* 2010;2(3):a000539-a000539. doi:10.1101/cshperspect.a000539
149. Linnemann AK, Krawetz SA. Maintenance of a functional higher order chromatin structure: The role of the nuclear matrix in normal and disease states. *Gene Ther Mol Biol.* 2009;13(1):231-243. <http://www.ncbi.nlm.nih.gov/pubmed/20948980>. Accessed April 8, 2019.
150. Hetzer MW, Wenthe SR. Border Control at the Nucleus: Biogenesis and Organization of the Nuclear Membrane and Pore Complexes. *Dev Cell.* 2009;17(5):606-616. doi:10.1016/j.devcel.2009.10.007

151. Aebi U, Cohn J, Buhle L, Gerace L. The nuclear lamina is a meshwork of intermediate-type filaments. *Nature*. 1986;323(6088):560-564. doi:10.1038/323560a0
152. Reddy S, Comai L. Lamin A, farnesylation and aging. *Exp Cell Res*. 2012;318(1):1-7. doi:10.1016/j.yexcr.2011.08.009
153. Holtz D, Tanaka RA, Hartwig J, McKeon F. The CaaX motif of lamin A functions in conjunction with the nuclear localization signal to target assembly to the nuclear envelope. *Cell*. 1989;59(6):969-977. <http://www.ncbi.nlm.nih.gov/pubmed/2557160>. Accessed April 8, 2019.
154. Strelkov S V., Schumacher J, Burkhard P, Aebi U, Herrmann H. Crystal Structure of the Human Lamin A Coil 2B Dimer: Implications for the Head-to-tail Association of Nuclear Lamins. *J Mol Biol*. 2004;343(4):1067-1080. doi:10.1016/j.jmb.2004.08.093
155. Ng Z, Ong ZH, Liu F, Xiao M, Ing D. *Assembly of Lamins in Vitro*. Vol 6.; 1996. doi:10.1038/cr.1996.2
156. Mattout A, Dechat T, Adam SA, Goldman RD, Gruenbaum Y. Nuclear lamins, diseases and aging. *Curr Opin Cell Biol*. 2006;18(3):335-341. doi:10.1016/j.ceb.2006.03.007
157. Dechat T, Pflieger K, Sengupta K, et al. Nuclear lamins: major factors in the structural organization and function of the nucleus and chromatin. *Genes Dev*. 2008;22(7):832. doi:10.1101/GAD.1652708
158. Cau P, Navarro C, Harhour K, et al. Nuclear matrix, nuclear envelope and premature aging syndromes in a translational research perspective. *Semin Cell Dev Biol*. 2014;29:125-147. doi:10.1016/J.SEMCDB.2014.03.021
159. Barrowman J, Hamblet C, George CM, Michaelis S. Analysis of Prelamin A Biogenesis Reveals the Nucleus to be a CaaX Processing Compartment. Wentz SR, ed. *Mol Biol Cell*. 2008;19(12):5398-5408. doi:10.1091/mbc.e08-07-0704
160. Kuga T, Nozaki N, Matsushita K, Nomura F, Tomonaga T. Phosphorylation statuses at different residues of lamin B2, B1, and A/C dynamically and independently change throughout the cell cycle. *Exp Cell Res*. 2010;316(14):2301-2312. doi:10.1016/j.yexcr.2010.05.017
161. Cenni V, Bertacchini J, Beretti F, et al. Lamin A Ser404 Is a Nuclear Target of

- Akt Phosphorylation in C2C12 Cells. *J Proteome Res.* 2008;7(11):4727-4735. doi:10.1021/pr800262g
162. Bertacchini J, Beretti F, Cenni V, et al. The protein kinase Akt/PKB regulates both prelamin A degradation and *Lmna* gene expression. *FASEB J.* 2013;27(6):2145-2155. doi:10.1096/fj.12-218214
163. Choudhary C, Kumar C, Gnad F, et al. Lysine Acetylation Targets Protein Complexes and Co-Regulates Major Cellular Functions. *Science (80-).* 2009;325(5942):834-840. doi:10.1126/science.1175371
164. Kim W, Bennett EJ, Huttlin EL, et al. Systematic and Quantitative Assessment of the Ubiquitin-Modified Proteome. *Mol Cell.* 2011;44(2):325-340. doi:10.1016/j.molcel.2011.08.025
165. Reyes-Turcu FE, Ventii KH, Wilkinson KD. Regulation and Cellular Roles of Ubiquitin-Specific Deubiquitinating Enzymes. *Annu Rev Biochem.* 2009;78(1):363-397. doi:10.1146/annurev.biochem.78.082307.091526
166. Heun P. SUMO Organization of the nucleus. *Curr Opin Cell Biol.* 2007;19(3):350-355. doi:10.1016/j.ceb.2007.04.014
167. Parnaik VK, Chaturvedi P, Muralikrishna B. Lamins, laminopathies and disease mechanisms: possible role for proteasomal degradation of key regulatory proteins. *J Biosci.* 2011;36(3):471-479. <http://www.ncbi.nlm.nih.gov/pubmed/21799258>. Accessed June 4, 2019.
168. Da Silva-Ferrada E, Lopitz-Otsoa F, Lang V, Rodríguez MS, Matthiesen R. Strategies to Identify Recognition Signals and Targets of SUMOylation. *Biochem Res Int.* 2012;2012:1-16. doi:10.1155/2012/875148
169. Matic I, van Hagen M, Schimmel J, et al. *In Vivo* Identification of Human Small Ubiquitin-like Modifier Polymerization Sites by High Accuracy Mass Spectrometry and an *in Vitro* to *in Vivo* Strategy. *Mol Cell Proteomics.* 2008;7(1):132-144. doi:10.1074/mcp.M700173-MCP200
170. Skoczyńska A, Budzisz E, Dana A, Rotsztein H. New look at the role of progerin in skin aging. *Menopausal Rev.* 2015;1(1):53-58. doi:10.5114/pm.2015.49532
171. Sieprath T, Darwiche R, De Vos WH. Lamins as mediators of oxidative stress. *Biochem Biophys Res Commun.* 2012;421(4):635-639. doi:10.1016/j.bbrc.2012.04.058

172. Pekovic V, Gibbs-Seymour I, Markiewicz E, et al. Conserved cysteine residues in the mammalian lamin A tail are essential for cellular responses to ROS generation. *Aging Cell*. 2011;10(6):1067-1079. doi:10.1111/j.1474-9726.2011.00750.x
173. Dalle-Donne I, Rossi R, Giustarini D, Colombo R, Milzani A. Actin S-glutathionylation: evidence against a thiol-disulphide exchange mechanism. *Free Radic Biol Med*. 2003;35(10):1185-1193. <http://www.ncbi.nlm.nih.gov/pubmed/14607517>. Accessed April 8, 2019.
174. Méjat A, Misteli T. LINC complexes in health and disease. *Nucleus*. 2010;1(1):40. doi:10.4161/NUCL.1.1.10530
175. Mewborn SK, Puckelwartz MJ, Abuisneineh F, et al. Altered Chromosomal Positioning, Compaction, and Gene Expression with a Lamin A/C Gene Mutation. Sullivan BA, ed. *PLoS One*. 2010;5(12):e14342. doi:10.1371/journal.pone.0014342
176. Manju K, Muralikrishna B, Parnaik VK. Expression of disease-causing lamin A mutants impairs the formation of DNA repair foci. *J Cell Sci*. 2006;119(13):2704-2714. doi:10.1242/jcs.03009
177. Heessen S, Fornerod M. The inner nuclear envelope as a transcription factor resting place. *EMBO Rep*. 2007;8(10):914-919. doi:10.1038/sj.embor.7401075
178. Malhas AN, Lee CF, Vaux DJ. Lamin B1 controls oxidative stress responses via Oct-1. *J Cell Biol*. 2009;184(1):45-55. doi:10.1083/jcb.200804155
179. De Vos WH, Houben F, Kamps M, et al. Repetitive disruptions of the nuclear envelope invoke temporary loss of cellular compartmentalization in laminopathies. *Hum Mol Genet*. 2011;20(21):4175-4186. doi:10.1093/hmg/ddr344
180. Fabrini R, Bocedi A, Pallottini V, et al. Nuclear Shield: A Multi-Enzyme Task-Force for Nucleus Protection. *PLoS One*. 2010;5(12). doi:10.1371/JOURNAL.PONE.0014125
181. Libotte T, Zaim H, Abraham S, et al. Lamin A/C-dependent Localization of Nesprin-2, a Giant Scaffold at the Nuclear Envelope. *Mol Biol Cell*. 2005;16(7):3411-3424. doi:10.1091/mbc.e04-11-1009
182. Weyemi U, Lagente-Chevallier O, Boufraquech M, et al. ROS-generating

- NADPH oxidase NOX4 is a critical mediator in oncogenic H-Ras-induced DNA damage and subsequent senescence. *Oncogene*. 2012;31(9):1117-1129. doi:10.1038/onc.2011.327
183. de Mochel NSR, Seronello S, Wang SH, et al. Hepatocyte NAD(P)H oxidases as an endogenous source of reactive oxygen species during hepatitis C virus infection. *Hepatology*. 2010;52(1):47-59. doi:10.1002/hep.23671
 184. Capell BC, Collins FS. Human laminopathies: nuclei gone genetically awry. *Nat Rev Genet*. 2006;7(12):940-952. doi:10.1038/nrg1906
 185. Navarro CL, Cau P, Lévy N. Molecular bases of progeroid syndromes. *Hum Mol Genet*. 2006;15(suppl_2):R151-R161. doi:10.1093/hmg/ddl214
 186. Richards SA, Muter J, Ritchie P, Lattanzi G, Hutchison CJ. The accumulation of un-repairable DNA damage in laminopathy progeria fibroblasts is caused by ROS generation and is prevented by treatment with N-acetyl cysteine. *Hum Mol Genet*. 2011;20(20):3997-4004. doi:10.1093/hmg/ddr327
 187. Muteliefu G, Shimizu H, Enomoto A, Nishijima F, Takahashi M, Niwa T. Indoxy sulfate promotes vascular smooth muscle cell senescence with upregulation of p53, p21, and prelamin A through oxidative stress. *Am J Physiol Physiol*. 2012;303(2):C126-C134. doi:10.1152/ajpcell.00329.2011
 188. Lattanzi G, Ortolani M, Columbaro M, et al. Lamins are rapamycin targets that impact human longevity: a study in centenarians. *J Cell Sci*. 2014;127(1):147-157. doi:10.1242/jcs.133983
 189. Stuurman N, Meijne AM, van der Pol AJ, de Jong L, van Driel R, van Renswoude J. The nuclear matrix from cells of different origin. Evidence for a common set of matrix proteins. *J Biol Chem*. 1990;265(10):5460-5465. <http://www.ncbi.nlm.nih.gov/pubmed/2180926>. Accessed April 10, 2019.
 190. Salomoni P, Pandolfi PP. The role of PML in tumor suppression. *Cell*. 2002;108(2):165-170. <http://www.ncbi.nlm.nih.gov/pubmed/11832207>. Accessed April 10, 2019.
 191. Lallemand-Breitenbach V, de Thé H. PML nuclear bodies. *Cold Spring Harb Perspect Biol*. 2010;2(5):a000661. doi:10.1101/cshperspect.a000661
 192. Bernardi R, Pandolfi PP. Structure, dynamics and functions of promyelocytic leukaemia nuclear bodies. *Nat Rev Mol Cell Biol*. 2007;8(12):1006-1016.

doi:10.1038/nrm2277

193. Dellaire G, Bazett-Jones DP. PML nuclear bodies: dynamic sensors of DNA damage and cellular stress. *BioEssays*. 2004;26(9):963-977. doi:10.1002/bies.20089
194. Boisvert FM, Hendzel MJ, Bazett-Jones DP. Promyelocytic leukemia (PML) nuclear bodies are protein structures that do not accumulate RNA. *J Cell Biol*. 2000;148(2):283-292. <http://www.ncbi.nlm.nih.gov/pubmed/10648561>. Accessed April 10, 2019.
195. Eskiw CH, Dellaire G, Bazett-Jones DP. Chromatin Contributes to Structural Integrity of Promyelocytic Leukemia Bodies through a SUMO-1-independent Mechanism. *J Biol Chem*. 2004;279(10):9577-9585. doi:10.1074/jbc.M312580200
196. Grande MA, van der Kraan I, van Steensel B, et al. PML-containing nuclear bodies: Their spatial distribution in relation to other nuclear components. *J Cell Biochem*. 1996;63(3):280-291. doi:10.1002/(SICI)1097-4644(19961201)63:3<280::AID-JCB3>3.0.CO;2-T
197. Aoto T, Saitoh N, Ichimura T, Niwa H, Nakao M. Nuclear and chromatin reorganization in the MHC-Oct3/4 locus at developmental phases of embryonic stem cell differentiation. *Dev Biol*. 2006;298(2):354-367. doi:10.1016/j.ydbio.2006.04.450
198. Flenghi L, Fagioli M, Tomassoni L, et al. Characterization of a new monoclonal antibody (PG-M3) directed against the aminoterminal portion of the PML gene product: immunocytochemical evidence for high expression of PML proteins on activated macrophages, endothelial cells, and epithelia. *Blood*. 1995;85(7):1871-1880. <http://www.ncbi.nlm.nih.gov/pubmed/7535592>. Accessed April 10, 2019.
199. Stadler M, Chelbi-Alix MK, Koken MH, et al. Transcriptional induction of the PML growth suppressor gene by interferons is mediated through an ISRE and a GAS element. *Oncogene*. 1995;11(12):2565-2573. <http://www.ncbi.nlm.nih.gov/pubmed/8545113>. Accessed April 10, 2019.
200. de Stanchina E, Querido E, Narita M, et al. PML is a direct p53 target that modulates p53 effector functions. *Mol Cell*. 2004;13(4):523-535. <http://www.ncbi.nlm.nih.gov/pubmed/14992722>. Accessed April 10, 2019.

201. Hubackova S, Novakova Z, Krejcikova K, et al. Regulation of the PML tumor suppressor in drug-induced senescence of human normal and cancer cells by JAK/STAT-mediated signaling. *Cell Cycle*. 2010;9(15):3157-3171. doi:10.4161/cc.9.15.12521
202. Novakova Z, Hubackova S, Kosar M, et al. Cytokine expression and signaling in drug-induced cellular senescence. *Oncogene*. 2010;29(2):273-284. doi:10.1038/onc.2009.318
203. Chang KS, Fan YH, Andreeff M, Liu J, Mu ZM. The PML gene encodes a phosphoprotein associated with the nuclear matrix. *Blood*. 1995;85(12):3646-3653. <http://www.ncbi.nlm.nih.gov/pubmed/7780148>. Accessed April 10, 2019.
204. Hayakawa F, Privalsky ML. Phosphorylation of PML by mitogen-activated protein kinases plays a key role in arsenic trioxide-mediated apoptosis. *Cancer Cell*. 2004;5(4):389-401. <http://www.ncbi.nlm.nih.gov/pubmed/15093545>. Accessed April 10, 2019.
205. Bernardi R, Scaglioni PP, Bergmann S, Horn HF, Vousden KH, Pandolfi PP. PML regulates p53 stability by sequestering Mdm2 to the nucleolus. *Nat Cell Biol*. 2004;6(7):665-672. doi:10.1038/ncb1147
206. Yang S, Kuo C, Bisi JE, Kim MK. PML-dependent apoptosis after DNA damage is regulated by the checkpoint kinase hCds1/Chk2. *Nat Cell Biol*. 2002;4(11):865-870. doi:10.1038/ncb869
207. Borden KLB. Pondering the promyelocytic leukemia protein (PML) puzzle: possible functions for PML nuclear bodies. *Mol Cell Biol*. 2002;22(15):5259-5269. <http://www.ncbi.nlm.nih.gov/pubmed/12101223>. Accessed April 11, 2019.
208. Ivanschitz L, De Thé H, Le Bras M. PML, SUMOylation, and Senescence. *Front Oncol*. 2013;3:171. doi:10.3389/fonc.2013.00171
209. Wilkinson KA, Henley JM. Mechanisms, regulation and consequences of protein SUMOylation. *Biochem J*. 2010;428(2):133-145. doi:10.1042/BJ20100158
210. Rodriguez MS, Dargemont C, Hay RT. SUMO-1 Conjugation *in Vivo* Requires Both a Consensus Modification Motif and Nuclear Targeting. *J Biol Chem*. 2001;276(16):12654-12659. doi:10.1074/jbc.M009476200
211. Kim JH, Baek SH. Emerging roles of desumoylating enzymes. *Biochim Biophys*

- Acta - Mol Basis Dis.* 2009;1792(3):155-162. doi:10.1016/j.bbadis.2008.12.008
212. Wilkinson KA, Henley JM. Mechanisms, regulation and consequences of protein SUMOylation. *Biochem J.* 2010;428(2):133-145. doi:10.1042/BJ20100158
213. Kerscher O. SUMO junction-what's your function? New insights through SUMO-interacting motifs. *EMBO Rep.* 2007;8(6):550-555. doi:10.1038/sj.embor.7400980
214. Hecker C-M, Rabiller M, Haglund K, Bayer P, Dikic I. Specification of SUMO1- and SUMO2-interacting Motifs. *J Biol Chem.* 2006;281(23):16117-16127. doi:10.1074/jbc.M512757200
215. Gostissa M, Hengstermann A, Fogal V, et al. Activation of p53 by conjugation to the ubiquitin-like protein SUMO-1. *EMBO J.* 1999;18(22):6462-6471. doi:10.1093/emboj/18.22.6462
216. Li T, Santockyte R, Shen R-F, et al. Expression of SUMO-2/3 induced senescence through p53- and pRB-mediated pathways. *J Biol Chem.* 2006;281(47):36221-36227. doi:10.1074/jbc.M608236200
217. Campagna M, Herranz D, Garcia MA, et al. SIRT1 stabilizes PML promoting its sumoylation. *Cell Death Differ.* 2011;18(1):72-79. doi:10.1038/cdd.2010.77
218. Li X, Luo Y, Yu L, et al. SENP1 mediates TNF-induced desumoylation and cytoplasmic translocation of HIPK1 to enhance ASK1-dependent apoptosis. *Cell Death Differ.* 2008;15(4):739-750. doi:10.1038/sj.cdd.4402303
219. Kim HJ, Yun J, Lee J, et al. SUMO1 attenuates stress-induced ROS generation by inhibiting NADPH oxidase 2. *Biochem Biophys Res Commun.* 2011;410(3):555-562. doi:10.1016/J.BBRC.2011.06.025
220. Pandey D, Chen F, Patel A, et al. SUMO1 Negatively Regulates Reactive Oxygen Species Production From NADPH Oxidases. *Arterioscler Thromb Vasc Biol.* 2011;31(7):1634-1642. doi:10.1161/ATVBAHA.111.226621
221. Jeanne M, Lallemand-Breitenbach V, Ferhi O, et al. PML/RARA Oxidation and Arsenic Binding Initiate the Antileukemia Response of As₂O₃. *Cancer Cell.* 2010;18(1):88-98. doi:10.1016/j.ccr.2010.06.003
222. Harhour K, Navarro C, Depetris D, et al. MG132-induced progerin clearance is mediated by autophagy activation and splicing regulation. *EMBO Mol Med.* 2017;9(9):1294-1313. doi:10.15252/emmm.201607315

223. Phinney DG. Functional heterogeneity of mesenchymal stem cells: Implications for cell therapy. *J Cell Biochem.* 2012;113(9):2806-2812. doi:10.1002/jcb.24166
224. McLeod C, Mauck R. On the origin and impact of mesenchymal stem cell heterogeneity: new insights and emerging tools for single cell analysis. *Eur Cells Mater.* 2017;34:217-231. doi:10.22203/eCM.v034a14
225. Wang J, Liao L, Wang S, Tan J. Cell therapy with autologous mesenchymal stem cells—how the disease process impacts clinical considerations. *Cytotherapy.* 2013;15(8):893-904. doi:10.1016/j.jcyt.2013.01.218
226. Phinney DG, Kopen G, Righter W, Webster S, Tremain N, Prockop DJ. Donor variation in the growth properties and osteogenic potential of human marrow stromal cells. *J Cell Biochem.* 1999;75(3):424-436. doi:10.1002/(SICI)1097-4644(19991201)75:3<424::AID-JCB8>3.0.CO;2-8
227. Colter DC, Sekiya I, Prockop DJ. Identification of a subpopulation of rapidly self-renewing and multipotential adult stem cells in colonies of human marrow stromal cells. *Proc Natl Acad Sci.* 2001;98(14):7841-7845. doi:10.1073/pnas.141221698
228. Wagner W, Ho AD, Zenke M. Different facets of aging in human mesenchymal stem cells. *Tissue Eng Part B Rev.* 2010;16(4):445-453. doi:10.1089/ten.TEB.2009.0825
229. Russell KC, Phinney DG, Lacey MR, Barrilleaux BL, Meyertholen KE, O'Connor KC. In Vitro High-Capacity Assay to Quantify the Clonal Heterogeneity in Trilineage Potential of Mesenchymal Stem Cells Reveals a Complex Hierarchy of Lineage Commitment. *Stem Cells.* 2010;28(4):788-798. doi:10.1002/stem.312
230. Mareddy S, Broadbent J, Crawford R, Xiao Y. Proteomic profiling of distinct clonal populations of bone marrow mesenchymal stem cells. *J Cell Biochem.* 2009;106(5):776-786. doi:10.1002/jcb.22088
231. Mareddy S, Dhaliwal N, Crawford R, Xiao Y. Stem Cell-Related Gene Expression in Clonal Populations of Mesenchymal Stromal Cells from Bone Marrow. *Tissue Eng Part A.* 2010;16(2):749-758. doi:10.1089/ten.tea.2009.0307
232. Berdasco M, Esteller M. DNA methylation in stem cell renewal and multipotency. *Stem Cell Res Ther.* 2011;2(5):42. doi:10.1186/scrt83

233. Hernandez-Segura A, de Jong T V., Melov S, Guryev V, Campisi J, Demaria M. Unmasking Transcriptional Heterogeneity in Senescent Cells. *Curr Biol.* 2017;27(17):2652-2660.e4. doi:10.1016/j.cub.2017.07.033
234. Choi JR, Yong KW, Wan Safwani WKZ. Effect of hypoxia on human adipose-derived mesenchymal stem cells and its potential clinical applications. *Cell Mol Life Sci.* 2017;74(14):2587-2600. doi:10.1007/s00018-017-2484-2
235. Skiles ML, Sahai S, Rucker L, Blanchette JO. Use of culture geometry to control hypoxia-induced vascular endothelial growth factor secretion from adipose-derived stem cells: optimizing a cell-based approach to drive vascular growth. *Tissue Eng Part A.* 2013;19(21-22):2330-2338. doi:10.1089/ten.TEA.2012.0750
236. Jauniaux E, Watson A, Ozturk O, Quick D, Burton G. In-vivo measurement of intrauterine gases and acid-base values early in human pregnancy. *Hum Reprod.* 1999;14(11):2901-2904. <http://www.ncbi.nlm.nih.gov/pubmed/10548645>. Accessed April 28, 2019.
237. Choi JR, Pingguan-Murphy B, Wan Abas WAB, et al. In Situ Normoxia Enhances Survival and Proliferation Rate of Human Adipose Tissue-Derived Stromal Cells without Increasing the Risk of Tumorigenesis. Ivanovic Z, ed. *PLoS One.* 2015;10(1):e0115034. doi:10.1371/journal.pone.0115034
238. Choi JR, Pingguan-Murphy B, Wan Abas WAB, et al. Impact of low oxygen tension on stemness, proliferation and differentiation potential of human adipose-derived stem cells. *Biochem Biophys Res Commun.* 2014;448(2):218-224. doi:10.1016/j.bbrc.2014.04.096
239. Choi JR, Pingguan-Murphy B, Abas WABW, et al. Hypoxia Promotes Growth and Viability of Human Adipose-Derived Stem Cells with Increased Growth Factors Secretion. *J Asian Sci Res.* 2014;4(7):328-338. https://econpapers.repec.org/article/asijoasrj/2014_3ap_3a328-338.htm. Accessed April 28, 2019.
240. Gardner LB, Li Q, Park MS, Flanagan WM, Semenza GL, Dang C V. Hypoxia Inhibits G₁/S Transition through Regulation of p27 Expression. *J Biol Chem.* 2001;276(11):7919-7926. doi:10.1074/jbc.M010189200
241. Grayson WL, Zhao F, Izadpanah R, Bunnell B, Ma T. Effects of hypoxia on human mesenchymal stem cell expansion and plasticity in 3D constructs. *J Cell*

- Physiol.* 2006;207(2):331-339. doi:10.1002/jcp.20571
242. Lu Y, Qu H, Qi D, et al. OCT4 maintains self-renewal and reverses senescence in human hair follicle mesenchymal stem cells through the downregulation of p21 by DNA methyltransferases. *Stem Cell Res Ther.* 2019;10(1):28. doi:10.1186/s13287-018-1120-x
243. Greer Card DA, Hebbar PB, Li L, et al. Oct4/Sox2-Regulated miR-302 Targets Cyclin D1 in Human Embryonic Stem Cells. *Mol Cell Biol.* 2008;28(20):6426-6438. doi:10.1128/MCB.00359-08
244. Kim JH, Kim S-H, Song SY, et al. Hypoxia induces adipocyte differentiation of adipose-derived stem cells by triggering reactive oxygen species generation. *Cell Biol Int.* 2014;38(1):32-40. doi:10.1002/cbin.10170
245. Hsu S-H, Chen C-T, Wei Y-H. Inhibitory Effects of Hypoxia on Metabolic Switch and Osteogenic Differentiation of Human Mesenchymal Stem Cells. *Stem Cells.* 2013;31(12):2779-2788. doi:10.1002/stem.1441
246. Hung S-P, Ho JH, Shih Y-R V., Lo T, Lee OK. Hypoxia promotes proliferation and osteogenic differentiation potentials of human mesenchymal stem cells. *J Orthop Res.* 2012;30(2):260-266. doi:10.1002/jor.21517
247. Wagegg M, Gaber T, Lohanatha FL, et al. Hypoxia Promotes Osteogenesis but Suppresses Adipogenesis of Human Mesenchymal Stromal Cells in a Hypoxia-Inducible Factor-1 Dependent Manner. Covas DT, ed. *PLoS One.* 2012;7(9):e46483. doi:10.1371/journal.pone.0046483
248. Valorani MG, Montelatici E, Germani A, et al. Pre-culturing human adipose tissue mesenchymal stem cells under hypoxia increases their adipogenic and osteogenic differentiation potentials. *Cell Prolif.* 2012;45(3):225-238. doi:10.1111/j.1365-2184.2012.00817.x
249. Korski KI, Kubli DA, Wang BJ, et al. Hypoxia Prevents Mitochondrial Dysfunction and Senescence in Human c-Kit⁺ Cardiac Progenitor Cells. *Stem Cells.* 2019;37(4):555-567. doi:10.1002/stem.2970
250. Hu X, Yu SP, Fraser JL, et al. Transplantation of hypoxia-preconditioned mesenchymal stem cells improves infarcted heart function via enhanced survival of implanted cells and angiogenesis. *J Thorac Cardiovasc Surg.* 2008;135(4):799-808. doi:10.1016/j.jtcvs.2007.07.071

251. Hung S-C, Pochampally RR, Chen S-C, Hsu S-C, Prockop DJ. Angiogenic Effects of Human Multipotent Stromal Cell Conditioned Medium Activate the PI3K-Akt Pathway in Hypoxic Endothelial Cells to Inhibit Apoptosis, Increase Survival, and Stimulate Angiogenesis. *Stem Cells*. 2007;25(9):2363-2370. doi:10.1634/stemcells.2006-0686
252. Roda B, Reschiglian P, Zattoni A, et al. A tag-less method of sorting stem cells from clinical specimens and separating mesenchymal from epithelial progenitor cells. *Cytom Part B Clin Cytom*. 2009;76B(4):285-290. doi:10.1002/cyto.b.20472
253. Lattuada D, Roda B, Pignatari C, et al. A tag-less method for direct isolation of human umbilical vein endothelial cells by gravitational field-flow fractionation. *Anal Bioanal Chem*. 2013;405(2-3):977-984. doi:10.1007/s00216-012-6337-4
254. Ghi T, Sotiriadis A, Calda P, et al. ISUOG Practice Guidelines: invasive procedures for prenatal diagnosis. *Ultrasound Obstet Gynecol*. 2016;48(2):256-268. doi:10.1002/uog.15945
255. Cruz-Lemini M, Parra-Saavedra M, Borobio V, et al. How to perform an amniocentesis. *Ultrasound Obstet Gynecol*. 2014;44(6):727-731. doi:10.1002/uog.14680
256. Tabor A, Alfirevic Z. Update on Procedure-Related Risks for Prenatal Diagnosis Techniques. *Fetal Diagn Ther*. 2010;27(1):1-7. doi:10.1159/000271995
257. Meron PM. Preparation, Culture, and Analysis of Amniotic Fluid Samples. In: *Current Protocols in Human Genetics*. Vol Chapter 8. Hoboken, NJ, USA: John Wiley & Sons, Inc.; 2001:Unit 8.4. doi:10.1002/0471142905.hg0804s05
258. Kalyanaraman B, Darley-Usmar V, Davies KJA, et al. Measuring reactive oxygen and nitrogen species with fluorescent probes: challenges and limitations. *Free Radic Biol Med*. 2012;52(1):1-6. doi:10.1016/j.freeradbiomed.2011.09.030
259. van de Loosdrecht AA, Beelen RH, Ossenkoppele GJ, Broekhoven MG, Langenhuijsen MM. A tetrazolium-based colorimetric MTT assay to quantitate human monocyte mediated cytotoxicity against leukemic cells from cell lines and patients with acute myeloid leukemia. *J Immunol Methods*. 1994;174(1-2):311-320. <http://www.ncbi.nlm.nih.gov/pubmed/8083535>. Accessed May 7, 2019.
260. Dimri GP, Lee X, Basile G, et al. A biomarker that identifies senescent human

- cells in culture and in aging skin in vivo. *Proc Natl Acad Sci.* 1995;92(20):9363-9367. doi:10.1073/pnas.92.20.9363
261. Bradford MM. A rapid and sensitive method for the quantitation of microgram quantities of protein utilizing the principle of protein-dye binding. *Anal Biochem.* 1976;72:248-254. <http://www.ncbi.nlm.nih.gov/pubmed/942051>. Accessed May 8, 2019.
262. Shevchenko A, Tomas H, Havli J, Olsen J V, Mann M. In-gel digestion for mass spectrometric characterization of proteins and proteomes. *Nat Protoc.* 2006;1(6):2856-2860. doi:10.1038/nprot.2006.468
263. Roda B, Lanzoni G, Alviano F, et al. A Novel Stem Cell Tag-Less Sorting Method. *Stem Cell Rev Reports.* 2009;5(4):420-427. doi:10.1007/s12015-009-9088-7
264. Mueller O, Lightfoot S, Schroeder A. *RNA Integrity Number (RIN)-Standardization of RNA Quality Control Application.* <https://www.agilent.com/cs/library/applications/5989-1165EN.pdf>. Accessed May 14, 2019.
265. Jin Q, Yan T, Ge X, Sun C, Shi X, Zhai Q. Cytoplasm-localized SIRT1 enhances apoptosis. *J Cell Physiol.* 2007;213(1):88-97. doi:10.1002/jcp.21091
266. Tanno M, Sakamoto J, Miura T, Shimamoto K, Horio Y. Nucleocytoplasmic Shuttling of the NAD⁺-dependent Histone Deacetylase SIRT1. *J Biol Chem.* 2007;282(9):6823-6832. doi:10.1074/jbc.M609554200
267. Haigis MC, Guarente LP. Mammalian sirtuins--emerging roles in physiology, aging, and calorie restriction. *Genes Dev.* 2006;20(21):2913-2921. doi:10.1101/gad.1467506
268. Ong ALC, Ramasamy TS. Role of Sirtuin1-p53 regulatory axis in aging, cancer and cellular reprogramming. *Ageing Res Rev.* 2018;43:64-80. doi:10.1016/j.arr.2018.02.004
269. Ruiz de Eguino G, Infante A, Schlangen K, et al. Sp1 transcription factor interaction with accumulated prelamin a impairs adipose lineage differentiation in human mesenchymal stem cells: essential role of sp1 in the integrity of lipid vesicles. *Stem Cells Transl Med.* 2012;1(4):309-321. doi:10.5966/sctm.2011-0010

270. Ivanschitz L, De Thé H, Le Bras M. PML, SUMOylation, and Senescence. *Front Oncol.* 2013;3:171. doi:10.3389/fonc.2013.00171
271. Barilani M, Banfi F, Sironi S, et al. Low-affinity Nerve Growth Factor Receptor (CD271) Heterogeneous Expression in Adult and Fetal Mesenchymal Stromal Cells. *Sci Rep.* 2018;8(1):9321. doi:10.1038/s41598-018-27587-8
272. Mulyawan IM. Role of Ki67 protein in colorectal cancer. *Int J Res Med Sci.* 2019;7(2):644. doi:10.18203/2320-6012.ijrms20190374
273. Xiao B, Sanders MJ, Underwood E, et al. Structure of mammalian AMPK and its regulation by ADP. *Nature.* 2011;472(7342):230-233. doi:10.1038/nature09932
274. Liberzon A, Birger C, Thorvaldsdóttir H, Ghandi M, Mesirov JP, Tamayo P. The Molecular Signatures Database Hallmark Gene Set Collection. *Cell Syst.* 2015;1(6):417-425. doi:10.1016/J.CELS.2015.12.004
275. Chen C, Liu Y, Liu Y, Zheng P. mTOR Regulation and Therapeutic Rejuvenation of Aging Hematopoietic Stem Cells. doi:10.1126/scisignal.2000559
276. Morita M, Gravel S-P, Chénard V, et al. mTORC1 Controls Mitochondrial Activity and Biogenesis through 4E-BP-Dependent Translational Regulation. *Cell Metab.* 2013;18(5):698-711. doi:10.1016/j.cmet.2013.10.001
277. Hetz C. The unfolded protein response: controlling cell fate decisions under ER stress and beyond. *Nat Rev Mol Cell Biol.* 2012;13(2):89-102. doi:10.1038/nrm3270
278. Childs BG, Baker DJ, Kirkland JL, Campisi J, van Deursen JM. Senescence and apoptosis: dueling or complementary cell fates? *EMBO Rep.* 2014;15(11):1139-1153. doi:10.15252/embr.201439245
279. Schmitz ML, Shaban MS, Albert BV, Gökçen A, Kracht M. The Crosstalk of Endoplasmic Reticulum (ER) Stress Pathways with NF- κ B: Complex Mechanisms Relevant for Cancer, Inflammation and Infection. *Biomedicines.* 2018;6(2). doi:10.3390/biomedicines6020058
280. Rizzino A, Wuebben EL. Sox2/Oct4: A delicately balanced partnership in pluripotent stem cells and embryogenesis. *Biochim Biophys Acta - Gene Regul Mech.* 2016;1859(6):780-791. doi:10.1016/j.bbagr.2016.03.006

281. Sheng L, Mao X, Yu Q, Yu D. Effect of the PI3K/AKT signaling pathway on hypoxia-induced proliferation and differentiation of bone marrow-derived mesenchymal stem cells. *Exp Ther Med.* 2017;13(1):55-62. doi:10.3892/etm.2016.3917
282. Solaini G, Baracca A, Lenaz G, Sgarbi G. Hypoxia and mitochondrial oxidative metabolism. *Biochim Biophys Acta - Bioenerg.* 2010;1797(6-7):1171-1177. doi:10.1016/j.bbabi.2010.02.011
283. Bethel M, Chitteti BR, Srour EF, Rohn Professor of Leukemia Research AS, Kacena MA, Professor A. The Changing Balance Between Osteoblastogenesis and Adipogenesis in Aging and its Impact on Hematopoiesis. doi:10.1007/s11914-013-0135-6
284. Kajkenova O, Lecka-Czernik B, Gubrij I, et al. Increased Adipogenesis and Myelopoiesis in the Bone Marrow of SAMP6, a Murine Model of Defective Osteoblastogenesis and Low Turnover Osteopenia. *J Bone Miner Res.* 1997;12(11):1772-1779. doi:10.1359/jbmr.1997.12.11.1772
285. Justesen J, Stenderup K, Ebbesen EN, Mosekilde L, Steiniche T, Kassem M. Adipocyte tissue volume in bone marrow is increased with aging and in patients with osteoporosis. *Biogerontology.* 2001;2(3):165-171. <http://www.ncbi.nlm.nih.gov/pubmed/11708718>. Accessed June 20, 2019.
286. Kim JE, Chen J. Regulation of Peroxisome Proliferator-Activated Receptor- Activity by Mammalian Target of Rapamycin and Amino Acids in Adipogenesis. *Diabetes.* 2004;53(11):2748-2756. doi:10.2337/diabetes.53.11.2748
287. Bruderer M, Richards RG, Alini M, Stoddart MJ. Role and regulation of RUNX2 in osteogenesis. *Eur Cell Mater.* 2014;28:269-286. <http://www.ncbi.nlm.nih.gov/pubmed/25340806>. Accessed June 26, 2019.
288. Zhang Y-Q, Sarge KD. Sumoylation regulates lamin A function and is lost in lamin A mutants associated with familial cardiomyopathies. *J Cell Biol.* 2008;182(1):35-39. doi:10.1083/jcb.200712124
289. Cruz FF, Rocco PRM. Hypoxic preconditioning enhances mesenchymal stromal cell lung repair capacity. *Stem Cell Res Ther.* 2015;6(1):130. doi:10.1186/s13287-015-0120-3

290. Lan Y-W, Choo K-B, Chen C-M, et al. Hypoxia-preconditioned mesenchymal stem cells attenuate bleomycin-induced pulmonary fibrosis. *Stem Cell Res Ther.* 2015;6(1):97. doi:10.1186/s13287-015-0081-6
291. Wakai T, Narasimhan P, Sakata H, et al. Hypoxic preconditioning enhances neural stem cell transplantation therapy after intracerebral hemorrhage in mice. *J Cereb Blood Flow Metab.* 2016;36(12):2134-2145. doi:10.1177/0271678X15613798
292. dos Santos F, Andrade PZ, Boura JS, Abecasis MM, da Silva CL, Cabral JMS. Ex vivo expansion of human mesenchymal stem cells: A more effective cell proliferation kinetics and metabolism under hypoxia. *J Cell Physiol.* 2009;223(1):n/a-n/a. doi:10.1002/jcp.21987
293. Fehrer C, Brunauer R, Laschober G, et al. Reduced oxygen tension attenuates differentiation capacity of human mesenchymal stem cells and prolongs their lifespan. *Aging Cell.* 2007;6(6):745-757. doi:10.1111/j.1474-9726.2007.00336.x
294. Basciano L, Nemos C, Foliguet B, et al. Long term culture of mesenchymal stem cells in hypoxia promotes a genetic program maintaining their undifferentiated and multipotent status. *BMC Cell Biol.* 2011;12(1):12. doi:10.1186/1471-2121-12-12
295. Grayson WL, Zhao F, Bunnell B, Ma T. Hypoxia enhances proliferation and tissue formation of human mesenchymal stem cells. *Biochem Biophys Res Commun.* 2007;358(3):948-953. doi:10.1016/j.bbrc.2007.05.054
296. Estrada JC, Albo C, Benguría A, et al. Culture of human mesenchymal stem cells at low oxygen tension improves growth and genetic stability by activating glycolysis. *Cell Death Differ.* 2012;19(5):743-755. doi:10.1038/cdd.2011.172